DEVELOPMENT OF LAYERED SILICATE / EPOXY NANOCOMPOSITES

A Thesis submitted to
the Graduate School of Engineering and Science of
Izmir Institute of Technology
in Partial Fulfillment of the Requirements for the Degree of

MASTER OF SCIENCE

in Materials Science and Engineering

by
Elçin Dilek KAYA

July 2006
Izmir, Turkey

We approve the thesis of **Elçin Dilek KAYA**

Date of Signature

..... **12 July 2006**

Assoc. Prof. Dr. Metin TANOĞLU
Supervisor
Department of Mechanical Engineering
Izmir Institute of Technology

..... **12 July 2006**

Assoc. Prof. Dr. Salih OKUR
Co-Supervisor
Department of Physics
Izmir Institute of Technology

..... **12 July 2006**

Assoc. Prof. Dr. Sacide ALSOY ALTINKAYA
Department of Chemical Engineering
Izmir Institute of Technology

..... **12 July 2006**

Assoc. Prof. Dr. Funda TIHMINLIOĞLU
Department of Chemical Engineering
Izmir Institute of Technology

..... **12 July 2006**

Asst. Prof. Dr. Seçil ALTUNDAĞ ARTEM
Department of Mechanical Engineering
Izmir Institute of Technology

..... **12 July 2006**

Prof. Dr. Muhsin ÇİFTÇİOĞLU
Head of Department
Izmir Institute of Technology

……

Assoc. Prof. Dr. Semahat Özdemir
Head of the Graduate School

ACKNOWLEDGEMENTS

I would like to express my gratitude to my advisor Assoc. Prof. Dr. Metin Tanoğlu and my co-advisor Assoc. Prof. Dr. Salih Okur for their invaluable advice, guidance, and encouragement. I would like to thank the Center for Materials Research staff at Izmir Institute of Technology for their help and patience during my study. I'd like to acknowledge The Scientific and Technical Research Council of Turkiye (TUBİTAK) for financial support to 104M365 project and Enercon A.Ş. (İzmir) for their support to my study.

I would also like to thank my friends Emrah Bozkurt, Kıvanç Işık and Levent Aydın for their encouragement, help and patience.

I am also grateful to my parents for their endless support during my thesis and all of my life.

ABSTRACT

DEVELOPMENT OF LAYERED SILICATE/EPOXY NANOCOMPOSITES

Layered silicate/polymer nanocomposites are materials that display rather unique properties, even at low silicate content, by comparison with more conventional particulate-filled polymers. These nanocomposites exhibit improved mechanical, thermal, optical, gas permeability resistance and fire retardancy properties when compared with the pure polymer.

In this study, layered silicate/polymer nanocomposites were prepared using Na^+ cation containing montmorillonite (MMT) and epoxy resins. Silicate particles were treated with hexadecyltrimethylammonium chloride (HTAC) to obtain the complete homogenous dispersion of the nano plaques within the polymer matrix which forms the exfoliated microstructure. In this way, organophilic silicates (OMMT) were obtained. Modification of the silicate expands the silicate galleries (from 14 Å to 18 Å) that promote the formation of exfoliated composite structure. SEM results showed that nanocomposites with organically modified MMT exhibited better dispersion than those with MMT. It was found that the tensile and flexural modulus values are increased, whereas the fracture toughness is decreased with increasing silicate content. Thermal analysis results revealed that the glass transition temperature (T_g) of the neat epoxy resin (63.6^{o}C) increases to 68.9 ^{o}C for the nanocomposites with 3 wt. % of OMMT. By incorporation of silicate particles, the dynamic mechanical properties of epoxy; including the storage and loss modulus and T_g are increased. Optical transmission values of the epoxy were affected by MMT and OMMT silicate incorporation. It was found that flame resistance at the polymer improved by the incorporation of MMT particles to the neat epoxy.

ÖZET

TABAKALI SİLİKA/EPOKSİ NANOKOMPOZİTLERİN GELİŞTİRİLMESİ

Tabakalı silika/epoksi nanokompozitler, geleneksel partikül içeren polimerlerle kıyaslandığında en düşük konsantrasyonlarda bile eşsiz özelliklere sahiptirler. Nanokompozitler, saf polimerlerle karşılaştırıldığında önemli derecede geliştirilmiş mekanik, ısıl, optik ve yanmazlık gibi özellikler sergilemektedir.

Bu çalışmada, tabakalı silika/polimer nanokompozitleri Na^+ katyonları içeren montmorillonite (MMT) ve epoksi reçine kullanılarak hazırlanmıştır. Silika partikülleri hexadecyltrimethylammonium chloride (HTAC) kullanılarak modifiye edilmiş ve polimer içerisinde homojen dağılmaya elverişli silika partikülleri (exfoliated) elde edilmiştir. Bu yöntemle, organik olarak modifiye edilmiş silikalar (OMMT) elde edilmiştir. X-ray ışını kırınımına göre modifiye edilmiş silikanın bazal boşluğu 14 Å' dan (saf silikanın değeri) 18 Å'a genişlemektedir, bu da silika tabakalarının epoksi reçine içinde tamamen dağılmış olduğunu göstermektedir. SEM sonuçları, organik olarak modifiye edilmiş OMMT içeren nanokompozitlerin MMT içerenlere göre daha iyi dağılım oluşturduğunu göstermektedir. Silika miktarının artmasıyla, çekme ve esneme modül değerleri artarken, kırılma tokluğu değeri azalmaktadır. Termal analiz sonuçları, camsı geçiş sıcaklığı (T_g), dolgusuz epoksi reçinede 63.6 ^oC iken organik olarak modifiye edilmiş, kütlece %3 silika içeren kompozitlerde 68.9 ^oC' ye yükselmekte olduğunu göstermektedir. Silika partiküllerinin eklenmesi ile epoksinin dinamik özellikleri, storage ve loss modulü ve T_g değeri artış göstermektedir. Epoksinin optik iletim değeri MMT ve OMMT partikül eklenmesiyle etkilenmektedir. Silika partiküllerinin epoksi reçineye eklenmesi ile yanmazlık direncinin arttığı gözlenmektedir.

TABLE OF CONTENTS

LIST OF FIGURES

LIST OF TABLES

CHAPTER 1

INTRODUCTION

There is a great demand to use of high-performance, low-weight materials, typically plastics to replace high density metals through practical synthesis and manufacturing technologies. The major drawback in engineering applications of polymers is the low stiffness, strength, thermal and flame retardancy behaviour as compared with metals. To overcome these deficiencies incorporation of particles or fibers to the polymer structures have been common way to the resin to form composite materials (Lee and Lichtenhan 1999). Nanocomposites are new class of materials that describe the combination of two phase materials that one of the phase is dispersed in the matrix on a nanometer scale (WEB_1 2000). Nanocomposites are generally based on polymer matrices such as nylon 6, polystyrene, polypropylene, epoxy, unsaturated polyester, and many others which are reinforced by inorganic particles (nanofiller) such as silica, silica-titanium oxides, carbon nanotubes and other particles.

The first known research was initiated to develop polymer based nanocomposites in Japan at Toyota Central Research and Development Labs to build a nanocomposite systems from nylon 6 and an organophilic silicate in 1988 (Subramaniyan and Sun 2006).

Nanocomposites have been widely used in diverse applications ranging from high barrier packaging for food and electronics (Ahmadi et al. 2004) to automotive and aerospace applications (Njuguna and Pielichowski 2003). Their improved mechanical and thermal properties, gas permeability resistance and fire retardancy is related to the microstructure achieved in processing these materials. Smectite silicates can be treated with onium type surfactants to exchange the sodium interlayer cations of the silicate with onium cation of the surfactant (Zanetti 2000). In this way, the silicate layers obtain organophilic characteristics that may lead to the complete homogenous dispersion of the nano plaques within the polymer matrix and obtain exfoliated microstructure (Nigam 2004). The exfoliated structure provides the desired enhancement of the thermal, mechanical, barrier and optical properties.

The aim of this study is to synthesis new nanocomposite materials composed of epoxy resin as the matrix and natural and organically modified montmorillonite (MMT)

as the filler. The second aim is to characterize the effects of content and silicate type on the structure and mechanical, thermal, optical and flame retardancy properties of the nanocomposites.

MMT is a special type of smectite silicate containing multiple layers that have 1nm thickness. Spacing between the silicate layers, which resemble a deck of card, can be increased so that they can be intercalated and separated from each other. MMT, kaolite, mica, and other type of silicates have been used for nanocomposite production so far. In the present study, natural and organically modified montmorillonite was used.

Silicate particles were treated with hexadecyltrimethylammonium chloride (HTAC) to obtain exfoliated microstructure in which homogenous dispersion of the nano plaques within the polymer matrix forms. The interlayer spacing of the silicates with and without modification was measured by X-Ray Diffraction (XRD) techniques.

A great number of polymers have been already used to synthesize layered silicate/polymer nanocomposites. Epoxy resins have been one of the best matrix materials for many fiber composites due to their high dimensional stability and good mechanical properties. The reactants of epoxy systems have a suitable polarity in order to diffuse between the silicate layers and form exfoliated nanocomposites after polymerization (Lee and Neville 1957). A diglycidyl ether of bisphenol A type epoxy system was used as the matrix in this study.

Silicate/polymer nanocomposites were processed through in-situ polymerization by blending 0-10 wt. % of the silicate particulates with the epoxy resin after ultrasonication.

Microstructure-property relation within the developed nanosystems was investigated at a fundamental level based on X-ray diffraction (XRD), scanning electron microscopy (SEM) and mechanical testing techniques. XRD was used to evaluate the exfoliation of the silicate particles within the matrix. The distribution of layered silicates was also evaluated based on the fracture surface SEM images of the sample after tensile test. Optical microscopy coupled with image analyzer software was used to determine the void content of the nanocomposites. The tensile, flexural, and fracture toughness tests were performed to characterize the mechanical properties of the nanocomposites in terms of strength, modulus, failure strength, elongation at break, and fracture toughness values. Spherical and non-spherical semi-empirical models developed for layered filler incorporated structures were also used to compare the predicted values with the experimentally measured tensile modulus values of the nanocomposites. Optical

transparency of the materials was analyzed by UV and IR transmittance spectroscopy. As a thermal property, glass transition temperature (T_g) of the nanocomposites was determined by differential scanning calorimeter (DSC). Burning rate of materials was measured using the UL-94 horizontal burning method. The effect of particle addition on t he optical, thermal, and flame retardant properties of the composite was also investigated.

CHAPTER 2

NANOCOMPOSITES

Nanocomposites are new class of materials that describe the combination of two phase materials that one of the phase is dispersed in the matrix on a nanometer scale. Dispersion of particles with nanometer sizes within the matrix provides improved mechanical, thermal and barrier properties and fire retardancy.

The nanocomposites have been already used widely in the various applications such as engine cover, timing belt cover, oil reservoir tank and fuel hose in automobile industries, floor adjuster and handrail in the construction fields and various connectors in the electrical fields (Ahmadi et al. 2004). The increased mechanical properties and dimensional stability makes the nanocomposites suitable to be used as high value construction materials. They are highly stable against aggressive chemicals, so they can also be carried out in corrosive protective coatings (Chang et al. 2004). Due to the decreased permeability for gases and water, as well as for hydrocarbons, they have a wide range of applications in packaging and automotive industries. In high temperature areas, such as internal combustion engines, nanocomposites are more attractive than other conventional materials because of good thermal stability, flame retardancy (Ahmadi et al. 2004).

These materials have a good perspective of application for the near future in daily life. Through the nano-silicate reinforcement, a new dimension in the polymer technology is expected.

Beneficial properties that fillers can give to a compound or composite are mainly:

· Increased modulus.

· Increased useful temperature range due to the higher modulus at high temperatures (increased heat distortion temperature (HDT)).

· Better dimensional stability, because of the reduced shrinkage upon crystallization, and the reduced thermal expansion.

· Reduced flammability.

· Sometimes increased toughness, in certain combinations of filler and polymer.

2.1. Structure and Properties of Layered Silicates

Silicate consists of small crystalline particles made up of aluminosilicates of various compositions, with possible iron and magnesium substitutions by alkalis and alkaline earth elements. The basic silicon-oxygen unit is a tetrahedron, with four oxygen atoms surrounding the central silicon. The tetrahedra are linked to form hexagonal rings. This pattern repeats in two dimensions to form a sheet. Aluminum, in combination with oxygen, forms an octahedron, with the aluminum at the center, and the octahedral link to form a more closely packed two-dimensional sheet as shown in Figure 2.1.

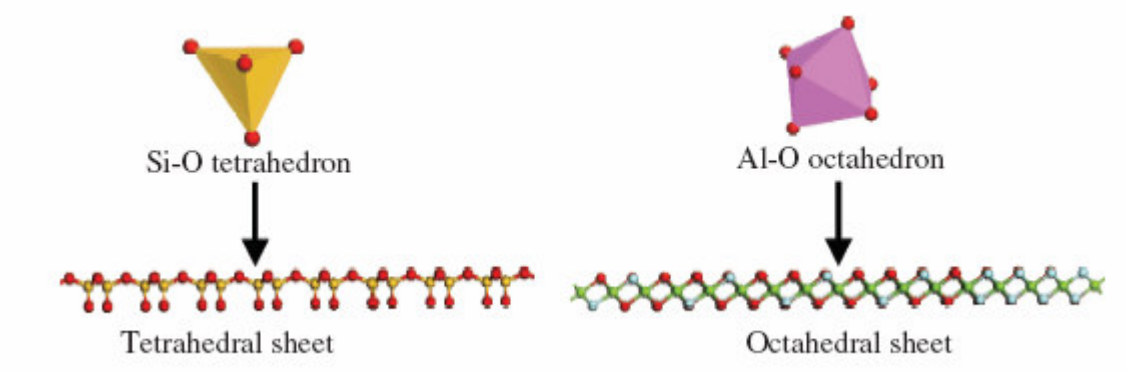

Figure 2.1. Structure of tetrahedral and octahedral sheets
(Source: Zeng et al. 2005)

There are two basic types of silicate structures (1: 1 and 2: 1) as seen in Table 2.1. Kaolinite is an example of 1:1 type of non-swelling dioctahedral silicate. In 2:1 layered silicates two tetrahedral layers surround one octahedral layer, and the oxygen atoms are shared, as an example in montmorillonite. Structures of montmorillonite and kaolinite are shown in Figure 2.2. Isomorphic substitution of Al with Mg, Fe, Li in the octahedron sheets and/or Si with Al in tetrahedron sheets gives each three-sheet layer an overall negative charge, which is counterbalanced by exchangeable metal cations residing in the interlayer space, such as Na, Ca, Mg, Fe, and Li (Qutubuddin and Fu 2001). In 1:1 layered structures a tetrahedral sheet is fused with one octahedral sheet, in which the oxygen atoms are shared. Each layer bears no charge due to the absence of isomorphic substitution in either octahedron or tetrahedron sheet. Thus, except for water molecules

neither cations nor anions occupy the space between the layers, and the layers are held together by hydrogen bonding between hydroxyl groups in the octahedral sheets and oxygen in the tetrahedral sheets of the adjacent layers (Zeng et al. 2005).

Table 2.1. Silicate minerals used for polymer nanocomposites
(Source: Zeng et al. 2005)

Type of silicate	Formula	Origin	Substitution	Layer Charge
2:1 type				
MMT	$Mx(Al_{2-x}Mg_x)Si_4O_{10}(OH)_2 \cdot nH_2O$	N	Octahedral	Negative
Hectorite	$Mx(Mg_{3-x}Li_x)Si_4O_{10}(OH)_2 \cdot nH_2O$	N	Octahedral	Negative
Saponite	$MxMg_3(Si_{4-x}Al_x)O_{10}(OH)_2 \cdot nH_2O$	N	Tetrahedral	Negative
Fluorohectorite	$Mx(Mg_{3-x}Li_x)Si_4O_{10}F_2 \cdot nH_2O$	S	Octahedral	Negative
Laponite	$Mx(Mg_{3-x}Li_x)Si_4O_{10}(OH)_2 \cdot nH_2O$	S	Octahedral	Negative
Fluoromica	$NaMg_{2.5}Si_4O_{10}F_2$	S	Octahedral	Negative
1:1 type				
Kaolinite	$Al_2Si_2O_5(OH)_4$	N	—	Neutral
Halloysite	$Al_2Si_2O_5(OH)_4 \cdot 2H_2O$	N	—	Neutral

M indicates exchangeable ions represented by monovalent ions. Symbols: N (nature) and S (synthetic).

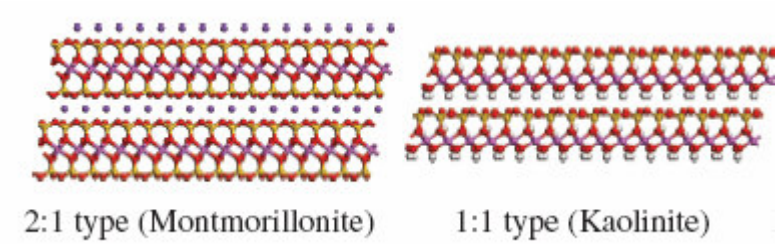

Figure 2.2 Structure of silicate minerals represented by montmorillonite and kaolinite
(Source: Zeng et al. 2005)

Silicates used in preparing layered silicate/polymer nanocomposites belong to the 2:1 layered structure type. Montmorillonite (MMT) is one of the most interesting and widely investigated silicates belong to the family of 2:1 layered silicates for polymer nanocomposites because of the weak bonding (Van der Waals) between layers. The chemical formula of MMT silicate is as follows:

$$Na_{0.33}\,(Al_{1.67}Mg_{0.33})\,Si_4O_{10}\,(OH)_2\,nH_2O \qquad (1.1)$$

The crystal structure of montmorillonite consists of two silica tetrahedra fused to an edge shared octahedral sheet of either alumina or magnesia as shown in Figure 2.3. Each layer is composed of a sheet of aluminum or magnesium octahedra sandwiched between two sheets of SiO_4 tetrahedra, which has a unit cell structure consisting of 20 oxygen atoms and 4 OH groups (Zanetti et al. 2000). These layers are continuous in the a and b directions and are stacked one above the other in the c direction. These layers have a stiffness of approximately 170 GPa (25 Msi), and have aspect ratios in the range of 100–1500. Each layer is approximately 1 nm thick, while the diameter may vary from 30 nm to several microns or larger. This provides a large surface area; approximately 700-800 m^2 per gram of silicate material. The silicate layers have a specific gravity of 2.5. The layer spacing (d-spacing) prior to processing with a polymer is 1.2 nm (Luo and Daniel 2003).

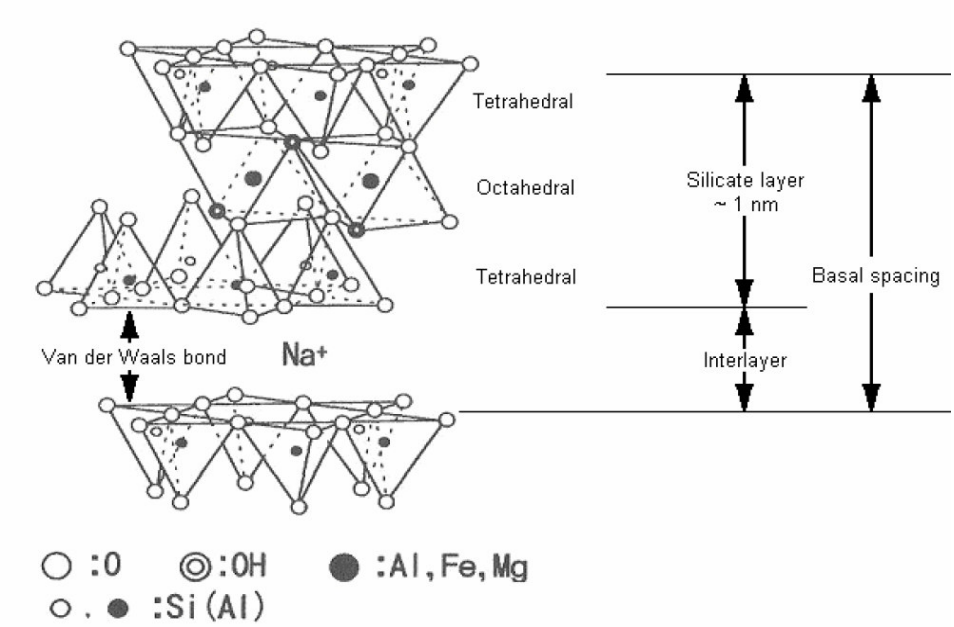

Figure 2.3. Schematic illustration of atomic arrangement in a typical MMT layer (Source: Qutubuddin and Fu 2001)

Hundreds or thousands of these layers are stacked together with weak Van der Waals forces to form a silicate particle. Isomorphic substitution within the layers (for example, Al^{3+} replaced by Mg^{2+} or by Fe^{2+}, or Mg^{2+} replaced by Li^{+}) generates excess negative charges, naturally balanced by exchangeable inorganic cations. The polar Si-O groups at the montmorillonite surface impart hydrophilic nature and these results in

affinity of montmorillonite to polar molecules (Ray and Okamoto 2003). Silicate is needed to be organophilic in order to disperse then in monomer phase. Before polymerization, silicate should become organophilic by treatment with suitable modifiers.

2.2. Structure and Properties of Organically Modified Layered Silicates

Montmorillonite is the most common type of layered silicates used in polymer nanocomposites due to its swellable layered structure. However, the charged nature of the silicate sheets in the silicate makes the silicate sheets incompatible with hydrophobic polymers. The lack of affinity between hydrophilic silicate and hydrophobic polymer tends to agglomeration of the mineral within the polymer matrix. Also, the interfacial interactions in the agglomerated morphology grow the problems at the interface (Thostenson et al. 2004). In this case, pre-treatment of the silicate is necessary. Pristine layered silicates (MMT) usually contain hydrated Na^+ or K^+ cations. They can be replaced trough on ion exchange reaction with cationic surfactants, including amino acids, organic ammonium salts, or tetra organic phosphoniums to render the normally hydrophilic silicate surfaces as organophilic (Gao 2004). This reaction is illustrated schematically in Figure 2.4. The most popular cationic surfactant is alkylammonium ion because it can be easily exchanged with the ions situated between the silicate layers. Depending on the layer charge density of the silicate, the alkylammonium ions adopt different structures between the silicate layers. The modified silicate becomes organophilic known as organosilicates (OMMT) and it becomes more compatible with organic polymers. By this way, polymer molecules may be able to intercalate within the galleries. The role of alkylammonium cations in the organosilicate is to lower the surface energy of the inorganic host and improve its wetting characteristics with the polymer. The purpose of the pre-treatment is to increase the interlayer spacing as well as to provide better compatibility with polymer. Swelling of the silicate galleries is called intercalation. The basal spacing can be changed depending on the nature of the exchanged cations and/or the size of the organic molecule (Fischer 2003).

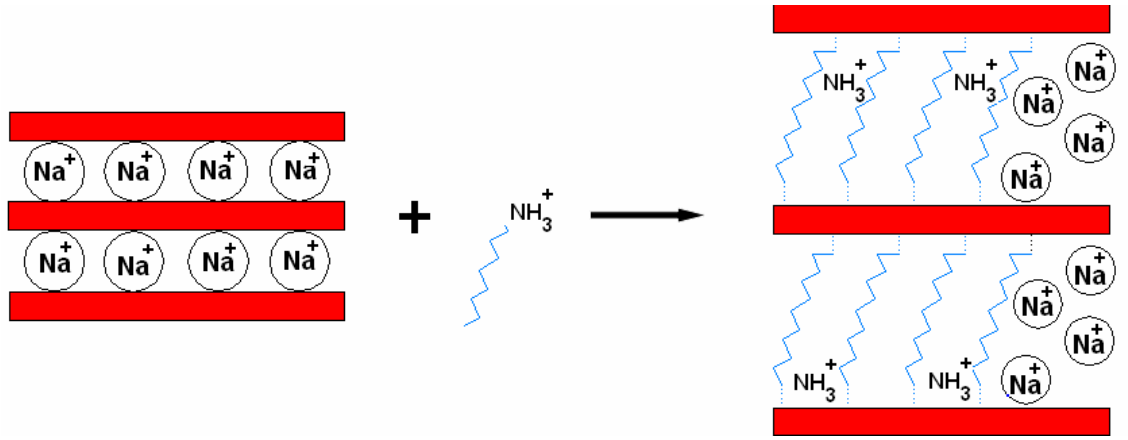

Figure 2.4. Modification of clay surfaces through ion exchange reaction by replacing the Na^+ cations with cationic surfactant

For a given silicate, the number of maximum exchangeable interlayer cations is known as the cation-exchange capacity (CEC) and it is usually described in milliequivalents per gram (meq/g) or more frequently milliequivalents per 100 g (meq/100g). CEC of MMT varies from 80 to 150 meq/100 g (Tolle and Anderson 2002).

The exchange of inorganic cations by organic surfactant ions in the silicate galleries not only makes the organosilicate surface compatible with monomer or polymer matrix, but also decreases the interlayer cohesive energy by expanding the d-spacing. The orientation of the surfactant in the galleries depends on its chemical structure, the cation-exchange capacity and the charge density of the silicate (Ajayan et al. 2003). This means that the length of the surfactant chain determines the distance between the layers. The adsorbed organic cations in swelling silicates (e.g. montmorillonite) may adopt several configurations in the interlayers. Some possible configurations, such as flat monolayer, bilayer, pseudo-trilayer, and inclined paraffin structure, are shown in Figure 2.5. At lower charge densities, the surfactant packs in monolayers and as the charge density increases, bilayers and trilayers can form. At very high CECs (≥120 mEq/100 g) and long surfactants (>15 carbons), the packing can be ordered in a paraffin-type structure (Qutubuddin and Fu 2001).

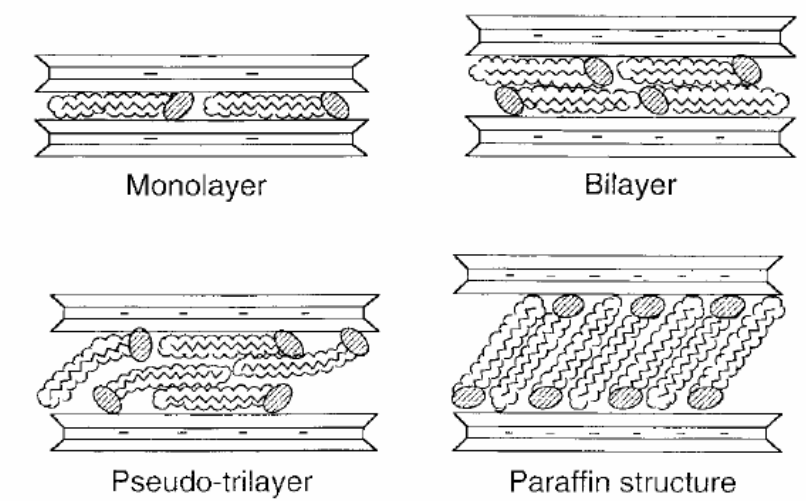

Figure 2.5. Schematic of the orientation of alkylammonium ions in the galleries of layered silicates with different layer charge densities (Source: Qutubuddin and Fu 2001).

2.3. Microstructure of Nanocomposites

The silicate particles or their layers (silicates, etc.) are incorporated into a polymer matrix to form an organic/inorganic composite. When layered silicates organically modified and dispersed within a polymer, the spacing expands to allow for the intercalation of polymer between the unit layers.

Three main types of composite morphology may be obtained when layered silicate is associated with a polymer. These primarily depend on the method of preparation and the nature of components used (Giannelis 1998).

1. Phase Separated Composites: Layered silicates exist in their original aggregated state with no intercalation of the polymer matrix into the galleries (Figure 2.6a). In this case, the particles act as microscale fillers. Their properties stay in the same range as seen in traditional microcomposites (Ray and M. Okamoto 2003).

2. Intercalated Composites: When polymer resin is inserted into the gallery between the adjacent layers, the spacing expands, and it is known as the intercalated state as shown in Figure 2.6b. In the intercalated form, matrix polymer molecules are introduced between the ordered layers of silicate resulting in an increase in the interlayer

spacing, but still maintaining the order. Intercalated nanocomposites are generally formed by melt blending or by in situ polymerization (Jordan 2004).

3. Exfoliated Composites: In an exfoliated nanocomposites, the individual nm scale thick silicate layers are separated and dispersed in a continuous polymer matrix with average distances between layers depending on the silicate concentration (Figure 2.6c). When the layers are fully separated, the silicate is considered to be exfoliated (Luo and Daniel 2003, Thostenson et al. 2004). Exfoliation ability depends on the nature of silicate, blending process, and the agents used for curing. Exfoliated nanocomposites improve specific properties better than intercalated one, that are affected by the degree of dispersion and resulting interfacial area between polymer and silicate nanolayers.

In addition, **Partially Intercalated or Exfoliated Composite** morphology may also be obtained. In this commonly occurring case, the exfoliated layers and intercalated clusters are randomly distributed in the matrix. The final structure of silicate composite has a wide range of variations, depending on the degree of intercalation and exfoliation.

X-ray diffraction measurements are used to characterize the intercalation and exfoliation structures (Gilman 1999). Reflections in the low angle region indicate intercalated composite, but if the peaks are extremely broad or disappear completely, this indicates complete exfoliation.

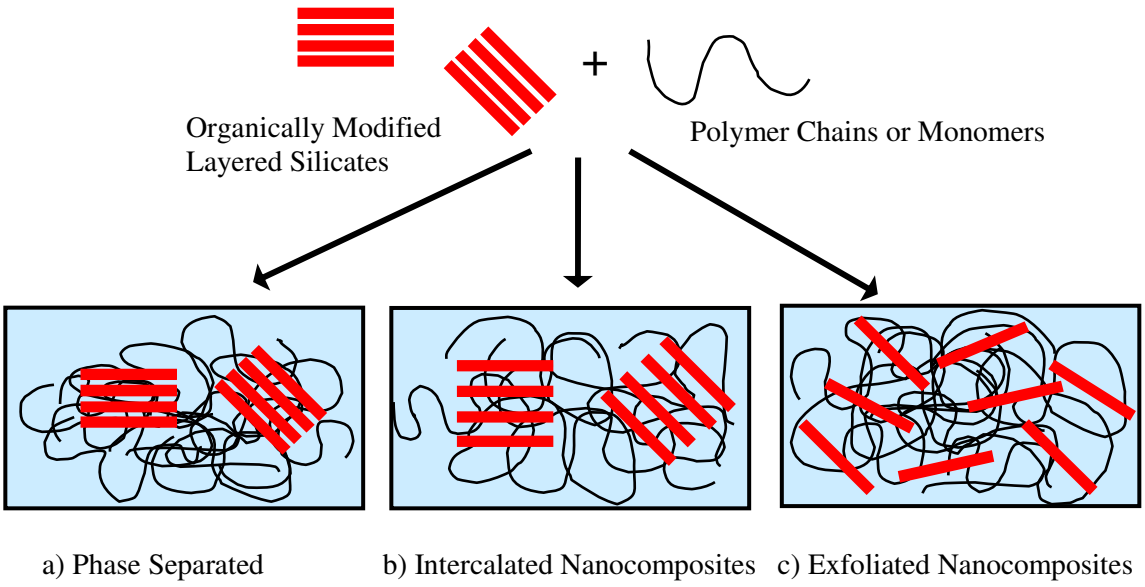

Figure 2.6. Different morphology of layered silicate/polymer nanocomposites

2.4. Synthesis of Nanocomposites

There are four general approaches for the synthesis of layered silicate/polymer nanocomposites as listed below. Each polymer system requires a special set of processing conditions to be formed, based on the processing efficiency and desired product properties as seen in Table 2.2.

- Solution Approach
- In-situ Polymerization
- Melt Intercalation
- Sol-gel Technology

Table 2.2. Processing techniques for layered silicate/polymer nanocomposites (Source: Zeng et al. 2005)

Processing	Drive Force	Advantages	Disadvantages	Examples
In-situ polymerization	Interaction strength between monomer and silicate surface: enthalpy evolvement during the interlayer polymerization.	Suitable for low or non-soluble polymers: a conventional process for thermoset nanocomposites.	Silicate exfoliation depends on the extent of silicate swelling and diffusion rate of monomers in the gallery: oligomer may be formed upon incompletely polymerization.	Nylon 6, epoxy, polyurethan, polystyrene, polyethylene oxide, unsaturated polyesters, polyethylene terephthalate.
Solution approach	Entropy gained by desorption of solvent, which compensates for the decrease in conformational entropy of intercalated polymers.	Prefer to water-soluble polymers.	Compatible polymer-silicate solvent system is not always available; use of large quantities of solvent; co-intercalation may occur for solvent and polymer	Epoxy, polyimide, polyethylene, polymethylm ethacrylate
Melt Intercalation	Enthalpic contribution of the polymer-organosilicate interactions.	Environmental benign approach: no solvent is required.	Slow penetration of polymer within the confined gallery.	Nylon 6, polystyrene, polyethylene terephthalate.

2.4.1 Solution Approach:

This is based on a solvent system in which the polymer or pre-polymer is soluble and the silicate layers are swellable. The layered silicate is first swollen in a solvent, such as water, chloroform, or toluene. When the polymer and layered silicate solutions are mixed, the polymer chains intercalate and displace the solvent within the interlayer of the silicate. Upon solvent removal, the intercalated structure remains, resulting in layered silicate/polymer nanocomposite, as shown in Figure 2.7 (Ray and Okamoto 2003).

This approach have several difficulties for the commercial production of nanocomposites for most engineering polymers because of the high costs of the solvents required and the phase separation of the synthesized products from those solvents. There are also health and safety concerns associated with the application of this technology (Gao 2004).

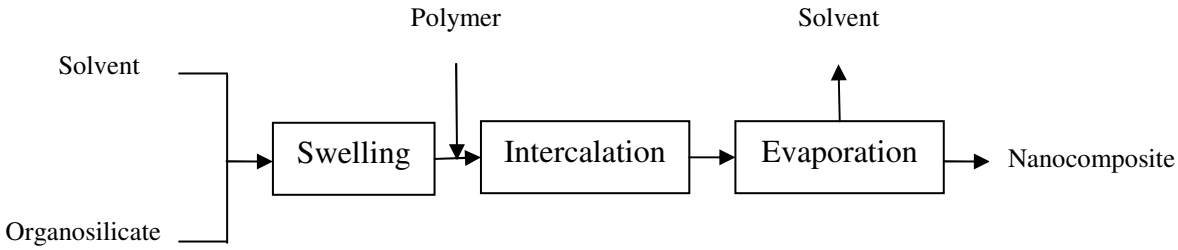

Figure 2.7. Flowchart of solution approach to synthesis nanocomposites

2.4.2. In-situ Polymerization Method

The in situ polymerization approach was the first strategy used to synthesize polymer-silicate nanocomposites and it is a convenient method for layered silicate/thermoset nanocomposites. This method is capable of producing well-exfoliated nanocomposites and has been applied to a wide range of polymer systems (Gao 2004). Once the organosilicate has been swollen in the liquid monomer or a monomer solution, the curing agent is added to the system, as shown in Figure 2.8. Upon polymerization, the silicate nanolayers are forced apart and no longer interact through the surfactant chains. Thus, highly exfoliated nanocomposites are formed (Ahmadi 2004).

There are advantages of utilizing the in situ polymerization technology with respect to the other methods (Avella 2001). It is a direct and easier dispersion of the nanoparticles into the liquid precursor of the polymeric matrix, avoiding the agglomeration of nanopowders in polymer matrices and improving the interfacial interactions between the two components. This method has the possibility of using less-expensive nanoparticles and conventional polymer processing technologies.

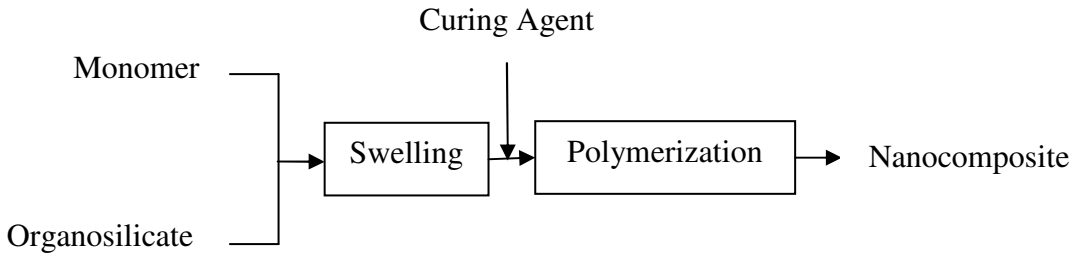

Figure 2.8. Flowchart of in-situ polymerization method to prepare nanocomposite

2.4.3. Melt Intercalation Method

In this technique, thermoplastic polymer is mechanically mixed with organophilic silicate above the glass transition or melting temperature, as shown in Figure 2.9. The polymer chains are then intercalated between the individual layers of the silicate. Silicate/Nylon-6 and silicate/polypropylene nanocomposites are the examples prepared via this approach (Ma et al. 2004).

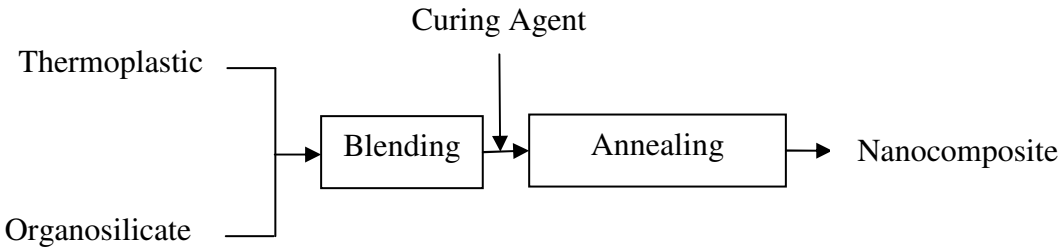

Figure 2.9. Flowchart of melt intercalation method to synthesis nanocomposite

2.4.4. Sol-gel technology

It consists in a direct crystallization of the silicates by hydrothermal treatment of a gel containing organics and organometallics, including polymer. As the precursor for the silicate silica sol, magnesium hydroxide sol and lithium fluoride are used. This method has the potential of promoting the high dispersion of the silicate layers in a one-step process, without the presence of the onium ions (Zanetti 2000).

2.5 Properties of Layered Silicate/Polymer Nanocomposites

Due to the nanometer-scale dimensions and the high aspect ratios of exfoliated silicate layers, nanocomposites show different properties as compared to traditional filled polymers. The high aspect ratio of layered silicates fillers results in a more effective modulus increase and the small dimensions of the particles lead to much larger interfacial areas than those in traditional microcomposites. In addition, improvements are obtained without the increase of polymer density and the loss of its optical properties at low particulate concentrations. For example, polymer nanocomposites containing 1–8 wt. % of silicate demonstrated great increase in mechanical properties (tensile stress-strain behavior) together with the thermal (dimensional) stability (Ratna et al. 2003). They also reduce the gas and liquid permeability and improve the flame retardancy while retaining optical clarity of pure polymers.

2.5.1. Effect of Layered Silicates on the Mechanical Properties of Nanocomposites

The enhancement in mechanical properties of polymer nanocomposites can be attributed to the high rigidity and aspect ratio together with the good affinity between polymer and organosilicate. The mechanical properties of silicate/nylon-6 nanocomposite synthesized by in-situ polymerization were first demonstrated by researchers at the Toyota Central Research Laboratories (Gao 2004). Such nanocomposites exhibit significant improvement in strength and modulus, namely, 40% in tensile strength, 60% in flexural strength, 68% in tensile modulus, and 126% in flexural modulus. The increase

in modulus is believed to be directly related to the high aspect ratio of silicate layers as well as the ultimate nanostructure.

Modulus improvement was also demonstrated in thermoplastic polymers such as polypropylene. Polypropylene nanocomposites were obtained by melt intercalation with organophilic silicate using maleic anhydride-modified PP oligomer (PP-MA) as a compatibilizer (Hasegawa 1998). The modulus of a silicate/PP hybrid with 5 wt. % of silicate and 22 wt. % PP-MA was 1.8 times higher than that of PP at 80°C. It was also shown that increasing the amount of PP-MA up to same concentrations improved intercalation and partial exfoliation, thus increased the tensile modulus.

Moreover, a dramatically increase in tensile modulus with increased silicate loading was also observed in exfoliated nanostructures such as MMT based thermoset amine-cured epoxy nanocomposite. The enhancement in modulus comes with reductions in both ultimate stress and strain at break, resulting in a loss of ductility. The strain at break was almost 50 % of the unmodified material at a silicate concentration of only 1.5 wt. %. At the highest concentrations, a decrease of over 75 % was observed in strain at break values as shown in Figure 2.10 (Zerda and Lesser 2001).

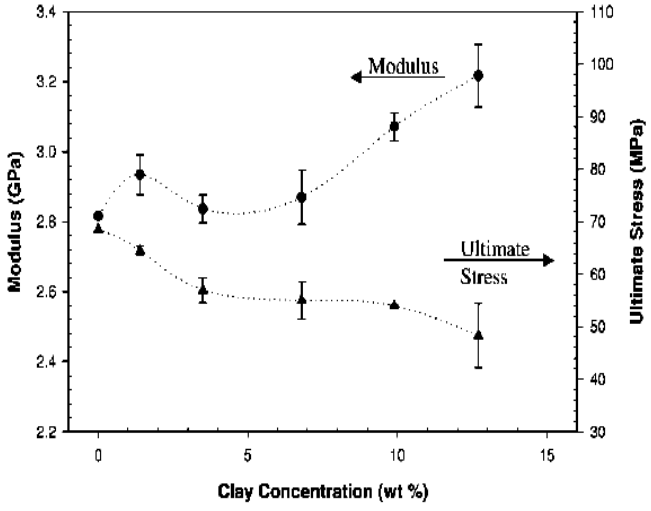

Figure 2.10. Tensile mechanical behavior of layered silicate /epoxy intercalated nanocomposites (Source: Zerda and Lesser 2001).

Isık et al. (Isık et al. 2003) investigated the nanocomposites of layered silicate/ epoxy prepared by in-situ intercalation method. The epoxy resin was diglycidyl ether of bisphenol A (DGEBA), Araldite M. It was cured with an aliphatic amine curing agent,

triethylenetetramine, Cloisite 30B was used as organically treated MMT silicate. The effect of silicate loading on the tensile properties of nanocomposites was investigated. As a result, it was observed that tensile strength decreased with increasing amount of MMT. This behaviour was explained as the higher stress concentration effect of silicate agglomerates at high silicate contents. Nanoexfoliated silicate particles formed larger agglomerates, and thus silicate-polymer surface interactions decreases as the silicate content increases resulting in lower tensile strength. The authors also concluded that the tensile modulus of the nanocomposite increased with increasing amount of MMT. The modulus of a composite depends on the ratio of filler modulus to matrix material modulus. Since MMT has a higher modulus than the polymeric matrix, the modulus increases with silicate content.

Also, Lin et al. (Lin et al. 2005) examined the effect of exfoliated nanoparticles on the mechanical properties of epoxy matrix. Two types of nanoparticles were applied into the epoxy matrix. Organically treated Na-montmorillonite (cloisite-30B) and inorganically treated titanium dioxide were used as the fillers. The epoxy matrix was used and it was cured by a polyamine hardener. As a result it was observed that the tensile strength for cloisite-30B composite decreased generally when the filler content is beyond 5 vol. %. This behavior was explained as that there was a lower degree of nanoparticle-polymer interaction at higher filler contents. This was attributed to interfacial debonding during tensile testing and thus reducing the tensile strength.

Similarly, the mechanical behaviour of the similar system was investigated by Zhang et al. (Zhang 2004). The silicate-epoxy nanocomposites were prepared by the dispersion of an organically modified Na-MMT (Cloisite-30B) in the epoxy resin (diglycidyl ether of bisphenol A). Nanocomposites were cured in the presence of methyl tetrahydro acid anhydride. When the silicate content was 3 wt%, the tensile strength of the nanocomposite was enhanced by 20.9 % (from 41.60 to 50.28 MPa) in comparison with the pristine epoxy resin.

Also, Chen and Yang (Chen and Yang 2004) studied the synthesis of epoxy-montmorillonite nanocomposites. Organically modified Na–montmorillonite with an exchange capacity of 125 mequiv/100 g and diglycidyl ether of bisphenol A (DGEBA, epoxide equivalent weight 178) was used in their study. As a result, it was observed that epoxy with modified silicate resulted in a decrease of tensile strength. This was related with that the interactions between the epoxy and the silicate surface were very weak.

Nigam et al. (Nigam et al. 2004) examined the nanocomposites of epoxy resin with montmorillonite K-10 silicate that were synthesized by swelling of different proportions of the silicates in a diglycidyl ether of bisphenol-A followed by in situ polymerization with aromatic diamine as a curing agent. The changes of the various mechanical properties of the composites with an increasing loading of the organosilicate were investigated. It was observed that a rise in the organosilicate concentration from 0 to 6% leads to 100% increased in the tensile modulus, 20% increased in ultimate tensile strength, and 80% decreased in elongation at break values. Also, comparison of inorganic and organosilicate composites for varied mechanical properties was studied and as a result it was observed that the organosilicate composite showed better mechanical properties than the inorganic one.

Similarly, Myskova et al. (Myskova 2003) investigated the influence of the modified silicate on the mechanical properties of epoxy matrix. A commercially produced epoxy resin based on Bisphenol A was mixed with different amounts of montmorillonite silicate modified with octadecyl amine. This system was cured by Jeffamine D 400 (amine-terminated polypropylene oxide). The tensile properties of systems with different silicate concentrations were investigated. The study was concluded as that the addition of silicate to the epoxy matrix increased the ultimate properties of the composite in tension. The breaking elongation increased more then five times in the silicate concentrations in the range of 0-10%. Also, Young's modulus increased by the incorporation of silicate.

Velmurugan and Mohan (Velmurugan et al. 2004) processed the nanocomposites of epoxy resin system DGEBA with garamite as a nanoparticle using triethyl tetra amine (TETA) curing agent. This silicate was alkyl quaternary ammonium silicate. The variation of elastic modulus with organosilicate and unmodified silicate content was investigated. It was observed that the modulus of the nanocomposites increased continuously with increasing silicate content. In unmodified silicate/ epoxy composite, there was not much improvement in the elastic modulus which indicated that the distribution of silicate in the molecular level was absent and hence did not contribute to the molecular strength. An improvement in modulus of about three times was observed with an addition of 10 wt% of organosilicate. The improvement of elastic modulus was explained as that it was due to the exfoliation/intercalation of nanoscale silicate particles in the matrix that restricts the mobility of polymer chains under loading and good interfacial adhesion between the particles and the epoxy matrix. The experimental results

showed that the tensile strength for all the silicate contents was less than that of pure epoxy. It was explained that it requires further investigation of the processing technique to understand the reduction in strength of the nanocomposites.

Silicate/epoxy nanocomposites have been further studied by Ranta et al. (Ranta et al. 2003) by in-situ polymerization method using an diglycidyl ether of bisphenol A (DGEBA) epoxy and commercial treated silicate I.30E which contains octadecylammonium organo-ions lining the surface of the galleries. Flexural properties (strength, modulus and strain) of the composites were investigated. The reinforcing effect of the silicate layers are reflected in higher flexural strength and modulus as compared to the neat epoxy. Nanocomposite containing 5 wt. % OMMT increased the flexural strength from 112 MPa to 146 MPa. Also, 42 % improvement was observed on the flexural modulus by the incorparation of 5 wt. % OMMT.

Silicate/epoxy nanocomposites were studied by swelling an organophilic montmorillonite in a diglycidyl ether of bisphenol A resin (Kornmann et al. 2001). Two different curing agents were used: an aliphatic diamine (Jeffamine D-230) and cycloaliphatic diamine (3, 3'-dimethylmethylenedi- (cyclohexylamine) (3DCM)). Polymer and nanocomposite samples were tested using the three-point bending testing to examine flexural properties of nanocomposites. The fexural modulus of the epoxy systems cured with Jeffamine D-230 and 3DCM without silicate additions were, 2.95 and 2.61 GPa, respectively. For both systems, the fexural modulus increased substantially with the silicate content, despite the small amounts of silicate added. Indeed, for the nanocomposite cured with Jeffamine D-230, the modulus was increased by 43% with only 4.2 vol% of silicate. The synthesis of an exfoliated nanocomposite structure allows the silicate layers to more efficiently swell in the epoxy matrix leading to better dispersion and larger stiffness improvement. The relative increase in flexural modulus was larger for the nanocomposite cured with Jeffamine D-230 than for the one cured with 3DCM. The degree of exfoliation of the silicate in the epoxy matrix was proportional to an increase of modulus of the nanocomposite. It was observed by TEM that a higher degree of exfoliation of the silicate was achieved with an epoxy cured with Jeffamine D-230 as compared with one cured with 3DCM.

The effect of the organosilicate nanoparticles on the flexural properties for organosilicate /epoxy nanocomposites has been studied by Dean et al. (Dean et al. 2005). Epon 828 Epoxy resin, Cloisite 30-B, montmorillonite silicate organically modified with a ternary ammonium salt and Epicure W curing agent were used. As the silicate loading

increased, the modulus increased by 35, 15, and 30% for the 2, 4, 6 wt. % OMMT incorporated epoxy, respectively. The strength values showed a decrease with silicate loading. This behaviour was explained as that variations in crosslink topology as well as homopolymerization may give rise to plastization and hence lower strength.

Organosilicate-modified high performance epoxy nanocomposites were studied by Liu (Liu 2005) and synthesized with a direct-mixing method (DMM) or a high-pressure mixing method (HPMM). As unmodified silicate, Cloisite Na+, a natural montmorillonite and as an organosilicate, Nanomer I.30E was an octadeyl amine modified montmorillonite were used. The epoxy resin was tetraglycidyl-4,4'-diaminodiphenylmethane (TGDDM) and the hardener was 4,4'-diaminodiphenyl sulphone. Fracture toughness of the specimens was measured using the single edge notch bending (SENB) technique. The nanocomposites made with the DMM showed a higher increase in K_{ic} than the composites prepared with inorganic silicate. DMM shows 80% increase in K_{ic} of epoxy by incorporation of 12 phr organosilicate, however only 45% improvement is observed by inorganic silicate loading at the same concentration. The nanocomposite made with the HPMM showed dramatic improvement in fracture toughness at very low silicate loading; that was, K_{ic} was increased by 1.89 times respectively, at only 1.5 phr (about 1 wt%) organosilicate loading. However, fracture toughness of the nanocomposite at 3 phr loading was decreased because high void contents were observed in the samples.

High performance layered silicate/epoxy nanocomposites based on tetra-glycidyl 4,4'-diamino-diphenyl methane (TGDDM) resin cured with 4.4-diaminodiphemyl sulfone (DDS) have been investigated (Kornman et al. 2002). Fluorohectorites modified by means of interlayer cation exchange of sodium cations for protonated dihydro-imidazolines and octadecylamine were used. The conventional composite based on MMT showed a lower increase in fracture toughness and fracture energy with silicate addition than the nanocomposites. The reason for this difference was related to apparent lower crosslink density of the epoxy matrix in the nanocomposites. Indeed, lowering the crosslink density of the epoxy may favour yielding in the matrix, which is known to improve toughness properties. However, it was also possible that the increase of effective particle volume fraction in the nanocomposites was responsible for the part of the fracture property improvement.

2.5.2. Effect of Layered Silicates on the Thermal Properties of Nanocomposites

The thermal stability of polymer composites is generally estimated from the weight loss upon heating which results in the formation of volatile products. The improved thermal stability in polymer nanocomposites is due to the silicate platelets which hinder the diffusion of volatiles and assist the formation of char after thermal decomposition. Velmurugan and Mohan reported a thermal stability improvement in epoxy nanocomposites, such that intercalated epoxy containing 10 wt. % OMMT silicate degraded at temperature which is about 60 °C higher than those for unfilled epoxy system (Velmurugan and Mohan 2004).

Thermal characterization of the nanocomposite materials investigated by differential scanning calorimetery (DSC) also implies evidence of enhanced thermal stabilities due to the presence of nanoparticles. The variation of glass transition temperature of the polymethylmethacrylate (PMMA) in the presence of $CaCO_3$ nanoparticles was investigated using DSC (Avella et al. 2001). The DSC results given in Table 2.3 show that the presence of nanoparticles shifts the T_g values to higher levels with respect to the neat polymer.

Table 2.3 Variation of glass transition temperature of PMMA based nanocomposites (Source: Avella et al. 2001)

Samples	T_g (°C)
PMMA	90
PMMA + 2% $CaCO_3$	120
PMMA + 3% $CaCO_3$	124
PMMA + 4% $CaCO_3$	127
PMMA + 6% $CaCO_3$	125

Chen and Yang examined the T_g of the organosilicate/epoxy nanocomposite using DSC. As shown in Figure 2.11, the epoxy polymer without the addition of silicate shows the T_g at 108.4°C. The addition of montmorillonite during the polymerization of the epoxy polymer decreased the T_g to 92.5°C. The epoxy resins polymerized in the presence

of 5 and 20 phr of organically modified montmorillonite silicate show higher T_g's at 117.4 and 146.1°C (Chen and Yang 2002).

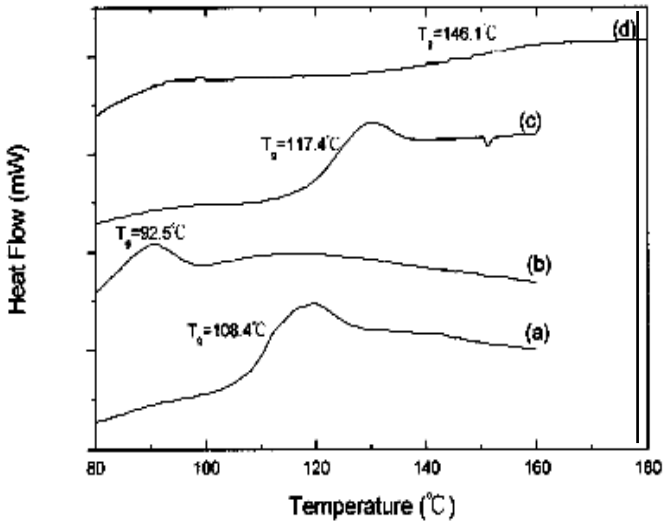

Figure 2.11. DSC thermograms of hybrids of silicate with (a) no silicate addition, (b) 20 % MMT, (c) 5 % OMMT, and (d) 20 % OMMT (Source: Chen and Yang 2002).

Isık et al. (Isik et al. 2003) also investigate the thermal properties of the nanocomposites of layered silicate/ epoxy prepared by in-situ intercalation method. The T_g of the nanocomposites was determined with DSC. Thermal characterization results indicated an increase in T_g with respect to montmorillonite contents. Nanocomposites having 3 wt% Cloisite 30B displayed higher T_g as compared the neat epoxy. This behaviour was explained as that the mobility of the polymer chains are reduced due to the interaction between the silicate and polymer molecules resulting in higher T_g.

Similarly, Nigam et al. (Nigam et al. 2004) processed the nanocomposites of epoxy resin with montmorillonite silicate synthesized by swelling of different proportions of the silicate in a diglycidyl ether of bisphenol A followed by in situ polymerization with aromatic diamine as a curing agent. The montmorillonite was modified with octadecylamine to obtain as organophilic. The results of the DSC experiments showed a gradual decrease of T_g with increasing concentration of silicate. Author related the decrease of T_g with the modification of the epoxy network by its homopolymerization within the silicate galleries. Indeed, if homopolymerization of the

epoxy is obtained between the layers, this caused a displacement of stoichiometry in the epoxy network so that the T_g is reduced. The excess of unreacted curing agent may also plasticize the epoxy network.

A commercial organosilicate with bis (2-hydroxylethyl) methyl tallow ammonium, modified by tolylene 2,4-diisocyanate and bisphenol A was studied by Feng (Feng et al. 2002). DSC tests were carried out on neat epoxy and organosilicate/epoxy composites to investigate the T_g values. The results showed that T_g increases with increasing the amount of organosilicate. This result was explained as that the layered silicates hindered the motion of molecules in the epoxy network at least in the vicinity of the silicate surface. It was also concluded that the layered silicates were dispersed and wetted relatively well in the epoxy matrix.

2.5.3. Effect of Layered Silicates on the Optical Transparency of Nanocomposites

Another significant property of the nanocomposites is their high optical transparency. Traditional composites tend to be largely opaque because of light scattering by the particles or fillers embedded within the continuous phase. In the nanocomposites, the sizes of the silicates are reduced to approximately 1nm thickness. Thus, when single layers are dispersed in a polymer matrix, the resulting nanocomposite is optically clear in visible light (Salahuddin 2004). Such as polyvinylacetate (PVA), various other polymers also showed optical transparency after nanocomposite preparation with organically modified silicate layers (Yano 1993).

Similarly, it was found by Deng et al. (Deng et al. 2003) who investigated the light transmission spectra of nanocomposites prepared by the reaction of alkylammonium-exchanged montmorillonite (AMT) with diglycidyl ether of bisphenol A (DGEBA) and triethylamine as the curing agent. The light transmission spectra of OMMT/ epoxy nanocomposites with different loadings were given as in Figure 2.12. As seen in the figures, OMMT loading affect the light transmittance of the nanocomposites. By increasing OMMT loading, the light transmittances in the whole wavelength range systematically decrease. This result was concluded as that when the number of silicate particles increases, the particle surface per unit volume increases, then the light extinction

resulting from the scattering at the interface of epoxy matrix and silicate particles is also increases.

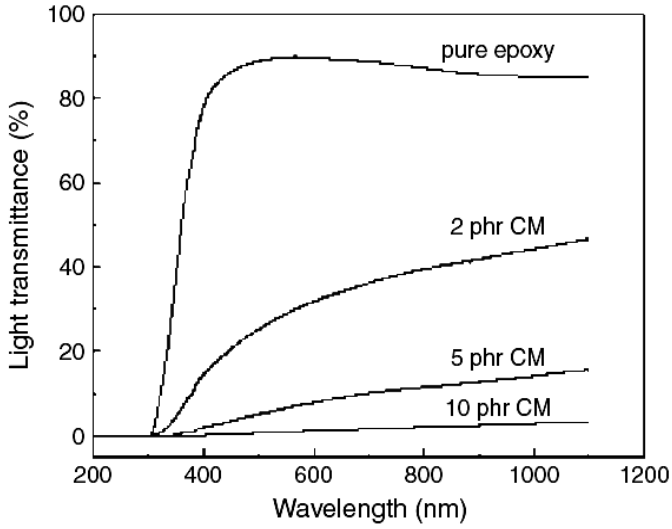

Figure 2.12. Light transmission spectra of pure epoxy, and OMMT/Epoxy nanocomposites with different OMMT contents (Source: Deng et al. 2003).

The optically transparent glass particle dispersed epoxy matrix composite was studied (Kagawa et al. 1998) and light transmission spectra for the pure epoxy matrix and the composites with particle volume fraction (f_p) are shown in Figure 2.13. The light transmittance of the pure matrix and the composites appeared at wavelength above 300 nm and they increased as the wavelength increased. The increase in the light transmittance rate with wavelength was large for the pure epoxy matrix and the composite with smaller particle volume fraction, respectively. The light transmittance of the composite decreased with increase in glass particle volume fraction.

The effect of the nanometer-order silica particle fraction (0%, 5%, 10%, 20%, and 24% by weight) on the light transmission of epoxy based nanocomposites was studied by Zhou et al. (Zhou and Shi 2004). The epoxy resin used in the experiments was a clear grade cycloaliphatic epoxide, the hardener was substituted hexahydro-phthalic anhydride and a tertiary amine salt was used as a catalyst. Light transmittances at a wavelength range from 300 to 900 nm were measured as shown in Figure 2.14. Addition of fillers reduced the light transmittance and, the magnitude of the reduction was wavelength dependent. The filler addition caused a greater light transmittance reduction at relatively

smaller wavelengths. This result was explained by authors as that it may be due to the size effect.

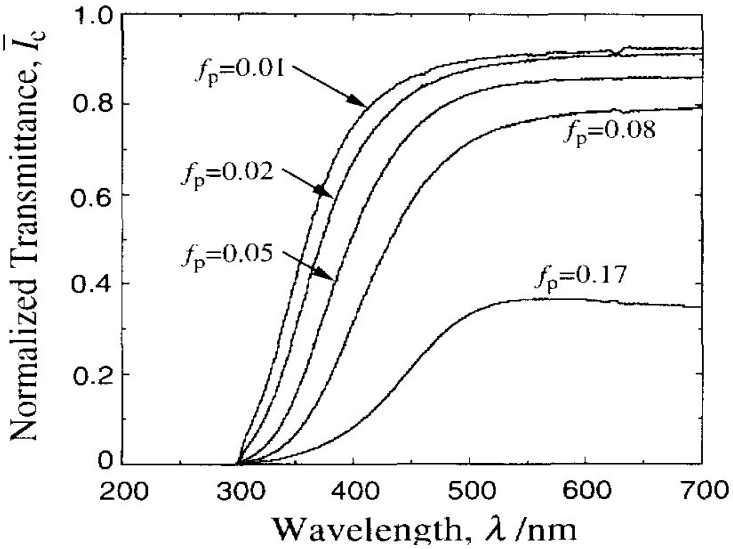

Figure 2.13. Light transmission spectra of the composite with the particle volume fraction, f_p (Source: Kagawa et al. 1998)

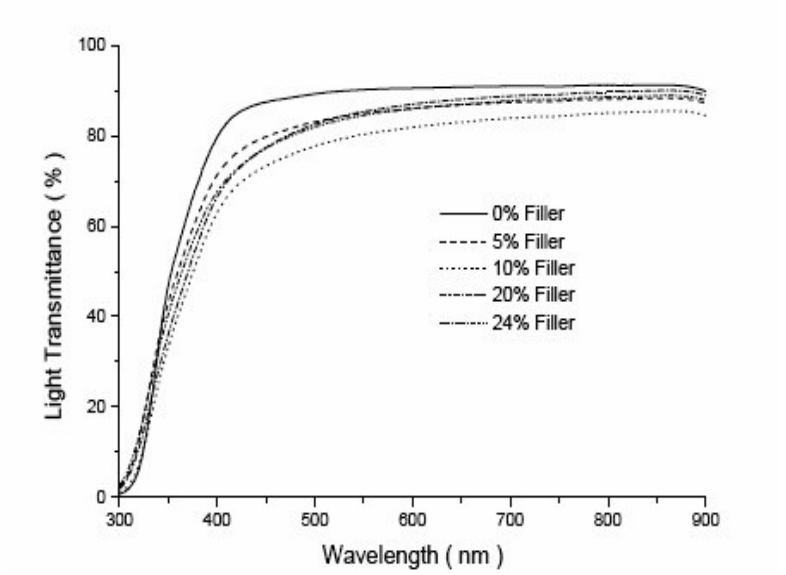

Figure 2.14. Light transmission spectra of the composite with the silica particle (Source: Zhou and Shi 2004).

2.5.4. Other Properties

Polymer nanocomposites have excellent barrier properties against gases (e.g., oxygen, nitrogen and carbon dioxide), water and hydrocarbons. Studies have showed that such reduction in permeability strongly depends on the aspect ratio of silicate platelets, with high ratios dramatically enhancing gaseous barrier properties. The water absorption of epoxy exfoliated nanocomposites as shown in Figure 2.15 has been reported by Chen and Yang. Figure 2.15 shows the water content of nanocomposites prepared with MMT and OMMT modified by dodecylamine ($H_2N(CH_2)_{11}CH_3$) in water at 23°C for 24 h. It was found that the OMMT/Epoxy nanocomposites showed excellent water resistance. The difference of water resistance of the composite containing modified silicate and unmodified silicate was explained such that the water resistance is strongly dependent on the delamination of silicate within the epoxy resin and modification of the silicate surface. The delamination of silicate within the epoxy resin increased the diffusion path of diffusing water in the epoxy resin. Therefore, it takes more time for water to pass through the epoxy matrix.

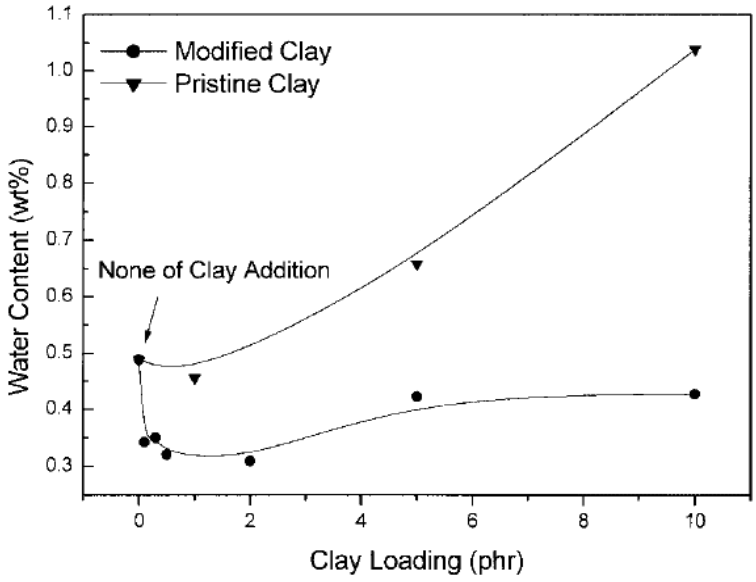

Figure 2.15. Water content of nanocomposites prepared with pristine and modified silicate as a function of silicate loadings (Source: Chen and Yang 2002).

Silicate minerals exhibit unique electrical properties, which is mainly attributed to their ionic conductivity. Although the silicate layers can be regarded as insulators, the hydrated interlayer cations and their mobility ensure a significant ionic conductivity of the system. Moreover, the intercalation of the silicate particles could affect the hydration shells of interlayer cations and therefore significantly modifies the ion mobility, electrical conductivity and other electrical parameters (Zeng et al. 2005).

CHAPTER 3

MODELING BACKROUND

A better understanding the mechanical behaviour and predict elastic modulus is essential in the development of nanocomposites. This also assists the improvement of material processing. For this reason, the modulus of polymer composites has been extensively studied experimentally and predicted with a two-phase model by various researchers. The main purpose of such theories is to see the predictive behaviour of the models on the mechanical properties of the composite material by considering the contribution of constituent (matrix and filler) properties, i.e. Poisson's ratio, modulus, volume fraction, filler aspect ratio, filler distribution, etc. In order to obtain tractable solutions, the theoretical approaches in general have the following assumptions (Whitney and McCullough 1990);

1. The phase surfaces are assumed to be in direct contact and bonded so that slip does not occur at the interface of the phases.

2. The overall average response of the materials to loads is considered rather than localized variations in the material response characteristics.

The earliest theory of rigid inclusions in a non-rigid matrix is based on Einstein's equation (Einstein 1956) for the viscosity of the suspension of rigid spherical particles in the compliant matrix. This model led to further development by Mooney (Mooney 1951), Brodyan (Brodyan 1959) and Guth (Guth 1945). The Hashin and Shtrikman modification model takes into account the Poisson contraction of the constituent phases (Hashin and Shtrikman 1963). The simplest case for a two phase system involves series and parallel models given by Broutman and Krock (Broutman and Krock 1967). A simpler model for two phase system was proposed by Counto (Counto 1964) assuming perfect bonding between the particle and the matrix. The two-phase model suggested by Takayanagi has been widely used to predict the modulus of polymers, polymer blends, and composites (Takayanagi et al. 1964). Halpin, who mathematically modelled laminated system of randomly oriented fibers or an oriented distribution of fibers in the bulk matrix (Halpin 1969), studied the stiffness of short fiber reinforced composites with variable fiber aspect ratios. Lewis and Nielsen studied dynamic mechanical properties of particulate-filed

composites and found that the moduli of composites increase with decreased particle size (Lewis and Nielsen 1970). Chantler et al. (Chantler et al. 1999) presented a new phenomenological model based on the classic Hertzian elastic contact theory. These expressions are generally based on some physical arguments and determination of fitting parameters (Lingois and Berglund 2002).

For traditional composites reinforced with inorganic fillers, a dispersed particle is in the range of micrometers, and the interfacial region is not often taken into account. Therefore, the interfacial contribution is often neglected. When the dispersed particle is reduced to a very small size, the specific surface area becomes very large that cause the areal fraction of the interfacial region to be so large. Some semi-empirical models that rely on the determination of adjustable parameters have been developed due to the complexity of the geometrical features (filler aspect ratio, volume fraction, filler orientation, etc.) and inadequacies of the theoretical models as mentioned above. All of the theoretical modeling approaches based on the relations of the elastic constants given in Equation 3.1. For an isotropic material, there are two elastic constants; the Young's modulus *(E)*, and the Poisson's ratio *(ν)* to define the elastic response of the composites:

$$G = \frac{E}{2(1+\nu)} \tag{3.1a}$$

$$E = \frac{9KG}{3K+G}, \quad \nu = \frac{3K-2G}{2(3K+G)} \tag{3.1b,c}$$

In the above equations, *K* refers to the bulk modulus of the material.

3.1 Semi Empirical Models for Spherical Particulate Systems

Semi-empirical models are based on some physical parameters and an expression of the following form (Mc Gee and Mc Cullough 1981)

$$P_C = \frac{P_m(1+\xi X V_f)}{1 - X\psi V_f}, X = (P_f - P_m)/(P_f + \xi P_m) \quad (3.2)$$

Here, P denotes the bulk modulus (K) or the shear modulus (G), V_f is the volume fraction. The subscripts c, m and f refer to the composite, matrix, and the filler, respectively. In this formulation ξ and ψ can be treated as adjustable parameters which are specifically defined in each model. Based on the formulation (3.2), there are several formulations proposed in the literature in order to predict the elastic modulus of the composites reinforced by spherical fillers. In these systems, the reinforcing particles are considered to be spherical or near spherical, therefore the effective aspect ratio is unity. The following three most commonly used models were developed by Guth and Gold, Halpin-Tsai (HT), Lewis-Nielsen (LN), Chantler, Hu, and Boyd (Ch) that are related with the adjustable parameters ξ and ψ.

3.1.1. Guth and Gold Model

Guth and Gold Model (Guth and Gold 1938) is based on the Einstein's model, the earliest theory of rigid inclusions in a non-rigid matrix. Einstein's model has an approach based not on elasticity, but on the assumption that changes in the viscosity of a suspension can have parallel changes in material properties, including elastic modulus. Hence, in the model given as in the following

$$\eta_C = \eta_m(1 + K_E V_f) \quad (3.3)$$

where, η is the viscosity that might be replaced by G or E. K_E is the Einstein coefficient, which is also called the "intrinsic viscosity," and it is a function of particle morphology and packing. K_E increases with increased filler aspect ratios (l/d > 1), and decreases slightly for Poisson's ratios<0.5 (Brown and Ellyin 2005).

By adapting the Einstein coefficient (K_E) is equal to 2.5 in the Einstein equation which is valid only very low concentrations (< %10) of the filler, Guth and Gold obtained the following formulation which is only applicable to elastomers filled with a certain amount of spherical fillers and the formulation can be used for concentrations up to 30 vol. %.

$$E_c = E_m[1 + 2.5Vf + 14.1Vf^2] \quad (3.4)$$

In this equation, the linear term accounts for the reinforcing effect of individual particles, and the second power term is the contribution of particle pair interactions (Flandin et. al. 2001).

To increase the capability of prediction of Guth and Gold model at higher volume fraction, the equation is modified in the following form which is valid at filler concentration of up to 45 vol. % (Kim et al.):

$$E_c = E_m[1 + 2.5Vf + 16.2Vf^2] \quad (3.5)$$

The terms E_c and E_m refers to the modulus of the composite and the matrix, respectively.

3.1.2. Halpin-Tsai (HT) Model

Halpin and Tsai developed a widely used composite theory to predict the stiffness of continuous-fiber composites as a function of aspect ratio. This theory is based on the early micromechanical work of Hermans (Hermans 1967) and Hill (Hill 1964). Hermans generalized the form of Hill's self-consistent theory by considering a single fiber encased in a cylindrical shell of matrix, which is embedded in an infinite medium assumed to possess the average properties of the composite. Halpin and Tsai adapted Hermans' model for particulate systems. Based on Equation 3.2, *P* represents the Young's modulus, ξ is a shape parameter that depends on the matrix Poisson's ratio, filler geometry, orientation, and loading direction and it was found to be 2 for particulate filled composites. Moreover, for shear modulus predictions, ξ = 1 can be used or the equality as in the below;

$$\xi_G = \frac{7 - 5\nu_m}{8 - 10\nu_m} \quad (3.6a)$$

By including the matrix Poisson's Ratio *(ν_m)*, the parameter can be calculated precisely. In the same manner for bulk modulus, the term is as below;

$$\xi_K = \frac{2(1-2\nu_m)}{1+\nu_m} \tag{3.6b}$$

The last parameter, ψ, used in Equation 2.3 is taken as 1 in Halpin-Tsai Model. The Halpin-Tsai equations are known to fit some experimental data very well at low volume fractions, but it under-estimates stiffness values at high volume fractions (Whitney and McCullough 1990). This has prompted some modifications to their model. By adapting this formulation to the short fiber composites, Halphin and Tsai noted that the shape parameter, ξ, lie between 0 and ∞. For example, if ξ is taken as ∞ then Equation 3.2 reduced to the rule of mixtures as in the following form (Halpin and Kardos 1976)

$$P = \nu_f P_f + \nu_m P_m \tag{3.7a}$$

However, for ξ = 0, Halphin-Tsai formulation becomes the inverse rule of mixture as given below.

$$\frac{1}{P} = \frac{\nu_f}{P_f} + \frac{\nu_m}{P_m} \tag{3.7b}$$

3.1.3. Lewis-Nielsen (NL) Model

This model was developed by Nielsen and Lewis (Lewis and Nielsen 1970, Nielsen 1970) using the analogy between the stiffness of the composite and viscosity of a suspension of rigid particle in a Newtonian fluid. This model is also a modification of the Halpin-Tsai model (Equation 3.5). It was designed to compensate the Halpin-Tsai model's lack for the prediction of modulus at high filler loading composites. In their formulation, an equation in which the stiffness not only matches with dilute theory at low volume fractions, but also displays rigid reinforcement as V_f approaches a packing limit $V_f^{\max}$. It is used to account for the limits imposed by the maximum packing for uniformly sized spherical particles. The following expressions are given for the model.

$$\xi_G = \frac{7 - 5\nu_m}{8 - 10\nu_m} \tag{3.8a}$$

$$\xi_K = \frac{2(1 - 2\nu_m)}{1 + \nu_m} \tag{3.8b}$$

$$\psi = 1 + \left(\frac{1 - Vf^{\max}}{(Vf^{\max})^2} \right) Vf \tag{3.7c}$$

Here, v_m is the matrix Poisson's ratio, $V_f^{\max}$ is the maximum volume fraction of filler. For uniform sizes of spheres, $V_f^{\max}$ is 0.66 for random packing and if the composite system do not have uniform size distribution of particles then $V_f^{\max}$ is considered to be between 0.66 and 1 (Lingois and Berglund 2002). The parameters, ξ_G and ξ_K are used for the prediction of shear and bulk modulus, respectively. It is obvious that ξ_G and ξ_K are the same as in Halpin-Tsai model, however, the parameter ψ is a function of volume fraction and maximum volume fraction of the filler in the Lewis-Nielsen model.

3.1.4. S Combining Rule

This approach considers a composite system with the stiff spherical inclusions in a more compliant matrix, such that for particulate filled polymers with $P_f > P_m$. For rigid uniformly sizes of spheres, the adjustable parameters ξ_G, ξ_K and ψ can be expressed as below (Whitney and McCullough 1990);

$$\xi_G = \frac{7 - 5\nu_m}{8 - 10\nu_m} \tag{3.9a}$$

$$\xi_K = \frac{2(1 - 2\nu_m)}{1 + \nu_m} \tag{3.9b}$$

$$\psi = 1 + \left(\frac{1 - Vf^{\max}}{(Vf^{\max})^2} \right) (Vf\, Vf^{\max} + (1 + Vf)(1 - Vf^{\max})) \qquad (3.9c)$$

Here, $V_f^{\max}$ is the maximum volume fraction of the filler. Comparing the Halpin-Tsai (HT), Lewis-Nilsen (LN) and S-combining rule, it can be seen that the parameter ψ has different mathematical form in each model. Therefore, it can be useful to investigate the variation of ψ for appropriate maximum volume fraction of filler and *Vf*. Figure 3.1 shows this effect for different values of $Vf^{\max}$. Another important difference among HT, LN, S-combining rule models is that Young's modulus values may not be predicted directly by LN or S-combining models while HT model allows prediction of Young's modulus of the composite without extra calculation. Young's modulus can be generated from the predicted values of bulk modulus *K* and shear modulus *G* through the auxiliary expression given in Equation 3.1 a-b for LN or S combining models.

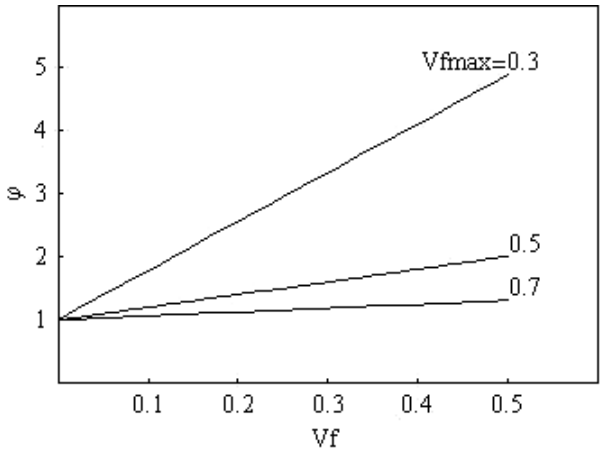

Figure 3.1.a. Effect of $V_f^{\max}$ on the adjustable parameter ψ for Lewis-Nilsen model as a function of $V_f^{\max}$.

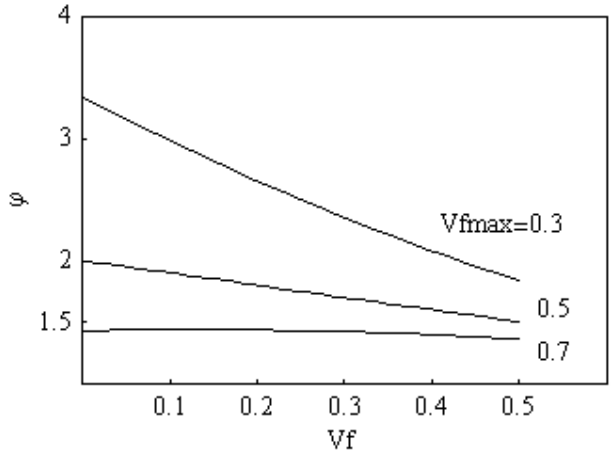

Figure 3.1.b. Effect of $V_f^{\max}$ on the adjustable parameter ψ for S-Combining Rule as a function of $V_f^{\max}$.

3.1.5. Chantler, Hu, and Boyd (CHB) Model

Chantler et al (Chantler et al. 1999) presented a new phenomenological model based on the classic Hertzian elastic contact theory. Following expression can be used to predict the elastic modulus of composites *(E_c)*.

$$E_c = E_m (E_f / E_m)^{1-(1-Vf)^{\beta}} \tag{3.10a}$$

The parameter β is determined by fitting Equation 3.10b to numerical simulation results for uniformly sized spherical particles. The resulting empirical expression is the following:

$$\beta = \frac{2[(1-{v_f}^2)/(1-{v_m}^2)]^{1.7}}{\ln(E_f / E_m)} \tag{3.10b}$$

Where, v_f and v_m are the Poisson's ratio of the filler and matrix, E_m and E_f are the elastic modulus of matrix and filler, respectively. In contrast to the previously mentioned models (HT, LN and S), CHB model consider the Poisson's ratio of the filler *(v_f)*. However, the reported studies about the nanocomposite modeling indicate that the effective material

parameter is only v_m. As in HT model, CHB model also allow calculation of the Young's modulus directly.

3.2. Semi Empirical Models for Non-spherical Particulate Systems

The composite systems such as in layered silicate/polymer nanocomposites contain platelet like non-spherical particles. Non-spherical particulate reinforced composites have slightly higher elastic modulus *(E)* than those based on spherical particulate systems. There are several important models which have appropriate prediction capability of elastic modulus of the non-spherical filled composite systems. In this section, we consider three different models developed for the estimation of elastic modulus of inorganic silicate layer incorporated thermoset polymer nanocomposites.

3.2.1. Guth and Gold Model

The relations between the Young's modulus and the concentration of filler given by Guth and Gold in Equation 3.3 were modified by Guth (Guth 1945) for non-spherical filled particulate composites. This modified model considers the chains composed of spherical fillers that are similar to rod like filler particles embedded in a continuous matrix. By introducing a shape factor to original Guth and Gold Equation, Guth developed a new expression as in the following form:

$$E_c = E_m[1 + 0.67\alpha Vf + 1.62(\alpha Vf)^2] \qquad (3.11)$$

where α is the shape factor (length/width of the filler), E_m is the elastic modulus of the matrix and E_c is the elastic modulus of the composite. The second term in Equation 3.11 is the contribution of particle-particle interaction that describes the mechanical reinforcement (Flandin et. al. 2001).

3.2.2. Brodnyan Model

The Mooney (Mooney 1951) equation is one of the many derivatives of the Einstein equation. It has the following form;

$$E_c = E_m \exp\left(\frac{K_E Vf}{(1 - Vf \ / \phi_m)}\right) \tag{3.12}$$

where φ_m is the maximum packing that the given filler, or is the ratio of true filler volume to the volume the filler actually occupies and K_E is the Einstein's coefficient. This relation was modified for non-spherical particles by Brodnyan to incorporate "α" the aspect ratio of the particle (1< α<15). Hence, Equation 3.12 becomes as in the following (Brown and Ellyin 2005).

$$E_c = E_m \exp\left(\frac{2.5V_f + 0.407(\alpha - 1)^{1.508} V_f}{(1 - V_f \ / \phi_m)}\right) \tag{3.13}$$

3.2.3. Halpin-Tsai (HT) Method

Halpin-Tsai equations are widely used expressions in order to predict reinforcement effect of fillers in nanocomposite systems with both spherical (or near spherical) and non-spherical filled systems (Fornes and Paul 2003). Halpin-Tasi equations was modified by Wu et al. (Wu et al. 2004) for the plate-like filler as expressed in the following form;

$$E_c = \frac{E_m(1 + \xi \eta Vf)}{1 - \eta Vf} \tag{3.14a}$$

where

$$\eta = \frac{E_f \ / E_m - 1}{E_f \ / E_m + \xi} \tag{3.14b}$$

Here, E_f denotes elastic modulus of the filler, and ξ is the shape factor depending on the filler orientation and loading direction. For the rectangular plate-like filler in a composite system, ξ is equal to *2w/t*, in which *w* is the width and *t* is the thickness of the dispersed phase. Figure 3.2 (a) shows two types of fillers (fiber and disk-like platelet), their orientation with respect to orthogonal axes, and their corresponding Halpin–Tsai quantities. Dispersed silicate platelets are expected as disk-like platelets: E_{11} and E_{22} are the composite modulus parallel (longitudinal) and perpendicular (transverse) to the major axis of the filler.

A number of assumptions are inherent to this approach. The Halpin–Tsai equations treat a fiber as a fiber and disk as a rectangular platelet, since the length and, in turn, aspect ratio across a disk is not constant as shown in Figure 3.3. In addition, the Halpin–Tsai equations for E_{11} and E_{22} are independent of the Poisson's ratio of the filler or the matrix. Also, the Halpin–Tsai equations for transverse modulus, i.e. perpendicular to the filler's major axis, are independent of aspect ratio as seen in Figure 3.2.

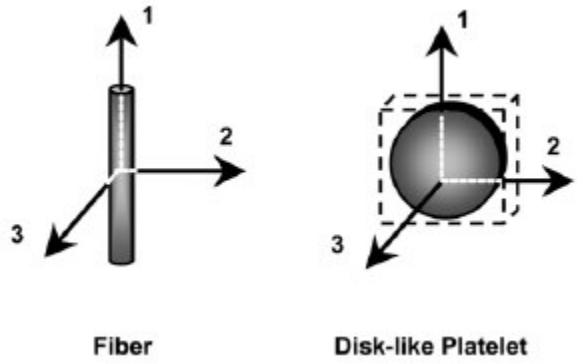

	Fiber	Disk-like Platelets	Fiber	Disk-like Platelets
Direction of Applied Load	Halpin-Tsai Composite Modulus		Shape Parameter, $\zeta^{(a)}$	
	Fiber	Platelets	Fiber	Platelets
1	$E_{11}=E_{//}$	$E_{11}=E_{//}$	$\zeta = 2(l/d)$	$\zeta = 2(l/t)$
2	$E_{22}=E_{\perp}$	$E_{22}=E_{//}$	$\zeta = 2$	$\zeta = 2(l/t)$
3	$E_{33}=E_{\perp}$	$E_{33}=E_{\perp}$	$\zeta = 2$	$\zeta = 2$

The symbol *l* represents the length of the fiber or diameter of the disk, *d* represents the fiber diameter, and *t* is thickness of the disk.

Figure 3.2. The two types of fillers, their orientation with respect to orthogonal axes, and their corresponding Halpin–Tsai quantities (Fornes and Paul 2003).

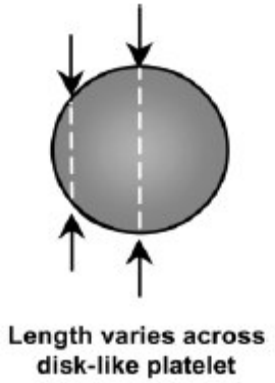

Figure 3.3. Inherent variation in length, and subsequently aspect ratio, across a disk-like platelet.

3.2.4. Modified Halpin-Tsai Model

Lewis and Nielsen (Lewis and Nielsen 1970, Nielsen 1970) modified the Equation 3.14 and considered the maximum volumetric packing fraction of the filler ψ as an additional parameter in order to improve the prediction ability of the classical HT model. Maximum volumetric packing fraction can be defined as the ratio of true volume of the filler to apparent volume occupied by the filler. Modified Halpin-Tsai model can be written in the following form;

$$E_c = \frac{E_m(1+\xi\eta Vf)}{1-\psi\eta Vf} \tag{3.15a}$$

$$\psi = 1+\left(\frac{1-Vf^{\max}}{(Vf^{\max})^2}\right)Vf \tag{3.15b}$$

CHAPTER 4

EXPERIMENTAL

4.1. Materials

Nanocomposite materials were prepared using an epoxy resin (Diglycidyl ether of bisphenol A (DGEBA)) as a polymer matrix and sodium montmorillonite (MMT, K10-Aldrich) as a filler with a cation exchange capacity of 120 meq/100g. Typical properties of montmorillonite based on the literature are shown in Table 4.1. An amine curing agent was blended to epoxy as a hardener agent. For the modification of MMT, hexadecyltrimethylammonium chloride (HTAC, Aldrich) with 25 wt. % sol. in water and hydrochloric acid were used.

Table 4.1. Typical properties of montmorillonite (WEB_2 2005)

Property	**Montmorillonite**
Size (μm)	0.01-1.0
Shape	Flakes
Swelling Capacity	High
Interlayer Spacing	1.0-2.0
Bonding	Van der Walls
Charge Exchange Capacity (CEC)	120 meq/100 g

4.2. Modification of Montmorillonite

Figure 4.1 is the schematic illustration of surface modification stages of montmorillonite (MMT) silicate particles. 20 grams of the MMT was dispersed into 400 mL distilled water and stirred at a temperature of 80 ^{0}C. 0.05 moles of HTAC was mixed with 4.8 ml HCl in 100 mL distilled water. This solution was poured into the hot silicate-water mixture and stirred at a temperature of 80 ^{0}C for 1 hour. The mixture was then filtered and washed with water until no chloride was detected. Chloride residue was

determined using $AgNO_3$ as described elsewhere (Salahuddin 2004). The organosilicate (OMMT) was then obtained after drying the filtered material at 75 ^{0}C for 2-3 days in a vacuum oven.

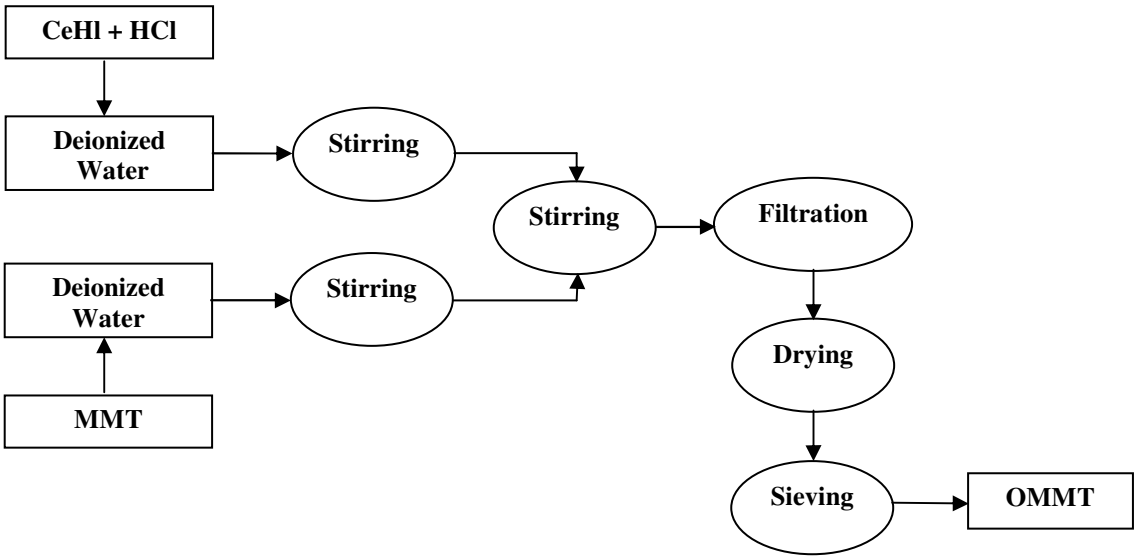

Figure 4.1. Schematic illustration of surface modification of montmorillonite

4.3. Synthesis of epoxy–montmorillonite nanocomposites

Layered silicate/epoxy nanocomposite samples were prepared with 1, 3, 6, and 10 wt. % of OMMT and MMT particles. Figure 4.2 illustrates the processing stages for in-situ polymerization process. The epoxy resin was blended with the desired amount (1, 3, 6, 10 wt. %) of OMMT and MMT at room temperature for 1 hour using a mechanical stirrer. The blend was further hold in an ultrasonic bath for 20 minutes to further disperse the silicate layers in the resin. Then, a stochiometric amount (35 parts curing agent: 100 parts epoxy by weight) of the amine curing agent was added and the mixture was outgassed by vacuuming to remove bubbles. The blend was casted into silicon molds and the nanocomposites were cured at room temperature and post cured for 1 hour at 80 ^{0}C and 2 hours at 150 ^{0}C.

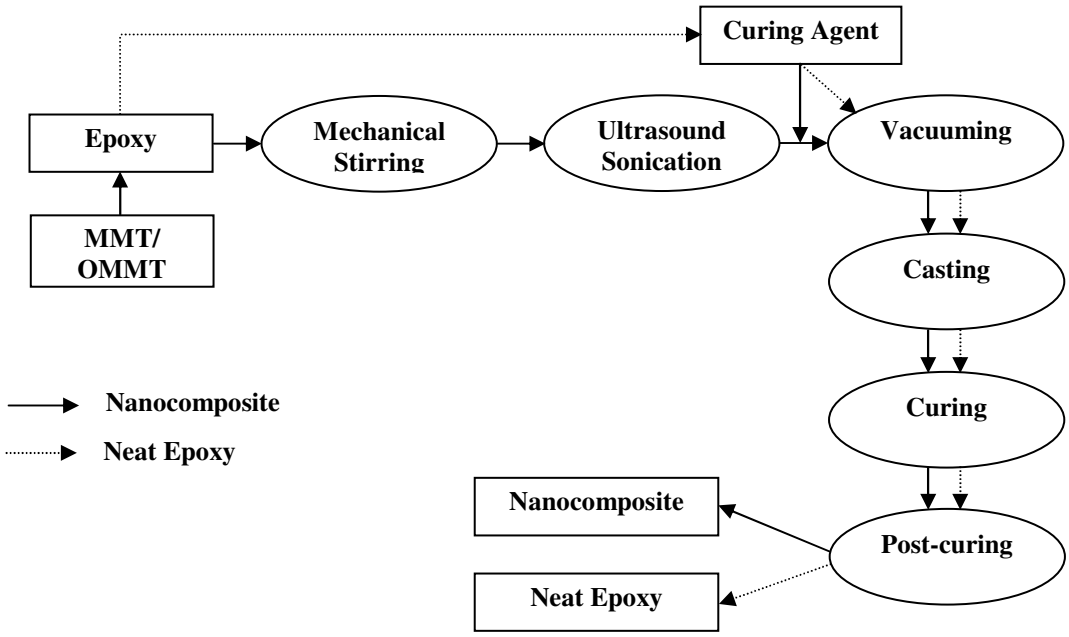

Figure 4.2. In-situ polymerization Method

4.4. Characterization of Nanocomposites

4.4.1 X-ray Diffraction

X-ray diffraction (XRD) is the most commonly used technique to identify intercalated structures due to the periodic arrangement of the silicate layers both in the pristine and the intercalated states. The x-ray diffraction peak due to the 001 silicate crystal orientation moves to lower 2θ angles as intercalation increases. The shift of the scattering peak related to the galleries of the silicate indicates intercalation. Based on the disappearance or the decrease of intensity of diffraction peaks, it can be concluded that the silicate is partially or completely exfoliated (Pozsgay et. al., 2004). The diffraction angle is related to the layer spacing through the well known Bragg's relation $\lambda = 2d\sin\theta$ where d is the distance between silicate lattice planes that are parallel, θ is the incident angle of the x-ray to the lattice plane, λ is the wavelength of x-ray used for analysis, n is the some number of wavelength periods. X-ray diffraction was conducted with a Phillips

X-Pert Pro diffractometer using CuKα radiation. Powder samples were scanned in the interval of 2Θ= 2°-12° at 40 kV and 30 mA.

4.4.2 Scanning Electron Microscopy (SEM)

Phillips™ Scanning Electron Microscopy (SEM) was used to study the fracture surface of tensile specimens and also used to determine the silicate agglomeration morphology. Gold vapor deposition onto the fracture surface permitted for the observation of the microstructure.

4. 5. Mechanical Property Characterization

4.5.1. Tensile Test

Tensile tests were conducted using a Schimadzu AG universal test machine and samples were stressed at a constant strain rate of 2.00 mm/min until failure. The test method and sample preparation was in accordance with ASTM D638M-91a. The tensile dogbone test coupons with 10 mm in wide and 6.0 mm in thickness were prepared. The gauge length of the specimen was approximately 50 mm. The overall length of the specimen was 200 mm. Figure 4.3 is the photo showing the tensile test specimen under load. At least five specimens from nanocomposites were used for the experiments.

The tensile strength (σ) in the units of MPa and strain was calculated using the following equations;

$$\sigma = \frac{F}{A} \tag{4.1}$$

$$\varepsilon = \frac{(L - L_0)}{L_0} \tag{4.2}$$

where, F is the applied load, A is the cross sectional area of the specimen, L_0 is the original distance between gage marks, and L is the distance between gage marks at any

time. Young's modulus (E) was obtained from the initial linear part of σ vs. ε graphs as below;

$$E = \frac{\sigma}{\varepsilon} \tag{4.3}$$

Figure 4.3. Photo of tensile test specimen under load

4.5.2. Flexural Test

The flexural test technique was used to determine the effects of organically modified and unmodified silicate loading on the flexural strength and modulus of the composites. The flexural test technique and sample preparation was in accordance with ASTM D 790M-86. Specimens were tested in 3-point bending configuration with a span to thickness ratio of 16. For this purpose, test specimens with 10 mm in width and 80 mm in length were sectioned using a diamond saw. Figure 4.4 is the photo showing the flexural test specimen under load. At least five specimens from nanocomposites were tested using the universal test machine at a cross-head speed of 1.7 mm/min. Force vs. deflection at the center of the beam was recorded.

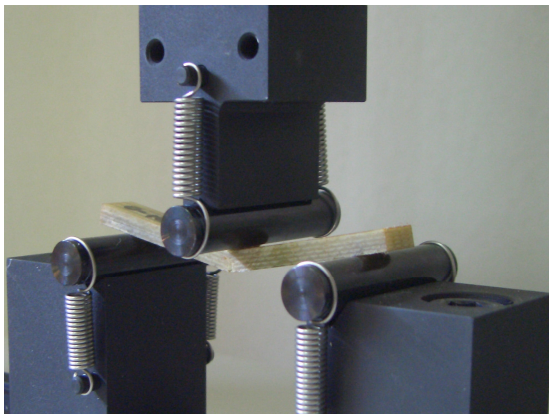

Figure 4.4. Photo of flexural test specimen under load.

The flexural strength (S) in the units of MPa was calculated using the following equation;

$$S = \frac{3PL}{2bd^2} \tag{4.4}$$

where P is the applied load at the deflection point, L is the span length, d and b are the thickness and the width of the specimen, respectively. The flexural modulus values (E_b) were calculated using the following equation;

$$E_b = \frac{L^3 m}{4bd^3} \tag{4.5}$$

where m is the slope of the tangent to the initial straight line portion of the load-deflection curve.

4.5.3. Fracture Toughness Test

Fracture toughness (K_{IC}) of nanocomposite materials, a measure of plane-strain fracture toughness, was measured by the Single-Edge-Notched Bending (SENB) method, following ASTM D-5045-91a. For this purpose, test specimens with the thickness of 4 mm and width of 8 mm were sectioned using a diamond saw. Each specimen was sawed to generate a notch. The samples were tested in a 3-point bending mode at a test rate of

10 mm/ min using the universal test machine. Five samples of each blend were tested and the K_{IC} values were calculated using the following equation in the units of $MPa.m^{1/2}$.

$$K_{IC} = \left(P_Q BW^{1/2}\right) f(x) \tag{4.6}$$

where P_Q is the applied load, B is the specimen thickness, W is the specimen width, and f(x) is the calibration factor.

4.6. Thermal Property Characterization

4.6.1. Differential Scanning Calorimetry (DSC)

Differential scanning calorimetry (DSC) is a thermal technique in which differences in heat flow into a substance and a reference are measured as a function of sample temperature while the two are subjected to a controlled temperature program (Skoog et al. 1998). TA Instrument Q10 model DSC was operated under nitrogen atmosphere at a flow rate of 50 mL/min. For this test, the samples of 5–6 mg of epoxy samples were placed into the aluminium crucible, respectively. Indium was used to calibrate the thermal response due to heat flow as well as the temperature prior to analysis. The dynamic measurements were made at a constant heat rate of 10°C/minute from 25 to 200°C to determine the effects of the montmorillonite silicate addition on the glass transition temperature (T_g) of epoxy. T_g was determined by the midpoint method.

4.6.2. Dynamic Mechanical Analysis

Dynamic Mechanical Analysis (DMA) is a thermal analysis technique used to measure changes in the viscoelastic response of a material as a function of temperature, time, or deformation frequency. DMA is commonly used to determine elastic modulus (or storage modulus, G'), viscous modulus (or loss modulus, G") and damping coefficient (Tan δ) of materials.

Typically, a sample is clamped into the DMA apparatus and subjected to an oscillatory deformation while being heated or cooled at some controlled rate (WEB_3).

The resonant frequency of the sample and mechanical clamp assembly is continuously monitored as a function of temperature. The modulus (stiffness) and viscoelastic loss properties of a specimen can be calculated as a function of temperature or time. Transition temperature is obtained by determining the peak temperature of tan delta profiles.

Dynamic Mechanical Analyzer (DMA Q800) was used at a fixed frequency of 10 Hz with 2 ^{o}C/min heating rate. 0.1% value was taken as a static strain. Storage modulus, viscous modulus and loss factors were obtained by strain sweep method for the sample of size 55 x 12 x 2 mm.

4.7. Flame Retardancy

The procedure applied within the study is generally considered the easiest test to observe the burning rate of materials according to the ASTM D 635-91. The test uses a 25mm specimen held at one end in a horizontal position with marks at 25 mm and 100 mm from the free end. Burner is mounted 45° to the horizontal and remote from the specimen, ignited, and adjusted it to produce a blue flame of 20 mm high. A flame is applied to the free end for 30 seconds or until the flame front reaches the 25 mm mark as shown in Figure 4.5. If combustion continued, the duration is timed between the 25mm mark and the 100mm mark. If combustion stopped before the 100 mm mark, the time of combustion and the damaged length between the two marks are recorded.

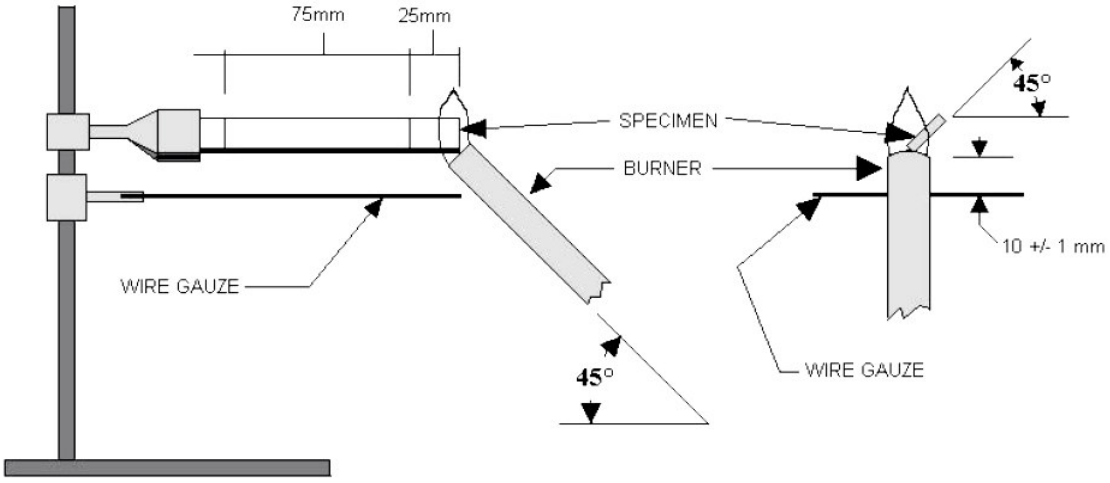

Figure 4.5. Schematic illustration of UL-94 test apparatus based on ASTM D 635-91 (Source: WEB_4 2006)

In this study, a set of 2 specimens, each has 125 mm length and 10 mm width were prepared and subjected to a 20 mm flame in accordance with the prescribed test procedures. After the flame was removed from the specimen, afterflame and afterglow times were measured. Also, the lengths of damaged material for each were measured. Average rate for burning was reported as the average of the burning rates of all specimens which have burned to the mark in cm/min.

$$\text{Rate of burning} = \text{length of burning} / (t_{\text{burning}} - t_{25\text{mm}}) \qquad (4.7)$$

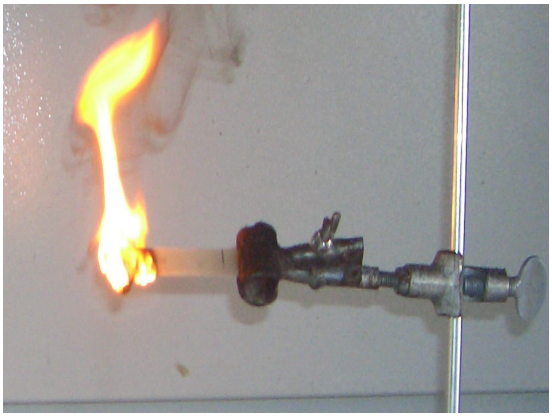

Figure 4.6. Photo of UL-94 test

4.8. Optical Property Characterization

HR 2000 High-resolution Miniature Fiber Optic Spectrometer (Ocean Optics) was used in this study which provides optical resolution as good as 0.065 nm. There are four basic optical measurements can be done: absorbance, transmission, reflection, and relative irradiance.

Absorbance spectra are a measure of how much light a sample absorbs. For most samples, absorbance is linearly related to the concentration of the substance. Absorbance (A_λ) can be calculated using the following equation;

$$A_\lambda = -\log_{10} \frac{(S_\lambda - D_\lambda)}{(R_\lambda - D_\lambda)} \qquad (4.10)$$

where S_λ is the sample intensity at wavelength λ, D_λ is the dark intensity at wavelength λ, R_λ is the reference intensity at wavelength λ.

Transmission is the percentage of energy passing through a sample relative to the amount that passes through the reference. The transmission is expressed as a percentage ($\%T_\lambda$) relative to a standard substance (such as air). $\%T_\lambda$ can be calculated with the following equation:

$$\%T_\lambda = -\log_{10} \frac{(S_\lambda - D_\lambda)}{(R_\lambda - D_\lambda)} \tag{4.11}$$

The fabricated nanocomposites were cut and four different specimen thicknesses (1, 2, 4, and 6 mm) were prepared for the measurement of optical transmittance of the samples. The light transmittance of the composites at a wavelength range of 200 to 1100 nm was measured using a transmission optical spectrometer. All the measurements were done at room temperature.

CHAPTER 5

RESULTS AND DISCUSSION

5.1. Microstructure and Dispersion of Silicate Layers

In this study, X-Ray diffraction (XRD) and Scanning Electron Micoscopy (SEM) analysis were performed to examine the microstructural properties of the neat epoxy and layered silicate/epoxy nanocomposites and the extend of silicate layer dispersion within the nanocomposites.

Figure 5.1 illustrates the X-ray diffractograms of natural silicate (MMT) and organically modified silicate (OMMT). MMT and OMMT exhibits characteristic XRD patterns corresponding to the d-spacing of 14.3 Å at $2\theta = 6.17^0$ and 18.1 Å at $2\theta = 4.87^0$, respectively. A greater d-spacing of OMMT implies intercalation (expansion) of the silicate galleries. The increase of the d-spacing is due to the penetration of the surfactant molecules within the galleries and exchange of Na^+ cations by the onium cation with a long alkyl chain of the surfactant during the surface modification process.

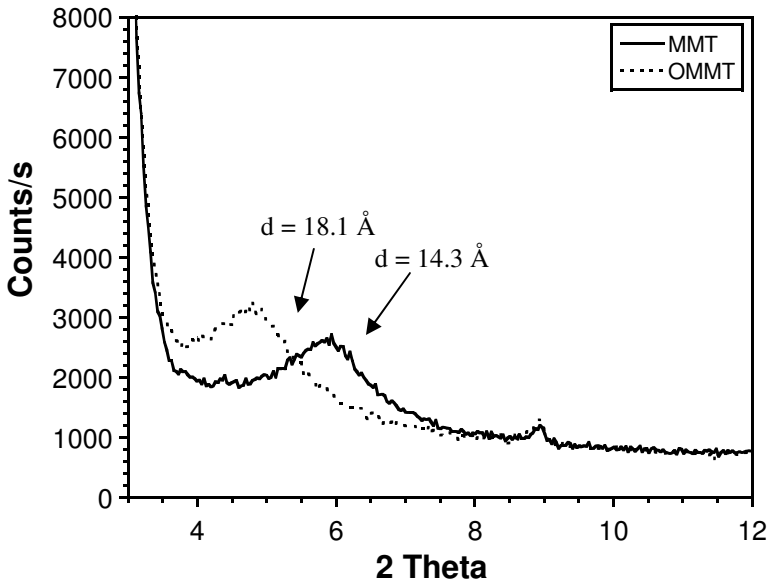

Figure 5.1. XRD patterns of MMT and OMMT

Figures 5.2 and 5.3 exhibit the XRD patterns of the nanocomposites made of MMT and OMMT silicates with various loadings. In general, the characteristic peak of the silicates observed in Fig. 1 are not detectable for the nanocomposites samples.

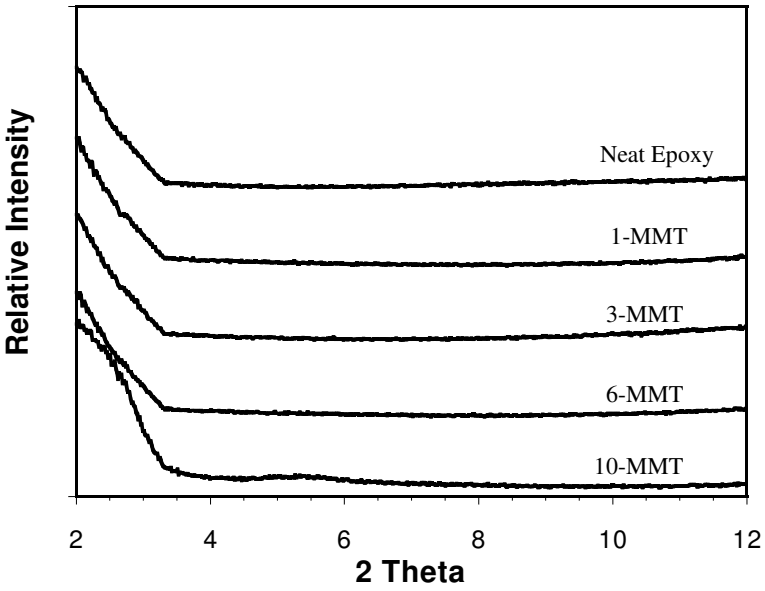

Figure 5.2. XRD patterns of neat epoxy and nanocomposites prepared with MMT loading of 1 to 10 wt%

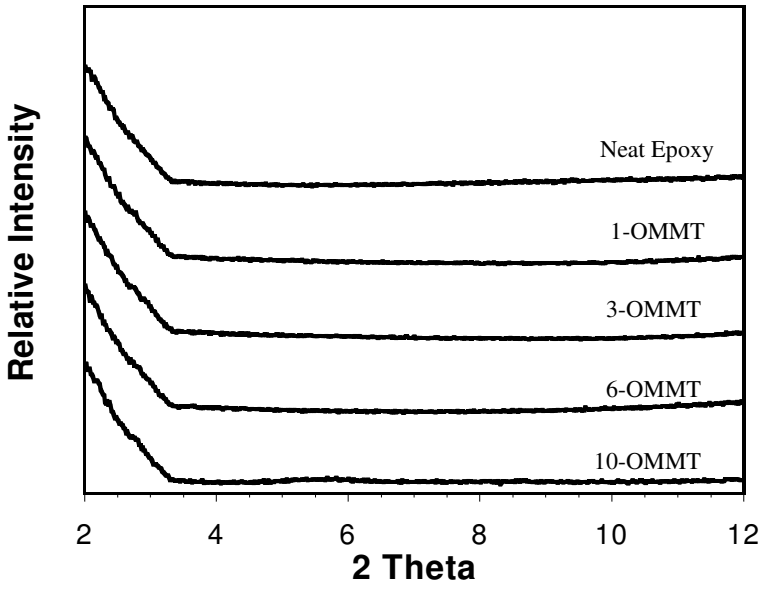

Figure 5.3. XRD patterns of neat epoxy and nanocomposites prepared with OMMT loading from 1 to 10 wt%

This indicates the further intercalation of the silicate layers within the polymer matrix due to penetration of epoxy molecules into the intercalated galleries and dispersion of the silicate plaques within the polymer matrix. For nanocomposites prepared at high loadings (10 wt. %), the broad peak at about 5.5^{o} implies a slight agglomeration of the silicate particles.

Fracture surfaces of neat epoxy and nanocomposites, after tensile testing, were examined by SEM to evaluate the extent of silicate dispersion within the matrix. Backscattered SEM images of the fracture surfaces of neat epoxy and nanocomposites prepared with various MMT and OMMT concentrations are shown in Figures 5.4 (a) to (g).

As seen in Fig 5.4 (a), relatively smooth fractured surface observed on neat epoxy indicate more brittle fracture as compared to those for nanocomposites. Figures 5.4 (b) to (e) illustrate the fracture surfaces of the nanocomposites prepared with MMT and OMMT (3 and 10 wt. %). The bright features on the backscattered images correspond to silicate particulates. At higher magnifications (Figure 5.4 (f) and (g)), the silicate layers incorporated into nanocomposites are more visible.

At high silicate concentrations, relatively higher fractions of silicate agglomerations are observed from SEM images. These agglomerations results in weaker silicate/epoxy interfacial interactions and higher stress concentration regions. As the dispersed particle size becomes smaller and the particle dispersion is more uniform, the mechanical properties are improved more significantly. Smaller sizes of the particles also imply better exfoliation of the silicate layers that result in improved mechanical properties.

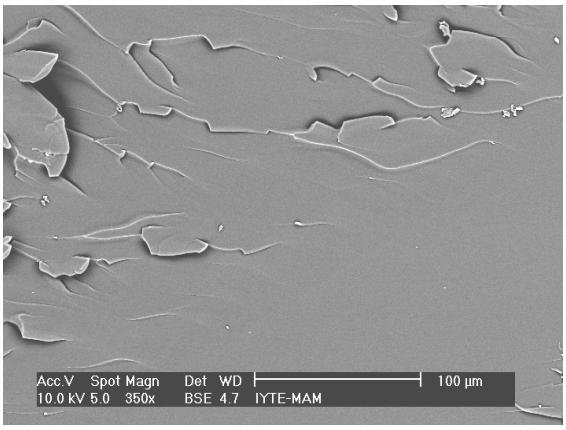
Acc.V Spot Magn Det WD 100 µm
10.0 kV 5.0 350x BSE 4.7 IYTE-MAM

(a)

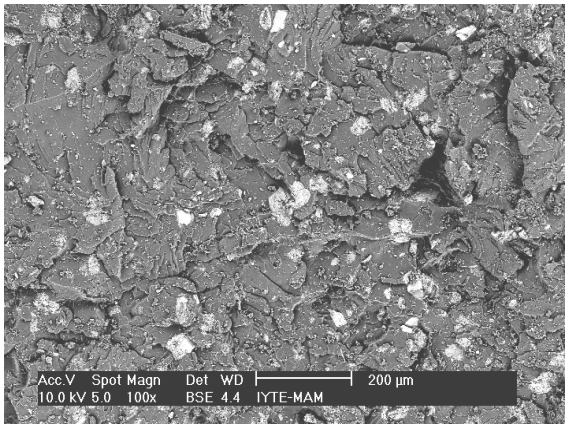
Acc.V Spot Magn Det WD 200 µm
10.0 kV 5.0 100x BSE 4.4 IYTE-MAM

(b)

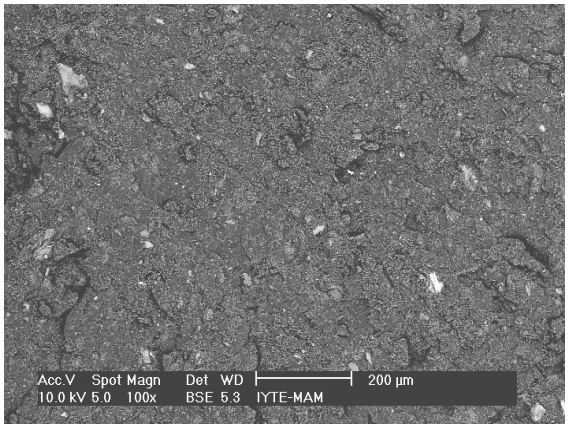
Acc.V Spot Magn Det WD 200 µm
10.0 kV 5.0 100x BSE 5.3 IYTE-MAM

(c)

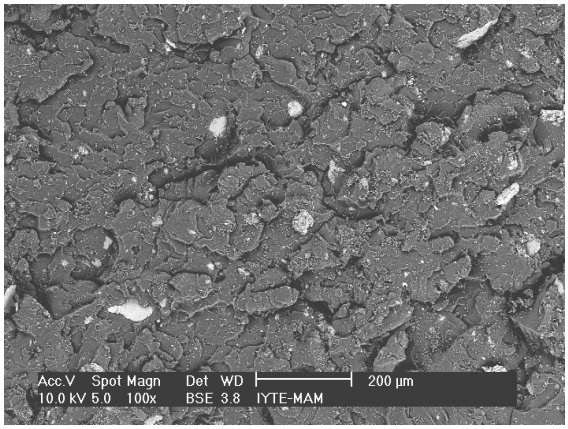
Acc.V Spot Magn Det WD 200 µm
10.0 kV 5.0 100x BSE 3.8 IYTE-MAM

(d)

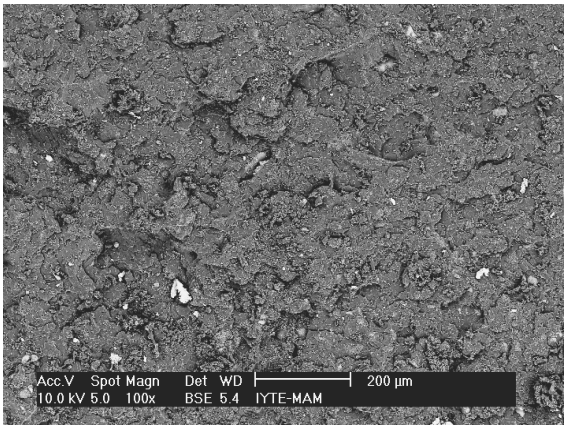
Acc.V Spot Magn Det WD 200 µm
10.0 kV 5.0 100x BSE 5.4 IYTE-MAM

(e)

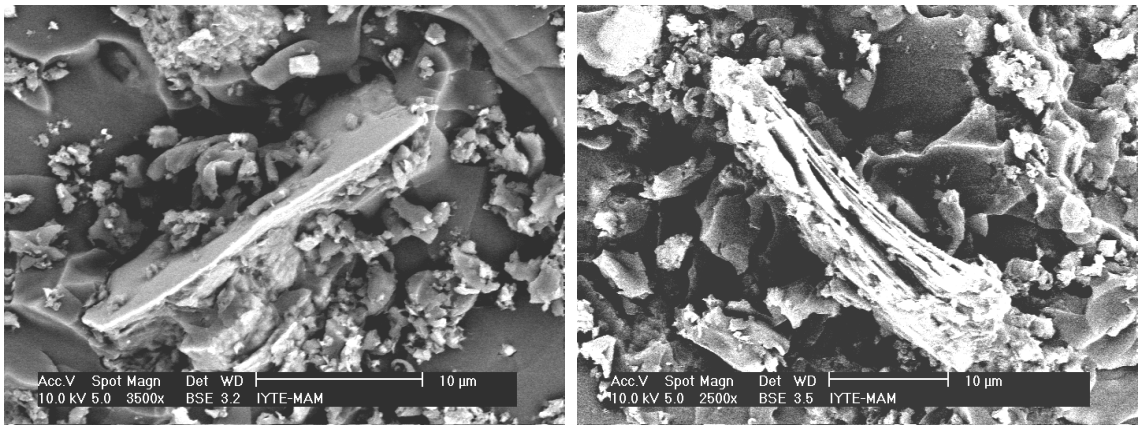

(f) **(g)**

Figure 5.4. SEM fracture surface micrographs after tensile testing of **(a)** neat epoxy (350X) **(b)** 3 wt. % MMT /Epoxy (100X) **(c)** 3 wt.% OMMT/Epoxy (100X) **(d)** 10 wt. % MMT /Epoxy (100X) **(e)** 10 wt. % OMMT/Epoxy (100X) **(f)** 10 wt. % MMT /Epoxy (3500X) **(g)** 10 wt .% OMMT /Epoxy (3500X)

Fracture surface images (Figures 5.4 (c) and (e)) observed from the nanocomposites that in made of OMMT/epoxy indicate that organosilicate platelets are better dispersed in the epoxy matrix as compared to those for MMT/epoxy nanocomposites. This implies the surface modification and thus intercalation of silicate layers results in better dispersion of the particles within the matrix. It is obvious that larger agglomerates are formed in the structure of the material with 10 wt. % MMT.

It is obvious that the fracture modes are affected by the incorporation of silicates into the epoxy structure. It is obvious that different fracture mechanisms are active during the fracture of the nanocomposites as compared to more brittle facture of neat epoxy.

5.2. Mechanical Properties

To evaluate mechanical properties of the nanocomposites developed in this study, tensile, flexural, and fracture toughness tests were performed. The tensile properties of layered silicate/epoxy nanocomposites were investigated to determine the effects of surface modification and silicate concentrations on the mechanical properties. The stress-

strain curves of neat epoxy and nanocomposites containing MMT and OMMT are given in Figures 5.5 and 5.6.

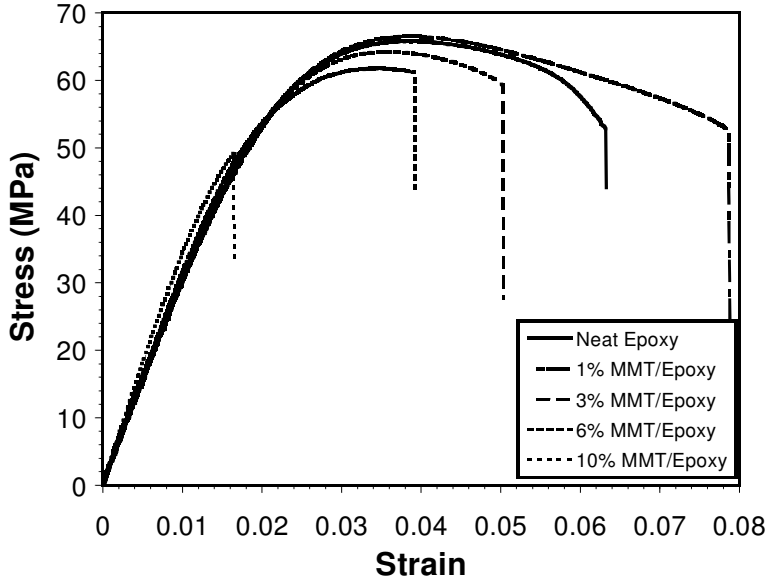

Figure 5.5. The stress-strain curves of neat epoxy and nanocomposites containing MMT

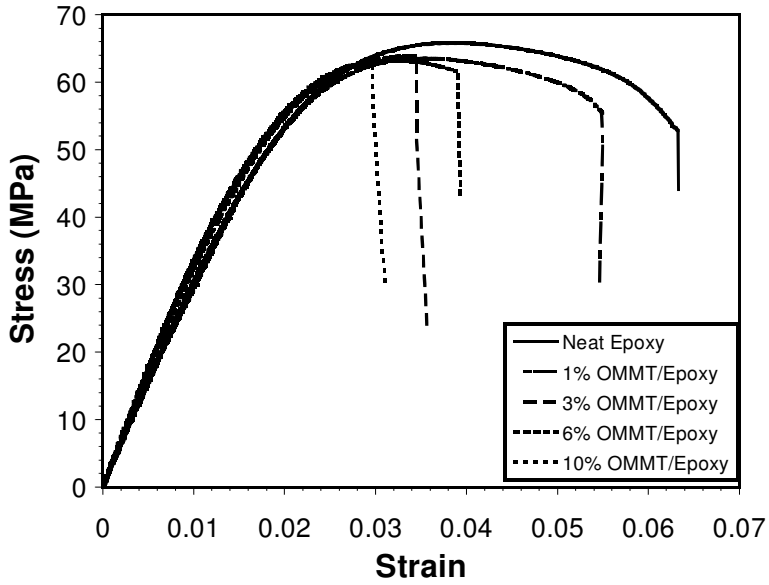

Figure 5.6. The stress-strain curves of neat epoxy and nanocomposites containing OMMT

The tensile modulus, tensile strength, yield strength, failure strength and % elongation at break with respect to type and content of silicate loading are given in Figures 5.7 to 5.10. Figures 5.7 exhibit the tensile modulus values of neat epoxy and nanocomposites made with various amount of MMT and OMMT, respectively. The tensile modulus values tend to increase with the increasing fraction of MMT and OMMT silicate particles up to 6 wt. % and approaches to a constant value at high loadings. The tensile modulus value is improved by 16% with 10 wt. % OMMT silicates loading as compared to neat epoxy. At high silicate loadings, OMMT exhibits slightly higher elastic modulus values as compared to those with MMT. Also, a dramatically increase in tensile modulus with increased silicate loading was also observed in exfoliated nanostructures such as MMT based thermoset amine-cured epoxy nanocomposite (Zerda and Lesser 2001). Similarly, it was found by Işık et al. (Işık et al. 2003) for silicate/epoxy systems that tensile modulus of nanocomposites increases by incorporation of silicate. It was reported that the increase in modulus is directly related to the high aspect ratio of silicate layers. Nigam et al. (Nigam et al. 2004) examined the nanocomposites of epoxy resin with montmorillonite K-10 silicate and it was observed that addition of the 6 wt. % organosilicate to the epoxy matrix leads to 100% increase in the tensile modulus. This results were obtained by using montmorillonite K-10 silicates in a diglycidyl ether of bisphenol A and polymerized by in situ polymerization using an aromatic diamine as a curing agent.

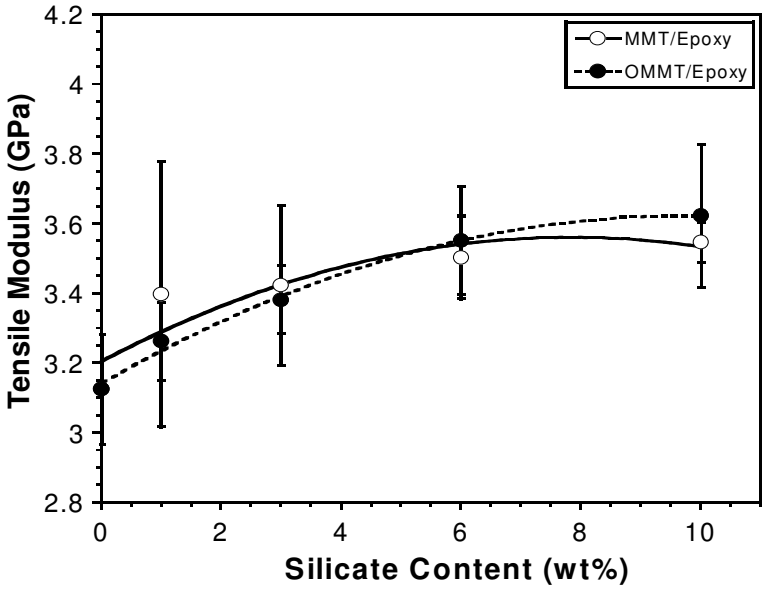

Figure 5.7. Tensile modulus of the neat epoxy and silicate/epoxy nanocomposites

Figure 5.8 presents the tensile strength values of neat epoxy resin and nanocomposites with MMT and OMMT. Maximum tensile strength value of neat epoxy was measured to be about 65 MPa. The addition of MMT reduces the tensile strength values of the epoxy while it remains almost constant with OMMT additions. This is related with the relatively higher amount of silicate agglomerates within the MMT/epoxy nanocomposites that have lower silicate intercalation and dispersion of the silicate particles. The agglomeration of the silicate particles prevents the penetration of the matrix resin into the galleries between the silicate layers that cause a decrease in silicate/polymer surface interaction. As the amount of the silicate content increases, these effects become more significant and it reduces the tensile strength of the composites. This behaviour also was observed by Isık et al. (Isık et al. 2003) and Chen and Yang (Chen and Yang 2004) for silicate/epoxy systems that tensile strength of the nanocomposites is decreased by the silicate incorporation due to the silicate agglomerates at high loadings and also the interactions between the epoxy and the silicate surface were very weak. On the other hand, it was observed that the tensile strength value of the organically modified Na-MMT (Cloisite-30B)/epoxy nanocomposite was increased by 20.9 % in comparison with the neat epoxy resin (Zhang 2004).

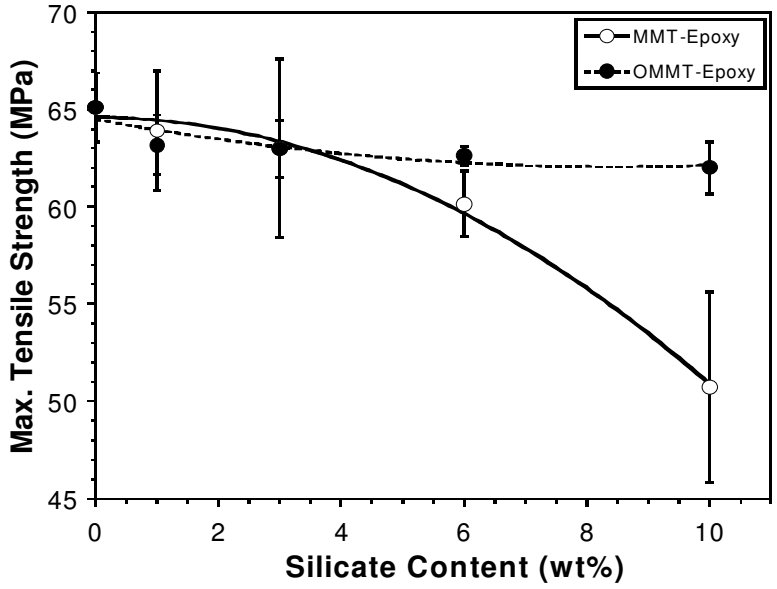

Figure 5.8. Tensile strength of the neat epoxy and silicate/epoxy nanocomposites

As shown in Figure 5.9, the failure strength values under tension for the nanocomposites increase with the incorporation of the silicates up to 6 wt. % and it decreases with further silicate loadings. The failure strength is improved by 21 and 28 % for composites prepared with up to 6 wt. % of MMT and OMMT, respectively, in comparison with neat epoxy. Similarly, Nigam et al. (Nigam et al. 2004) observed that failure strength of OMMT/epoxy nanocomposites increased by 20%. On the other hand, reductions in failure strength was found for the MMT based thermoset amine-cured epoxy nanocomposite (Zerda and Lesser 2001).

Figure 5.10 shows the % elongation at break values with respect to the type and content of the silicate. % elongation at break values decrease with increasing silicate content for both type of nanocomposites containing MMT and OMMT. This is because the rigid fillers do not elongate easily and the actual elongation in the matrix is higher than the filler that cause lower strain at break with increasing filler content. The stress concentrations around the filler particles also associate with the reduced deformation percentages. So, the stiff silicate particles are rigid fillers and make the nanocomposites more brittle. Similarly, Nigam et al. (Nigam et al. 2004) found that 80% decrease in elongation at break values of nanocomposites of epoxy resin with montmorillonite K-10 silicate resulted. However, Myskova et al. (Myskova 2003) investigated that the elongation break of the epoxy matrix increased more than five times by loading of silicate up to 10%.

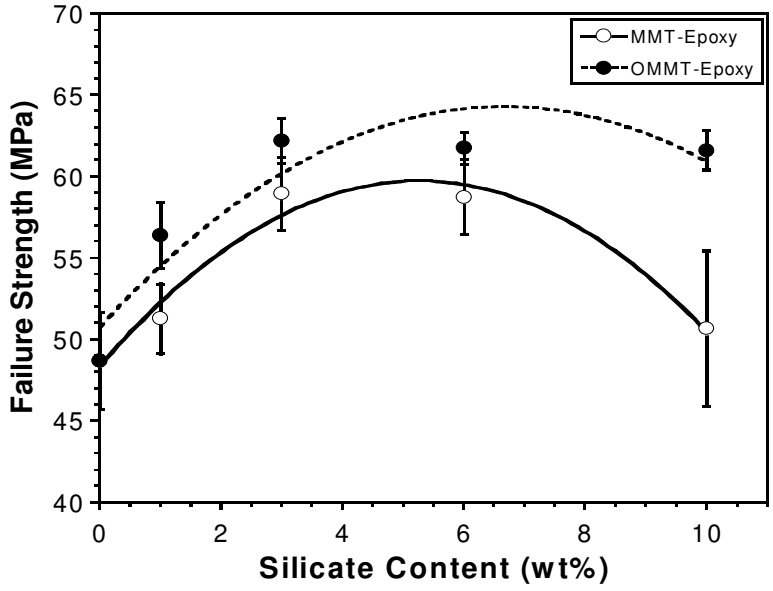

Figure 5.9. Failure strength of the neat epoxy and silicate/epoxy nanocomposites

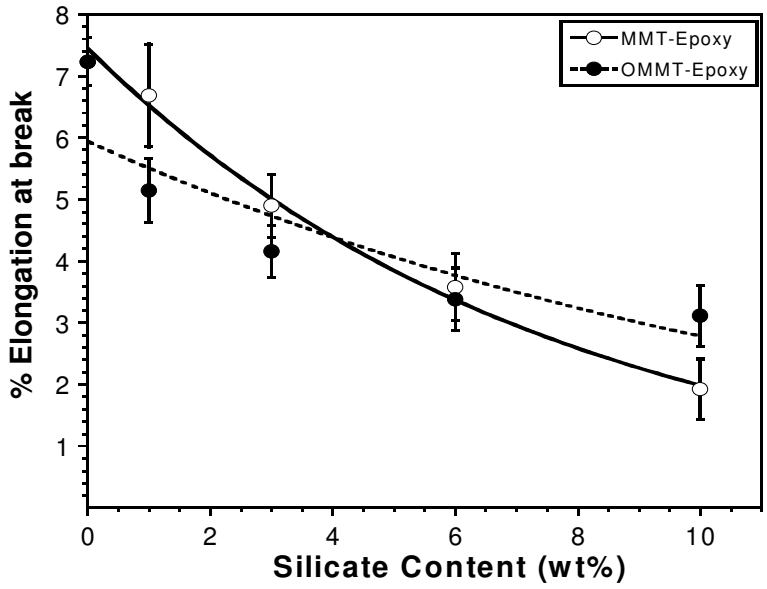

Figure 5.10. % Elongation at break of the neat epoxy and silicate/epoxy nanocomposites

The influence of the nano platelets on the flexural properties of epoxy resin was also investigated. Flexural stress-strain curves for neat epoxy and nanocomposites with MMT and OMMT are given in Figures 5.11 and 5.12, respectively.

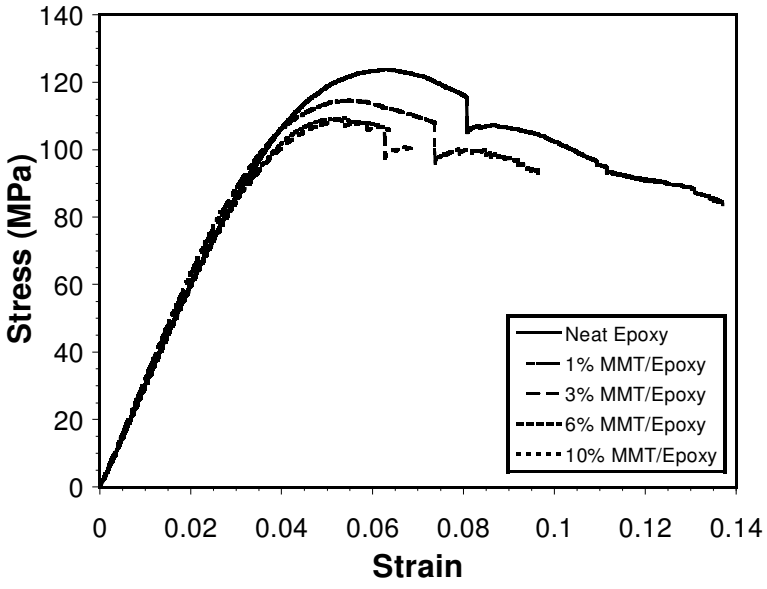

Figure 5.11. The flexural stress-strain curves of neat epoxy and nanocomposites containing MMT

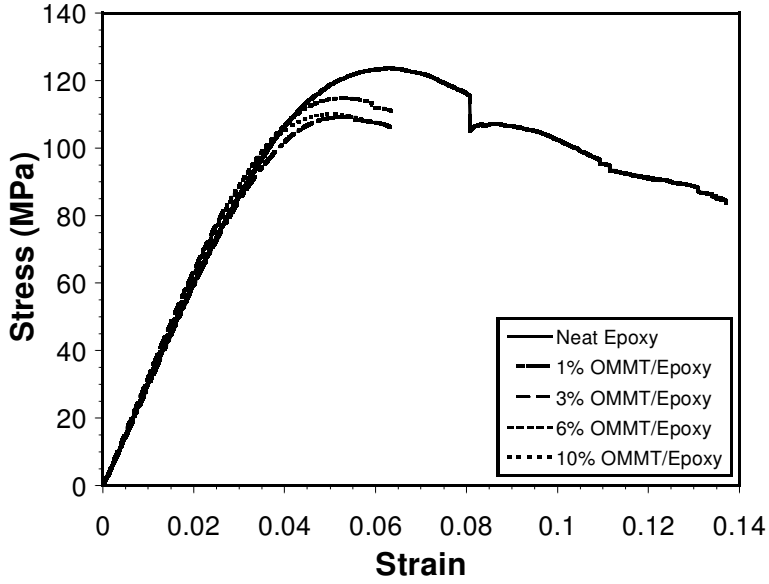

Figure 5.12. The flexural stress-strain curves of neat epoxy and nanocomposites containing OMMT

The flexural modulus of the neat epoxy is about 2.9 GPa. Addition of silicate layers within the epoxy increases the modulus values. OMMT particle addition to the polymer structure better enhances the flexural modulus of epoxy in comparison with MMT due to better dispersion and particle/matrix interfacial interactions. The flexural modulus values are enhanced by 24 % with 6 % OMMT loading. At high silicate loading, agglomeration of the particles reduces the particle/matrix interactions and thus modulus does not futher increase to higher levels. Silicate/Epoxy nanocomposites have been studied by Ranta et al. (Ranta et al. 2003) using diglycidyl ether of bisphenol A (DGEBA) epoxy and treated silicate I.30E which contains octadecylammonium organo-ions lining the surface of the galleries. Similarly, 42% increase in flexural modulus was observed by the incorporation of 5 wt. % OMMT. Also, Dean et al. (Dean et al. 2005) studied the organosilicate/epoxy nanocomposites and it was observed that at low silicate concentrations, as the silicate loading increased, the modulus increased.

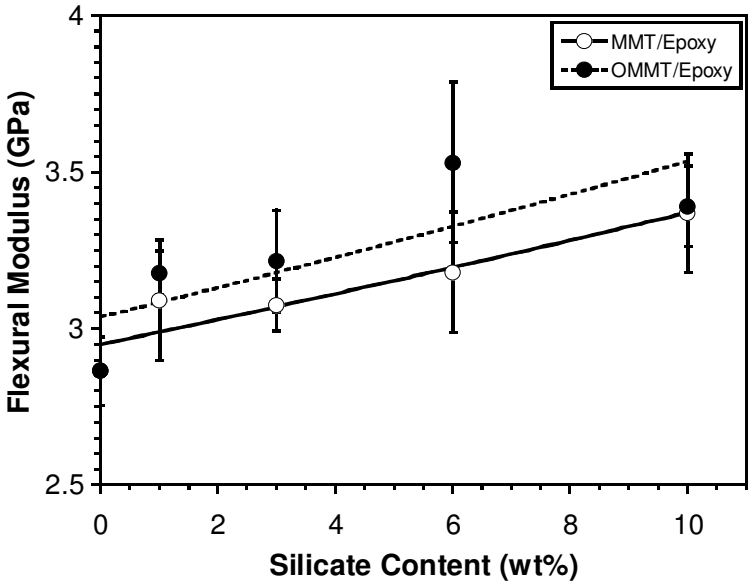

Figure 5.13. Flexural modulus of the neat epoxy and silicate/epoxy nanocomposites

Figure 5.14 shows the flexural strength of the neat epoxy and nanocomposites containing MMT and OMMT. It was found that the flexural strength values decreases for the nanocomposites prepared with MMT and OMMT as compared to neat epoxy. This may be due to the formation of voids, weak adhesion points along the particle/matrix interfacial and agglomerates formed during nanocomposite processing. On these microstructural defects, microcracks may initiate due to local stress concentrations that causes failure at relatively low stresses. On OMMT/epoxy nanocomposites systems, it was observed that a decrease in flexural strength is more than the MMT/epoxy systems. The void formation is dominant effect in these systems due to the surfactant which is used for the surface modification of silicate particles. Similarly, Wetzel et al. (Wetzel et al. 2003) and Dean et al. (Dean et al. 2005) found that the flexural strength of the nanocomposites is reduced with increasing filler content. On the other hand, it was observed that silicate/epoxy nanocomposite containing 5 wt. % OMMT increased the flexural strength by 30%. Also 42 % increase in flexural strength was observed by the incorporation of 5 wt. % OMMT in the silicate/epoxy system that was studied by Ratna et al. (Ranta et al. 2003).

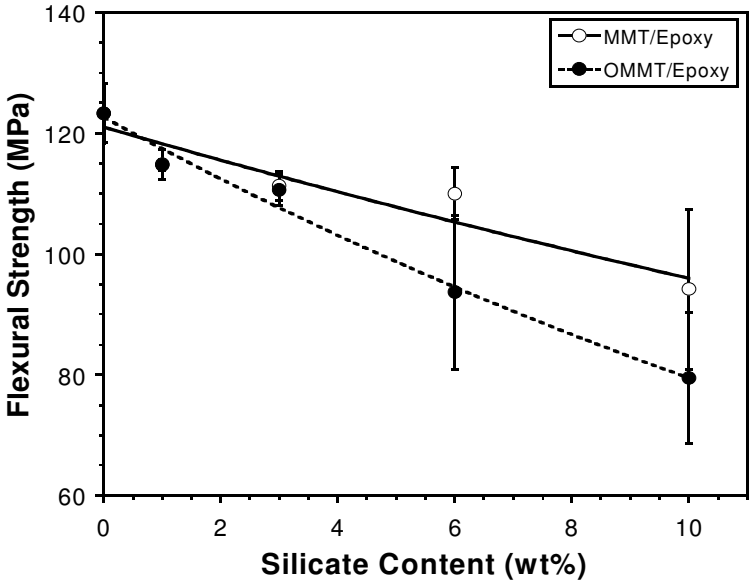

Figure 5.14. Flexural strength of the neat epoxy and silicate/epoxy nanocomposites

The fracture toughness (K_{IC}) values of the materials were measured using the SENB test configuration and Table 5.1 exhibits the fracture toughness values and void content of neat epoxy and nanocomposites made with MMT and OMMT. The K_{IC} value of neat epoxy was measured to be about 0.5 MPa.$m^{1/2}$. K_{IC} values decrease by 44 and 54% with the addition of 10 wt. % of MMT and OMMT silicate particles, respectively. The void content was measured to be about 14.7 and 20.16 % for the same materials. It was found that as the silicate loading is increasing void formation becomes more extensive in the matrix. Figure 15 shows void formation in the nanocomposite matrix containing 6 wt. % MMT particles obtained from the optical microscopy. Black features show the voids in the matrix. The results indicate that K_{IC} is decreasing as the silicate loading is increasing in the matrix. This is associated with the higher amount of voids in the structure. Also, it was found that addition of OMMT particles into the epoxy results in a higher void formation as compared with MMT incorporation. This may be related to the bubble formation due to the surfactant used for surface modifications. Kornmann et al. found that the layered silicate (MMT) /epoxy nanocomposite showed a lower increase in fracture toughness with silicate addition than the nanocomposites due to the apparent lower crosslink density of the epoxy matrix in the nanocomposites (Kornman et al. 2002). However, Liu (Liu 2005) investigated that the nanocomposites made with the direct-mixing method show a higher increase in Kıc than neat epoxy with increasing silicate loading. It showed 80% increase in Kıc of epoxy at 12 phr organosilicate loading but only 45% increase for untreated silicate.

Table 5.1. Fracture toughness (K_{IC}) and void content of neat epoxy and silicate/epoxy nanocomposites prepared with MMT and OMMT.

Nanocomposites	**Silicate Loading (wt%)**	**Fracture Toughness (K_{IC}) (MPa $m^{1/2}$)**	**Void Content (Volume Fraction) (%)**
Neat Epoxy	0	0.498 ± 0.034	0.21 ± 0.13
MMT/Epoxy	1	0.438 ± 0.054	1.21 ± 0.11
	3	0.354 ± 0.021	2.62 ± 0.64
	6	0.334 ± 0.044	5.89 ± 1.30
	10	0.276 ± 0.018	14.71 ± 4.1
OMMT/Epoxy	1	0.275 ± 0.029	3.63 ± 0.9
	3	0.257 ± 0.033	6.62 ±1.2
	6	0.227 ± 0.024	13.04 ± 1.3
	10	0.231 ± 0.023	20.46 ± 3.8

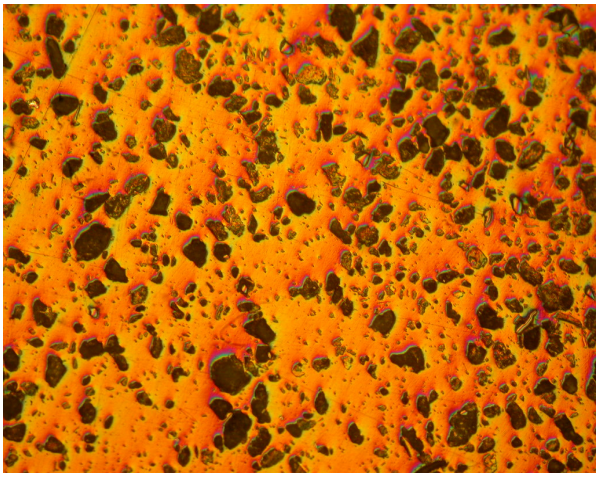

Figure 5.15. Optical microscopy result of 6 wt. % MMT/epoxy nanocomposite

5.2.1. Model Predictions

In this study, the data set given in Tables 5.2 and 5.3 is used to investigate predictive capability of different models. Semi-empirical models for spherical and non spherical particulate cases were used to predict the elastic modulus of the nanocomposites. For this purpose, the experimental data presented in Table 5.2 obtained within the study for MMT/epoxy and OMMT/epoxy nanocomposites. Table 5.3 gives the

values for elastic modulus and Poisson's ratio of the matrix and the filler used in model calculations. Figures 5.16 and 5.17 shows the experimentally measured and predicted elastic modulus values for MMT/epoxy and OMMT/epoxy systems, respectively.

Table 5.2. Elastic modulus of the nanocomposites determined experimentally within the study

Vol. % MMT	Elastic Modulus	Vol. % OMMT	Elastic Modulus
0	3.1255	0	3.1255
0.3	3.3979	0.3	3.2630
0.9	3.4233	0.9	3.3825
1.8	3.5037	1.8	3.5514
3.0	3.5472	3.0	3.6240

Table 5.3. Material data used in models (Source: Wang and Pyrz 2003)

Property	Value
Matrix Poisson's ratio, v_m	0.4
Filler Young's modulus, E_f(Gpa)	150
Filler Poisson's ratio, v_f	0.23

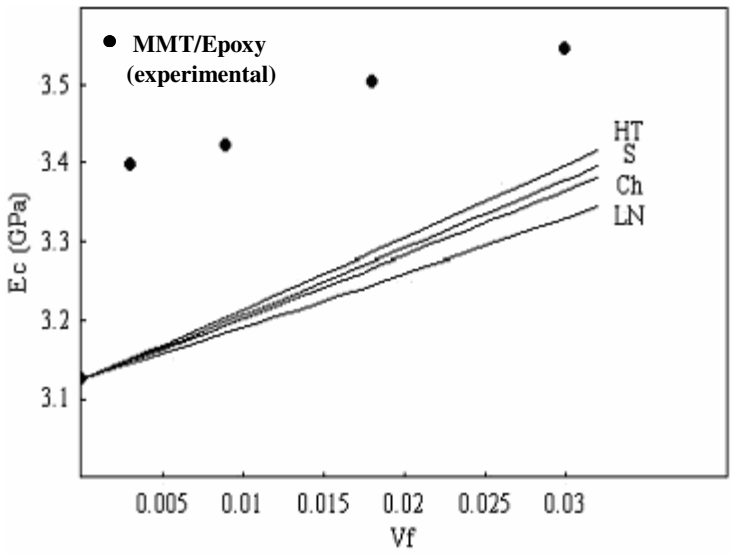

Figure 5.16. Comparison of the experimental data for MMT-Epoxy nanocomposite with semi emprical models (Halpin-Tsai: HT, Chantler: Ch, Lewis-Nilsen: LN, S combining rule: S) used for spherical particulates.

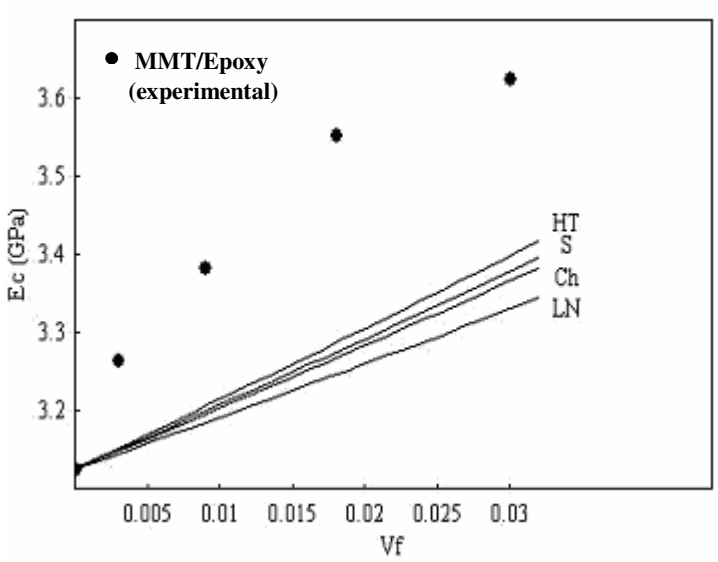

Figure 5.17. Comparison of the experimental data for OMMT-Epoxy nanocomposite with semi empirical models (Halpin-Tsai: HT, Chantler: Ch, Lewis-Nilsen: LN, S combining rule: S) used for spherical particulates.

The mentioned semi-empirical models (Halpin-Tsai, Chantler, Lewis-Nilsen, and S combining rule) were developed for prediction of elastic properties of composite systems that contain spherical particulates. As seen from the figures, the models that consider spherical particles can not satisfactorily correlate with the experimental data. These results also imply that non-spherical particle geometry is presented for silica/epoxy systems. Therefore, the other models that were developed considering non-spherical particle geometry are used in the following parts.

5.2.1.1. Determination of the aspect ratio and maximum volumetric fraction

5.2.1.1.1. The MMT-Epoxy nanocomposite

Modified Halpin-Tsai (Nielsen 1970) and Brodnyan model (Brown and Ellyin 2005) are the models developed recently considering non-spherical particulate reinforced composites. The detailed information about the models was given in Chapter III. These models require the consideration of maximum volumetric fraction of filler (V_f^{max}) and this value must be determined. Based on Modified Halpin-Tasi and Brodnyan models,

Figures 5.18 and 5.19 show the effect of V_f^{max} for various aspect ratio of the filler on the composite elastic modulus vs. filler volume fractions based on modified Halpin-Tsai model and Brodnyan model for MMT/epoxy nanocomposites, respectively. The experimental data is also presented in the same figures. It is observed that V_f^{max} has very small effect in both of the models since we consider low volume fractions of the filler (<%3.5). Therefore, determination of V_f^{max} is not critical and it can be taken as an arbitrary parameter. As reported in the literature, V_f^{max} value for nanocomposite systems is generally smaller than those obtained for standard composites (micro particulate, fiber filled...). For example, Wu et al. (Wu et al. 2004) determined the maximum volumetric fraction as a fitting parameter and the values of V_f^{max} was obtained as 0.2, 0.16 and 0.15 for styrene butadiene rubber (SNBR)-silicate, nitrile butadiene rubber (NBR)-silicate, carboxylated nitrile-butadiene rubber (CNBR)-silicate nanocomposites, respectively. Lingois and Berglund (Lingois et al. 2002) reported. V_f^{max} value of 0.66 for uniformly sized spheres and V_f^{max} value of 0.66 and 1 for random packing and for non-uniformly sized particles in dental composites. In the study of Kalaprasad et al. (Kalaprasad et al. 1997), for short sisal fibre-reinforced low density polyethylene composites, V_f^{max} has a value of 0.785 for square arrangement of fibers, 0.907 for hexagonal array of fibers and 0.82 for random packing of fibers. In the present study, V_f^{max} was assumed to be 0.20 for calculations in Modified Halpin-Tsai and Brodnyan models.

Figures 5.18, 5.19, 5.20 and 5.21 show the effect of aspect ratios on the elastic properties of the composite based on semi emprical models of Modified Halpin-Tsai, Brodnyan, Guth, and Halpin-Tsai and give a comparison with the experimental data for the MMT-epoxy nanocomposite. It is obvious that aspect ratio α is very effective parameter for all of the model at low and high volume fraction of fillers.

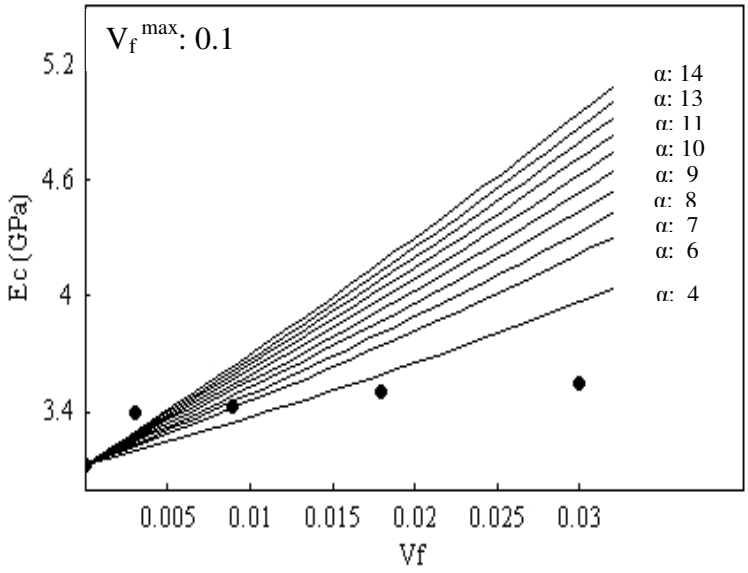
$V_f{}^{max}$: 0.1
5.2
4.6
4
3.4
Ec (GPa)
0.005
0.01
0.015
0.02
0.025
0.03
Vf
α: 14
α: 13
α: 11
α: 10
α: 9
α: 8
α: 7
α: 6
α: 4

(a)

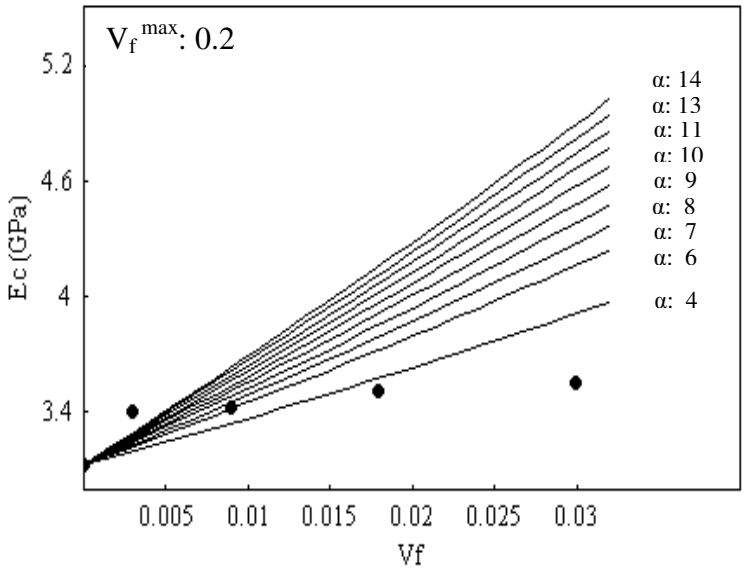
$V_f{}^{max}$: 0.2
5.2
4.6
4
3.4
Ec (GPa)
0.005
0.01
0.015
0.02
0.025
0.03
Vf
α: 14
α: 13
α: 11
α: 10
α: 9
α: 8
α: 7
α: 6
α: 4

(b)

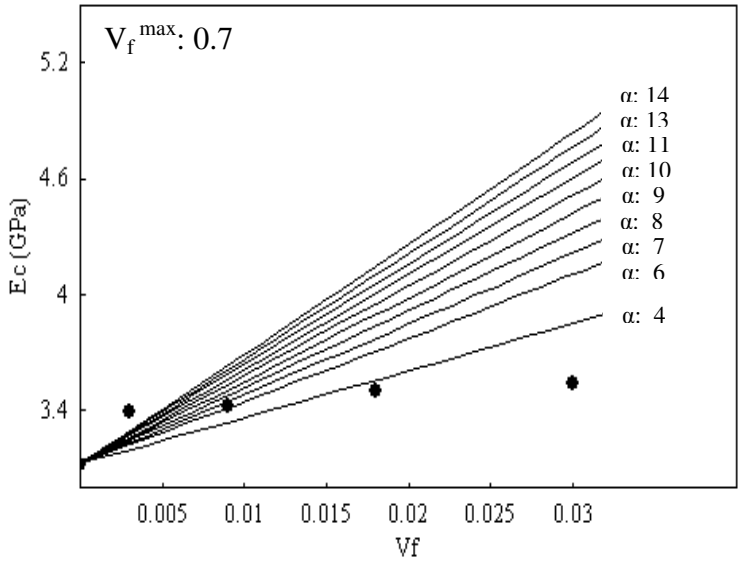

(c)

Figure 5.18. For $V_f{}^{max}$ is a) 0.1, b) 0.2, and c) 0.7, effect of the aspect ratio, α, on the elastic modulus of the composite reinforced by non-spherical particulate fillers based on Modified Halpin-Tsai equation for comparison experimental data for MMT/Epoxy is presented with (•) symbol.

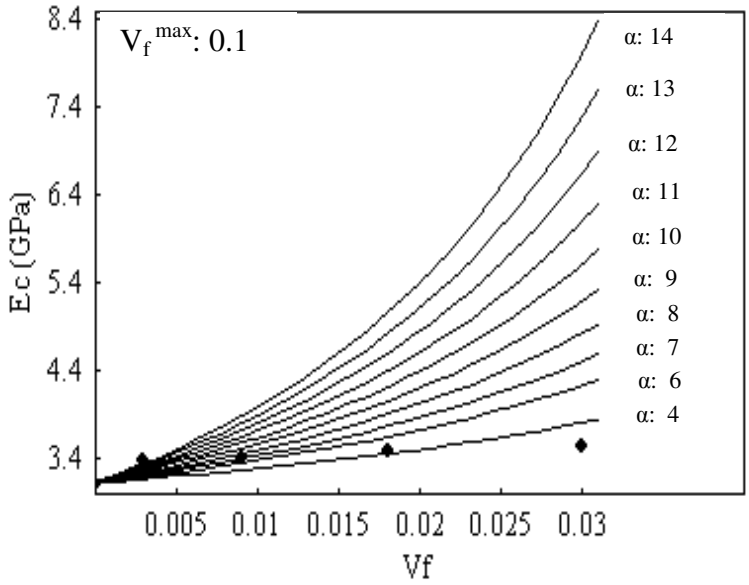

(a)

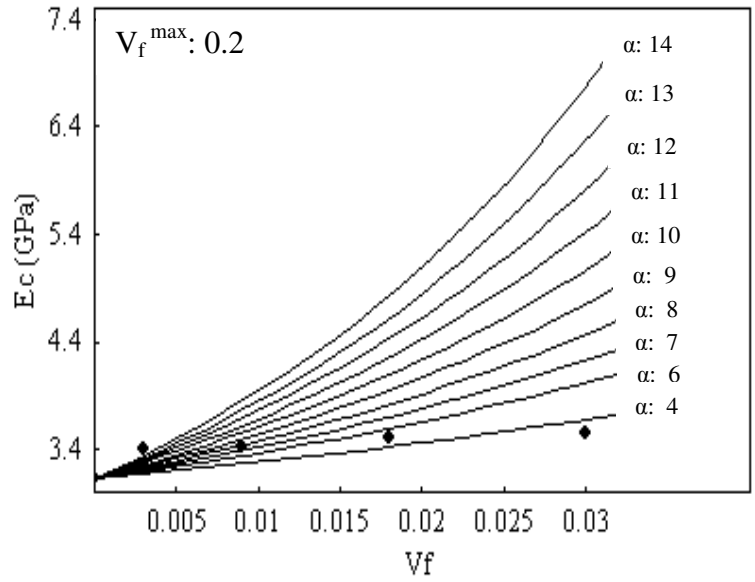

(b)

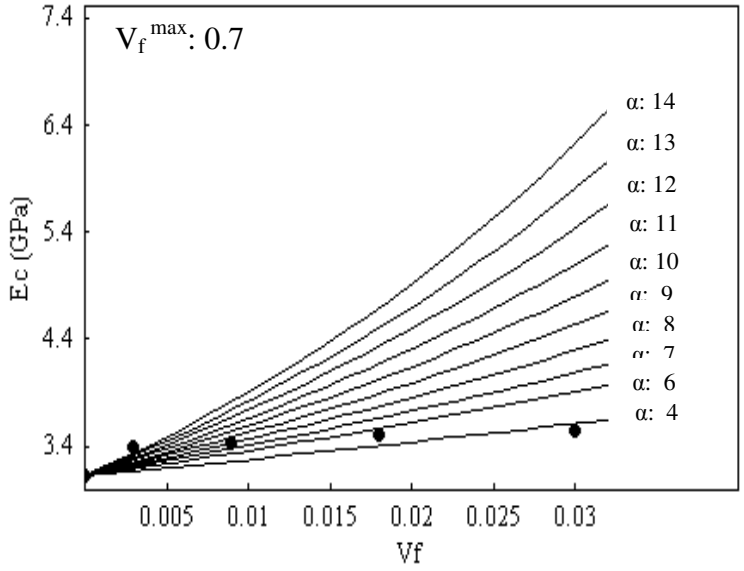

(c)

Figure 5.19. For V_f^{max} is a) 0.1, b) 0.2, and c) 0.7, effect of the aspect ratio, α, on the elastic modulus of the composite reinforced by non-spherical particulate fillers based on Brodnyan equation for comparison experimental data for MMT/Epoxy is presented with (•) symbol.

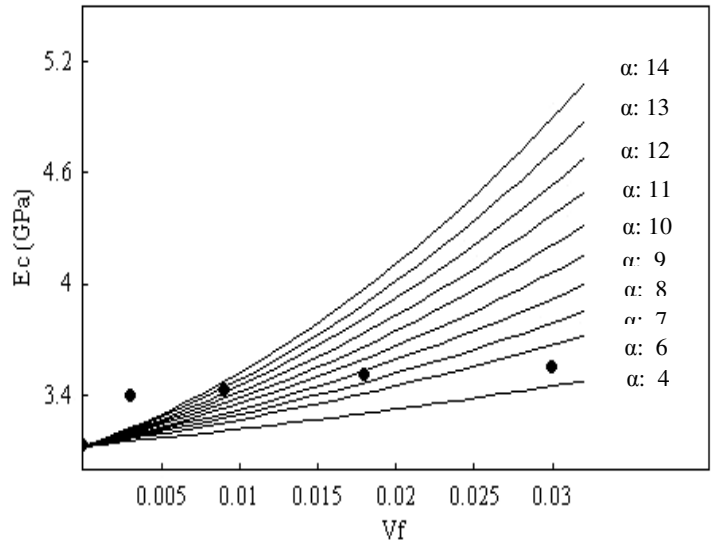

Figure 5.20. Effect of the aspect ratio, α, on the elastic modulus of the composite reinforced by non-spherical particulate fillers based on Guth equation for comparison experimental data for MMT/Epoxy is presented with (•) symbol.

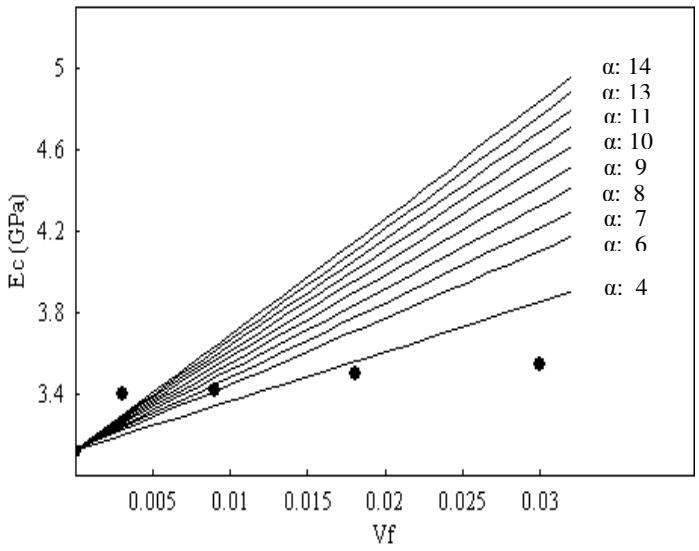

Figure 5.21. Effect of the aspect ratio, α, on the elastic modulus of the composite reinforced by non-spherical particulate fillers based on Halpin-Tsai equation for comparison experimental data for MMT/Epoxy is presented with (•) symbol.

In these models, the higher aspect ratio of silicate particle provides a higher improvement of the elastic modulus of the composite. In other words, as the surface area of the silicate layers that has thickness in nanometer level increases, the reinforcing efficiency of the particle is increasing and thus the elastic modulus is enhancing. As seen in Figures 5.18, 5.19, 5.20 and 5.21, it is clear that if the aspect ratio (α) is taken in the interval of 4-7, most of the models has a good match with the experimental data for MMT/epoxy nanocomposite and also best fit can be provided in the case of α =5. For the clarity, the E_c vs. V_f values are presented for α=5 and V_f^{max} = 0.2 in Figures 5.22 to 5.25.

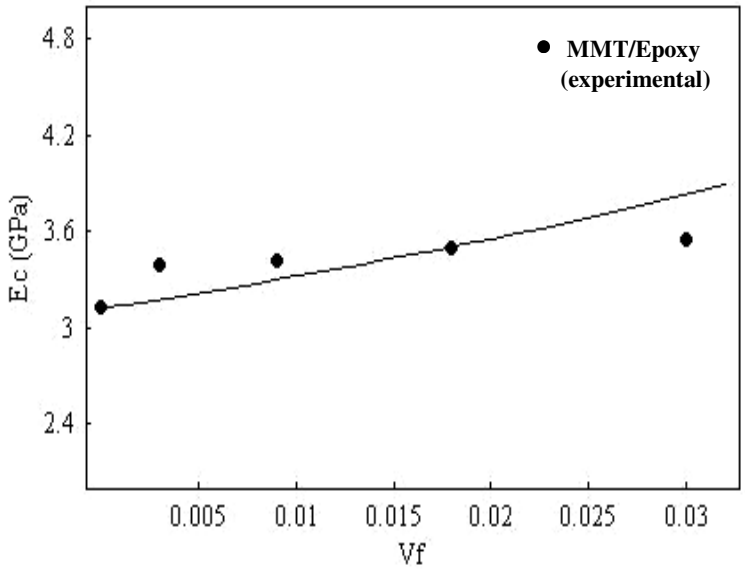

Figure 5.22. Comparison of the experimental data of E_c vs. V_f for MMT/Epoxy nanocomposites and theoretical prediction based on Brodnyan model for aspect ratio (α) =5 and V_f^{max} = 0.2

As seen from the figures, Brodnyan model has a much better agreement with the experimental data while Halpin-Tsai and Modified Halpin-Tsai models have relatively worse fit with the data for MMT/epoxy system. Modified Halpin-Tsai and Halpin Tsai produce almost the same value because of the low volume fraction of the particles taken into calculation within the study. With Guth model, we have an under estimation of E_c values for α =5.

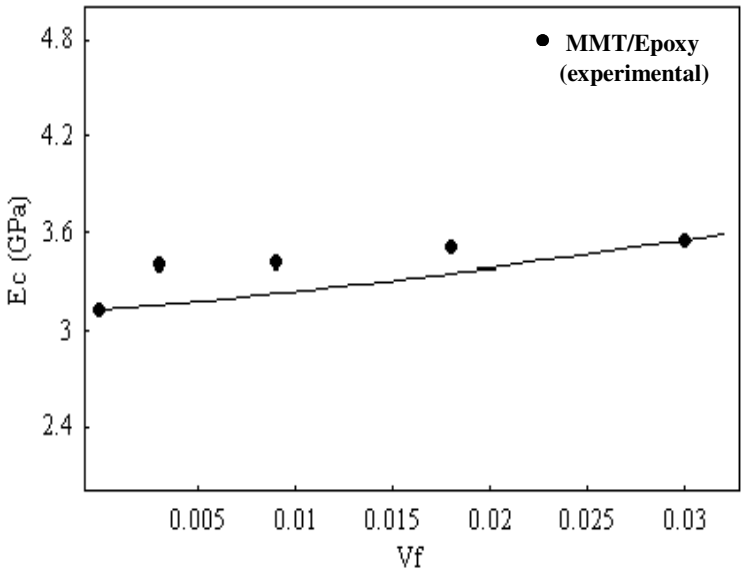

Figure 5.23. Comparison of the experimental data of E_c vs. V_f for MMT/Epoxy nanocomposites and theoretical prediction based on Guth model for aspect ratio (α) =5

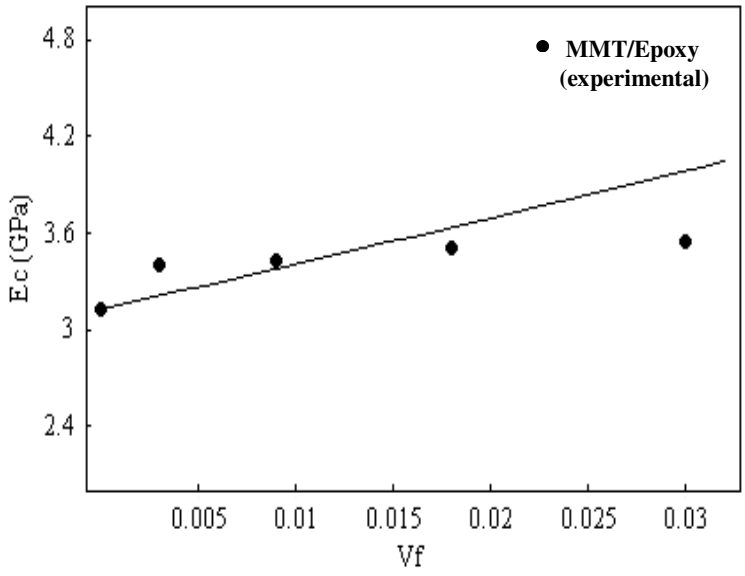

Figure 5.24. Comparison of the experimental data of E_c vs. V_f for MMT/Epoxy nanocomposites and theoretical prediction based on Halpin-Tsai model for aspect ratio (α) =5

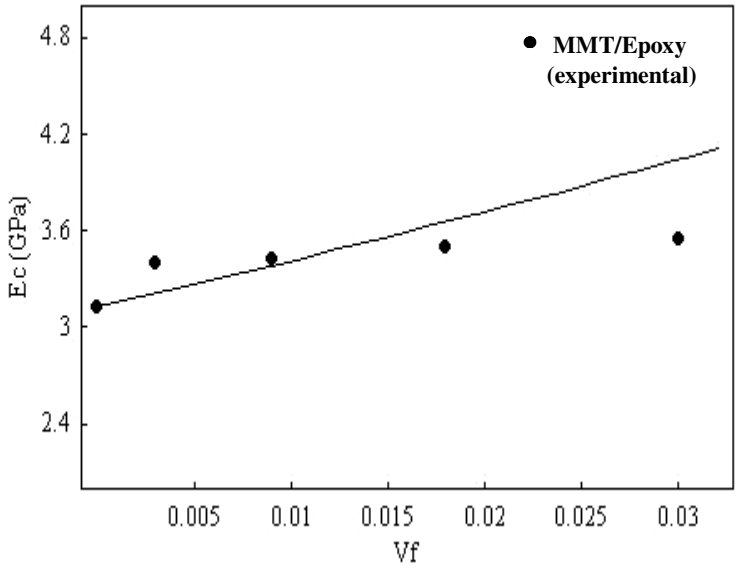

Figure 5.25. Comparison of the experimental data of E_c vs. V_f for MMT/Epoxy nanocomposites and theoretical prediction based on Modified Halpin-Tsai model for aspect ratio (α) =5 and $V_f^{max} = 0.2$

5.2.1.1.2. The OMMT/epoxy nanocomposite

It was revealed in the previous section that the V_f^{max} can be taken as an arbitrary parameter in an appropriate interval. Similar to MMT/epoxy, it is assumed that V_f^{max} is 0.2 for OMMT/epoxy nanocomposite system. As it can be also seen from Figures 5.26 and 5.27 for both of Modified Halpin-Tsai and Brodnyan models, the variation of E_c value as a function of V_f^{max} is almost negligible. Figures 5.27 to 5.29 also show the effect of aspect ratio on E_c vs. V_f graphs for Modified Halpin-Tsai, Brodnyan, Guth, and Halpin-Tsai and give a comparison with the experimental data for the OMMT/epoxy nanocomposite.

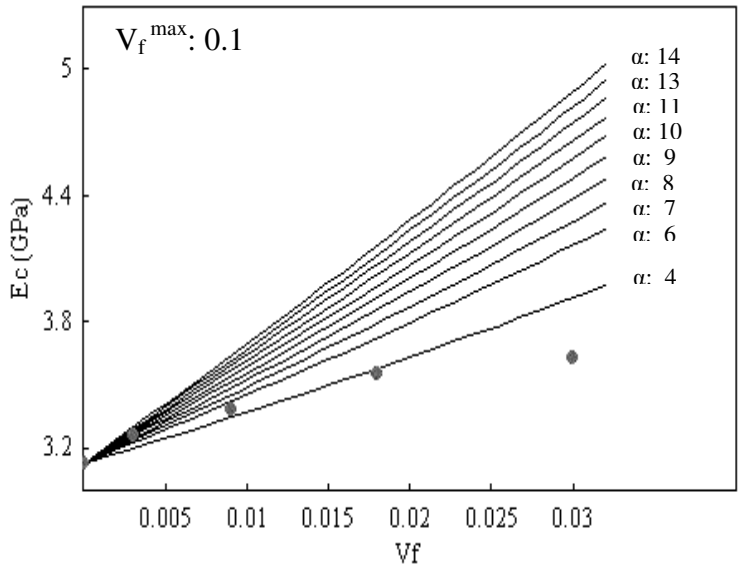
V_f^{max}: 0.1
α: 14
α: 13
α: 11
α: 10
α: 9
α: 8
α: 7
α: 6
α: 4
Ec (GPa)
5
4.4
3.8
3.2
0.005
0.01
0.015
0.02
0.025
0.03
Vf

(a)

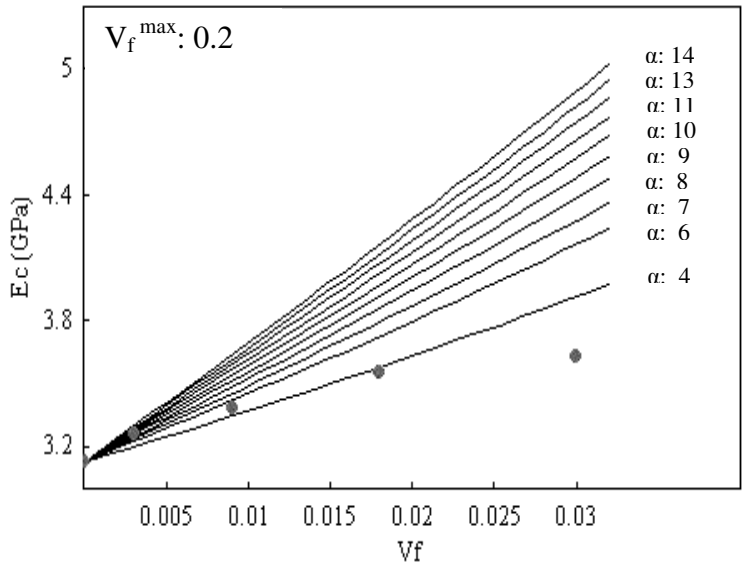
V_f^{max}: 0.2
α: 14
α: 13
α: 11
α: 10
α: 9
α: 8
α: 7
α: 6
α: 4
Ec (GPa)
5
4.4
3.8
3.2
0.005
0.01
0.015
0.02
0.025
0.03
Vf

(b)

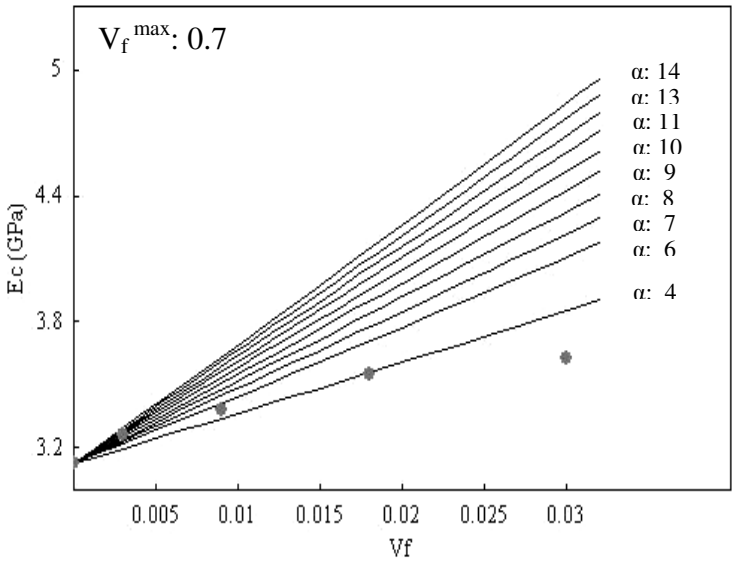

(c)

Figure 5.26. For V_f^{max} is a) 0.1, b) 0.2, and c) 0.7, effect of the aspect ratio, α, on the elastic modulus of the composite reinforced by non-spherical particulate fillers based on Modified Halpin-Tsai method for comparison experimental data for OMMT/Epoxy is presented with (•) symbol.

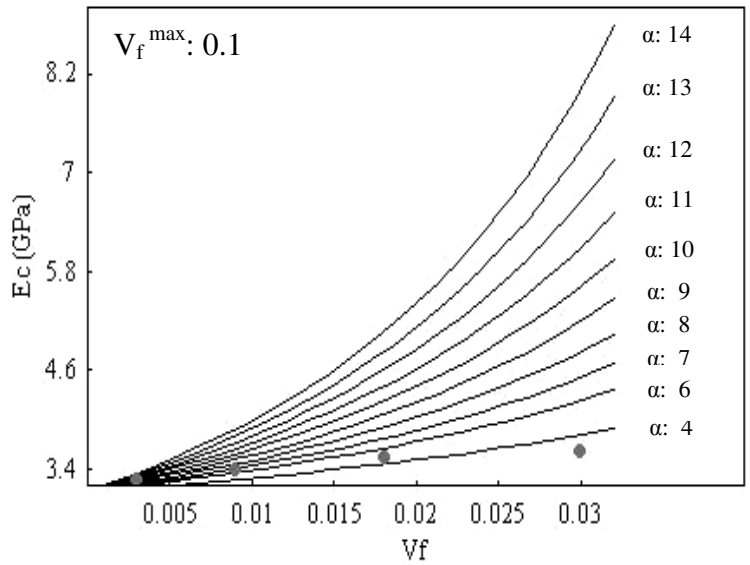

(a)

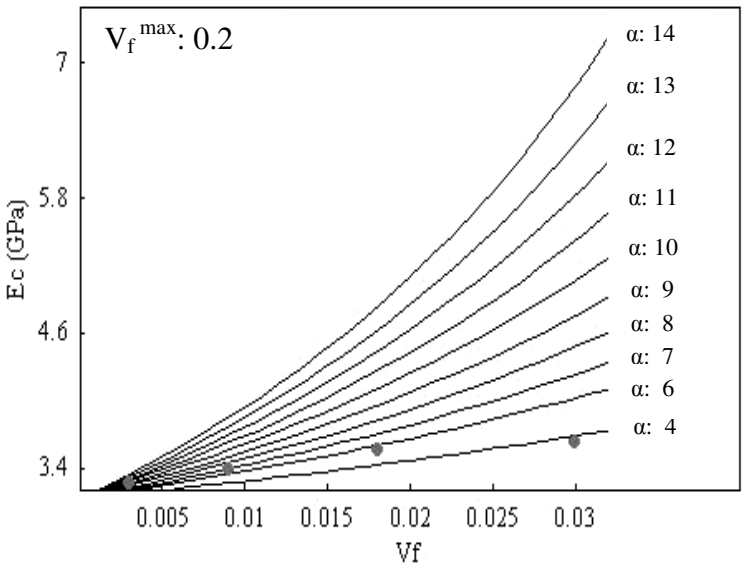

(b)

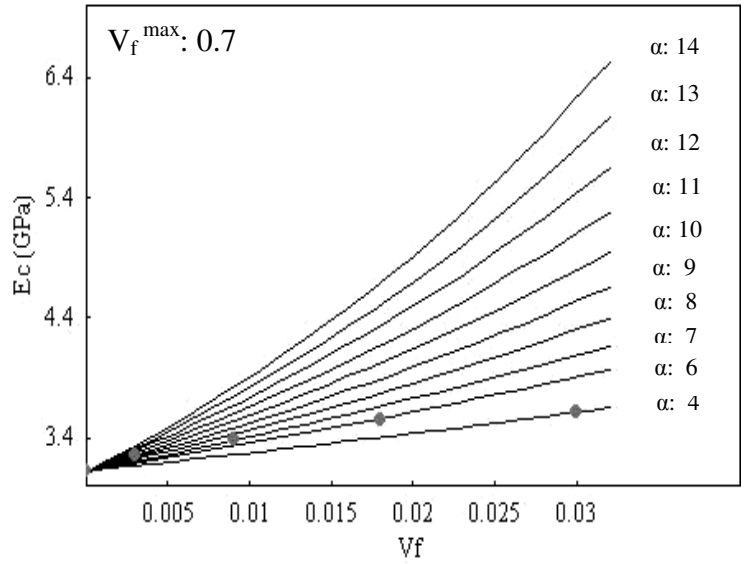

(c)

Figure 5.27. For V_f^{max} is a) 0.1, b) 0.2, and c) 0.7, effect of the aspect ratio, α, on the elastic modulus of the composite reinforced by non-spherical particulate fillers based on Brondyan equation for comparison experimental data for OMMT/Epoxy is presented with (•) symbol.

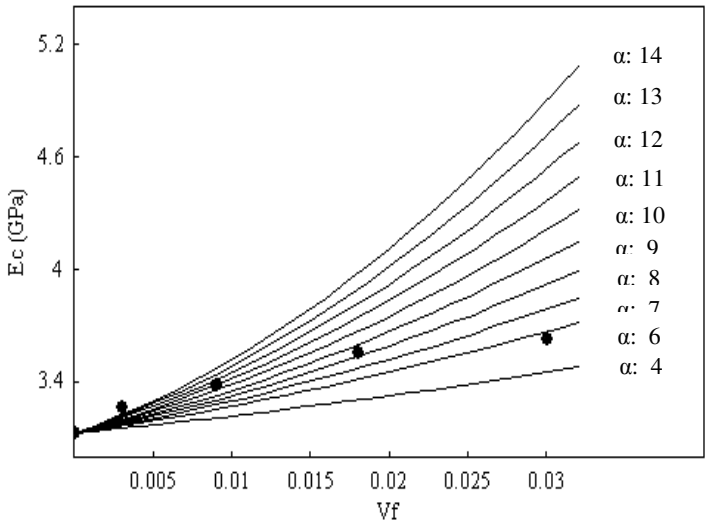

Figure 5.28. Effect of the aspect ratio, α, on the elastic modulus of the composite reinforced by non-spherical particulate fillers based on Guth equation for comparison experimental data for OMMT/Epoxy is presented with (•) symbol.

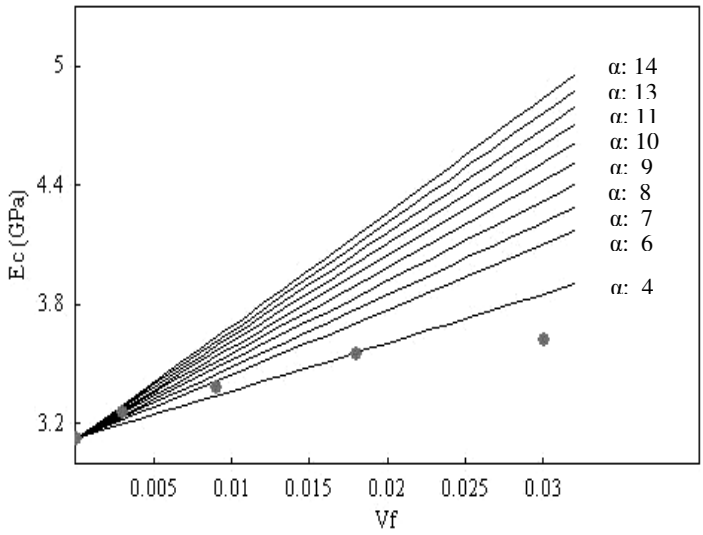

Figure 5.29. Effect of the aspect ratio, α, on the elastic modulus of the composite reinforced by non-spherical particulate fillers based on Halpin-Tsai equation for comparison experimental data for OMMT/Epoxy is presented with (•) symbol.

The same behaviour with MMT/epoxy is observed and therefore, if the aspect ratio α is taken as in the interval 4-7, most of the models have a good match with the experimental data for OMMT/epoxy nanocomposite and also best fit can be provided by α =5. The results are given in Figures 5.30, 5.31, 5.32 and 5.33.

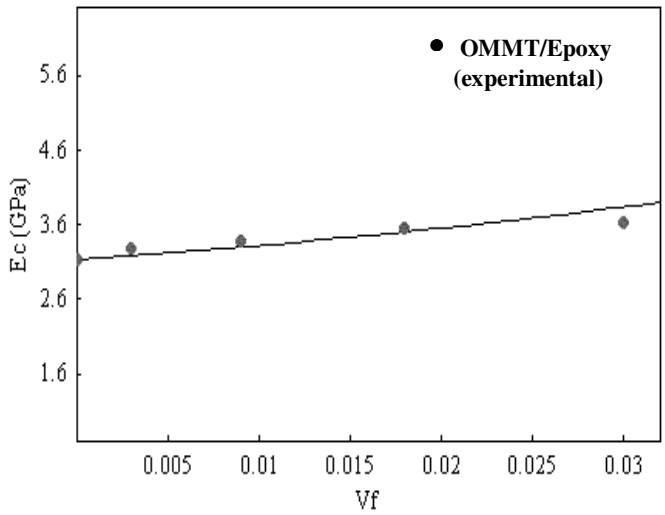

Figure 5.30. Comparison of the experimental data of E_c vs. V_f for OMMT/Epoxy nanocomposites and theoretical prediction based on Brodnyan model for aspect ratio (α) =5 and $V_f^{max} = 0.2$

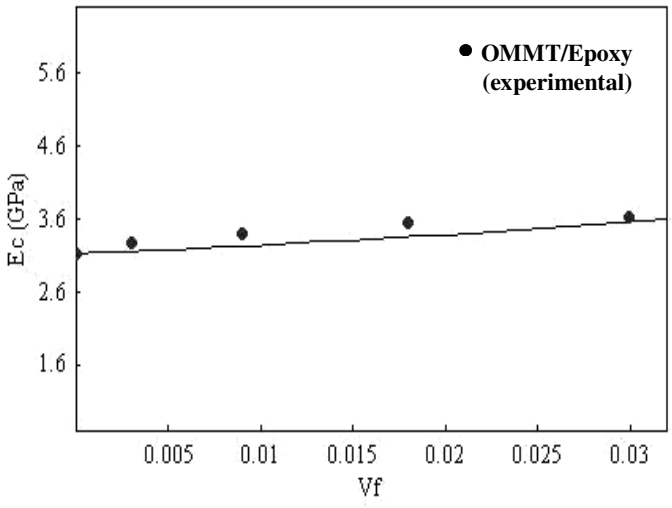

Figure 5.31. Comparison of the experimental data of E_c vs. V_f for OMMT/Epoxy nanocomposites and theoretical prediction based on Guth model for aspect ratio (α) =5

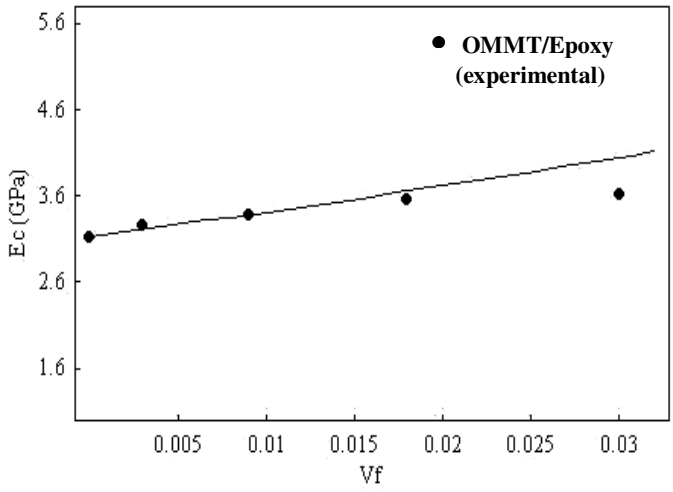

Figure 5.32. Comparison of the experimental data of E_c vs. V_f for OMMT/Epoxy nanocomposites and theoretical prediction based on Modified Halpin-Tsai model for aspect ratio (α) =5 and $V_f^{max} = 0.2$

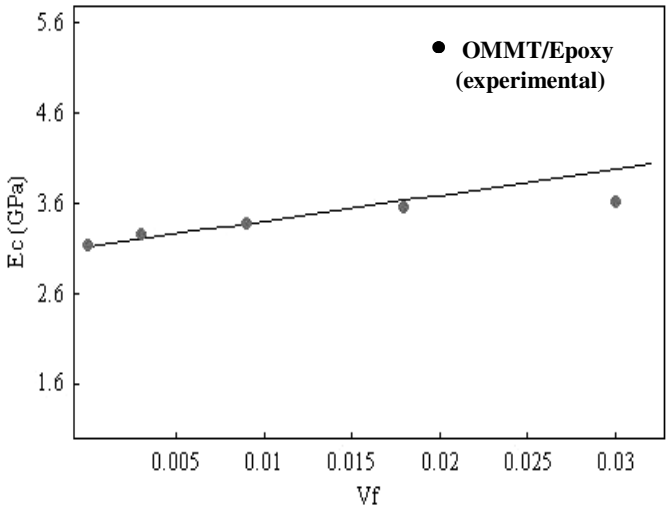

Figure 5.33. Comparison of the experimental data of E_c vs. V_f for OMMT/Epoxy nanocomposites and theoretical prediction based on Halpin Tsai model for aspect ratio (α) =5 and $V_f^{max} = 0.2$

Correlative capability of Brodnyan, Halpin-Tsai and Modified Halpin-Tsai models was found to be very good as compared to Guth model for OMMT-epoxy nanocomposites. Halpin-Tasi and Modified Halpin-Tsai models produced almost the same values because of the low volume fraction of the particles. With Guth model, similar to MMT system we have an under estimate of E_c values for α =5.

In summary, all of the used models considering non-spherical particles embedded within the polymer matrix showed good agreement with experimental data. Among various models, Brodnyan model produced the best correlation for elastic modulus of MMT/epoxy and OMMT/epoxy nanocomposite systems.

5.3. Thermal Behavior of Nanocomposites

Figures 5.34 and 5.35 show the DSC thermograms of neat epoxy and the nanocomposites prepared with MMT and OMMT, respectively. The T_g value of neat epoxy is 63.6 °C. The T_g values of epoxy remains almost constant with the addition of MMT. The For OMMT/epoxy nanocomposites, at low concentration of silicate addition, T_g increases up to 68.9 °C with 3 wt. % addition of OMMT. However, further addition of OMMT reduces the T_g up to T_g of neat epoxy. This observation suggests that organically modified silicates at relatively low contents better disperse in the polymer system and it restricts the motion of the epoxy network in the silicate/epoxy system.

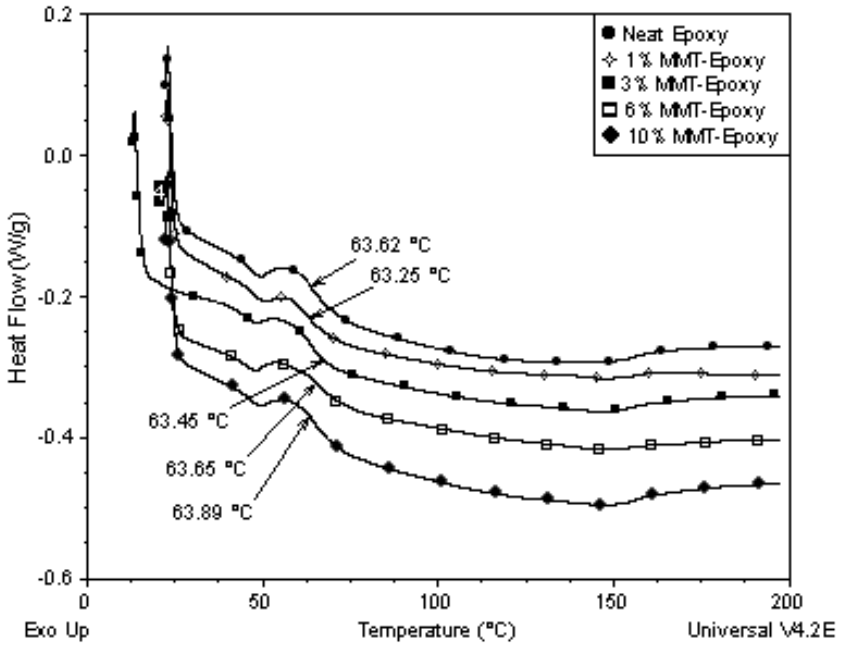

Figure 5.34. DSC thermograms for neat epoxy and MMT/epoxy nanocomposites for various MMT content

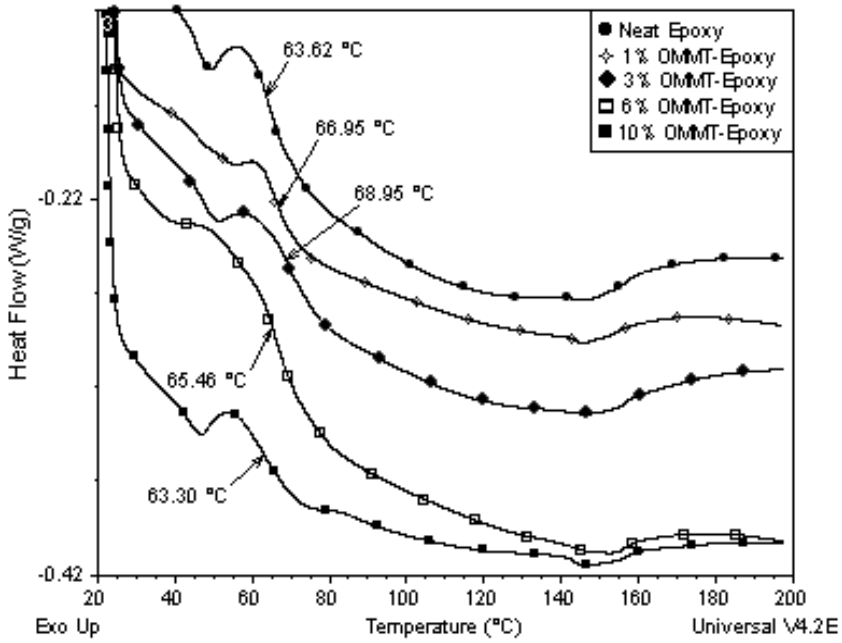

Figure 5.35. DSC thermograms for neat epoxy and OMMT/epoxy nanocomposites for various OMMT content

At relatively higher concentration, OMMT have plasticizing effect that compensates the stiffening effect of the silicate layers. Plasticizing effects may be due to the presence of higher fraction of the surfactant, used for surface modification, at high silicate contents. So, these two effects may have contribution on the chains to commence transition from the rigid glassy state to the soft rubbery state. Chen et al. (Chen et al. 2002) and Feng et al. (Feng et al. 2002) similarly investigated the thermal behaviour of nanocomposites and they found that the addition of MMT during the polymerization of the epoxy polymer decreased the T_g. On the other hand, higher T_g value was obtained by incorporation of OMMT. Isık et al. (Isik et al. 2003) also investigated the glass transition temperature of the nanocomposites of layered silicate/ epoxy. It was seen an increase in T_g with respect to montmorillonite loading. This behaviour was explained based on the mobility of the polymer chains hindered due to the interaction between the silicate and polymer molecules resulting in higher T_g. However, a gradual decrease of T_g by loading of silicate was observed for the montmorillonite/epoxy nanocomposites (Nigam et al. 2004). Authors have explained the decrease in T_g based on the plasticizing effect of the excess of unreacted curing agent.

The dynamic mechanical properties of composites were also studied. The dynamic storage modulus, loss modulus and tan δ versus temperature for neat epoxy and

nanocomposites prepared with 3 wt. % of MMT and OMMT are shown in Figures 5.36 to 5.38. Storage modulus values were taken at room temperature and the loss modulus was taken as a maximum value getting from peak of curve.

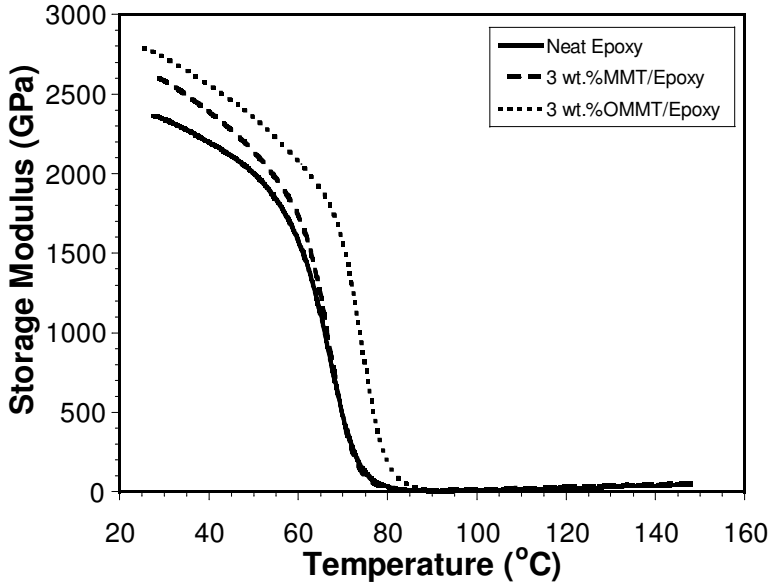

Figure 5.36. Storage modulus versus temperature plots of neat epoxy and nanocomposites containing 3 wt.% MMT and OMMT.

The storage modulus of the nanocomposites containing MMT and OMMT particles are significantly higher than that of the neat epoxy as shown in Figure 5.39. About 16 and 23 % increase in storage modulus are achieved as a result of incorporation of 10 wt.% of MMT and OMMT silicate layers into the epoxy matrix, respectively. The nanocomposites, in general, show higher loss modulus compared to the neat epoxy as shown in Figure 5.40. The loss modulus of nanocomposites prepared with 10 wt. % MMT and OMMT are increased by about 36.8 and 40.7 %. Zhang et al. (Zhang et al. 2004) also examined the dynamic mechanical properties of composites prepared with diglycidyl ether of bisphenol A type epoxy resin and sodium silicate. As a result it was found that when the temperature was lower than the T_g, the storage modulus of the composite are increased by 42.86 % (from 2.17 to 3.10 GPa) as compared to neat epoxy.

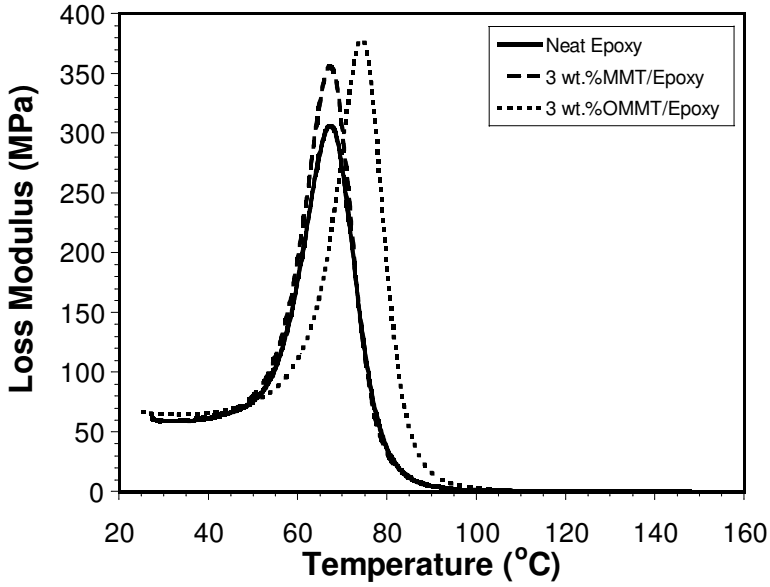

Figure 5.37. Loss modulus versus temperature plots of neat epoxy and nanocomposites containing 3 wt. % MMT and OMMT.

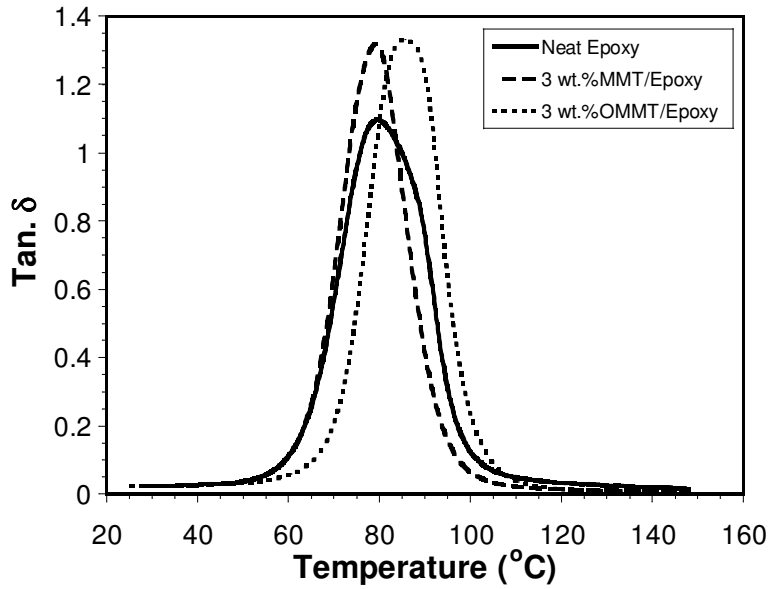

Figure 5.38. Tan. δ versus temperature plots of neat epoxy and nanocomposites containing 3 wt.% MMT and OMMT.

Similarly Ranta et al. (Ranta et al. 2003) and Chen and Curliss (Chen and Curliss 2003) reported a similar increase in storage modulus for the montmorillonite/epoxy

nanocomposite system. This behaviour was attributed to the high stiffness and high aspect ratio of the organoclay filler which is frequently assumed to exceed above 1000.

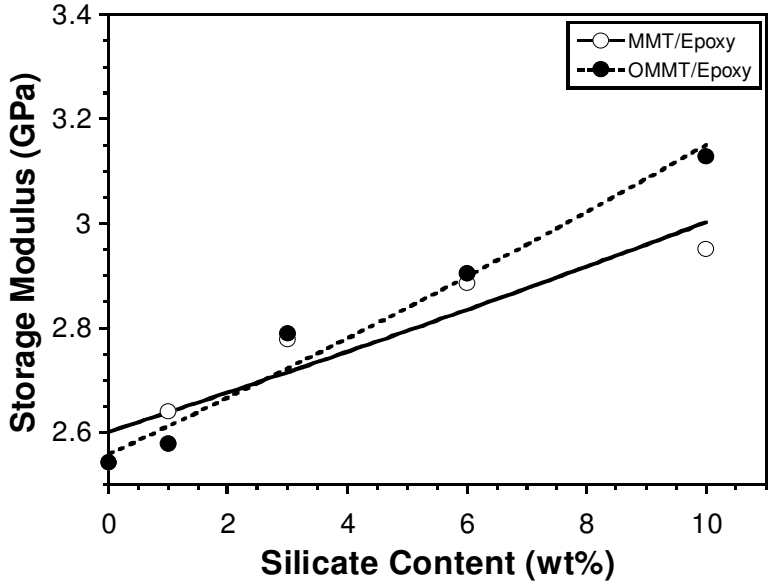

Figure 5.39. Storage modulus of the neat epoxy and silicate/epoxy nanocomposites as a function of silicate content.

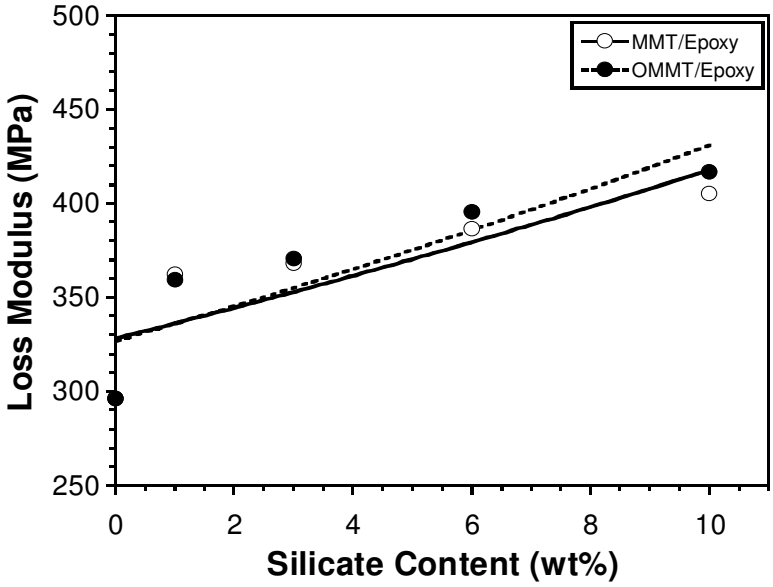

Figure 5.40. Loss modulus of the neat epoxy and silicate/epoxy nanocomposites as a function of silicate content.

Based on the tan δ peak temperature, as shown in Figure 5.38, the T_g of neat epoxy was determined as 77.94 ^oC. The T_g values of the nanocomposites contaning MMT particles are close to the pure resin as shown in Figure 5.41. The nanocomposites prepared with OMMT up to same concentration (6 wt. %) show higher T_g values as compared to neat epoxy. Incorporation of 3 % OMMT resulted by a 14.7 ^oC increase in the T_g of epoxy. However, it was observed that a futher addition of OMMT into the nanocomposites decreased the glass temperature. The decrease of the T_g of the nanocomposites at high concentrations may be associated with the plasticizing effect of the surfactant used, similar to the behaviour observed in the DSC analysis. Similarly, it was observed by DSC that incorporation of silicate increased up to 5 % the T_g of the epoxy resin. This may be related to the confinement of polymer chains as a result of intercalation into the interlayer gallery of the clay.

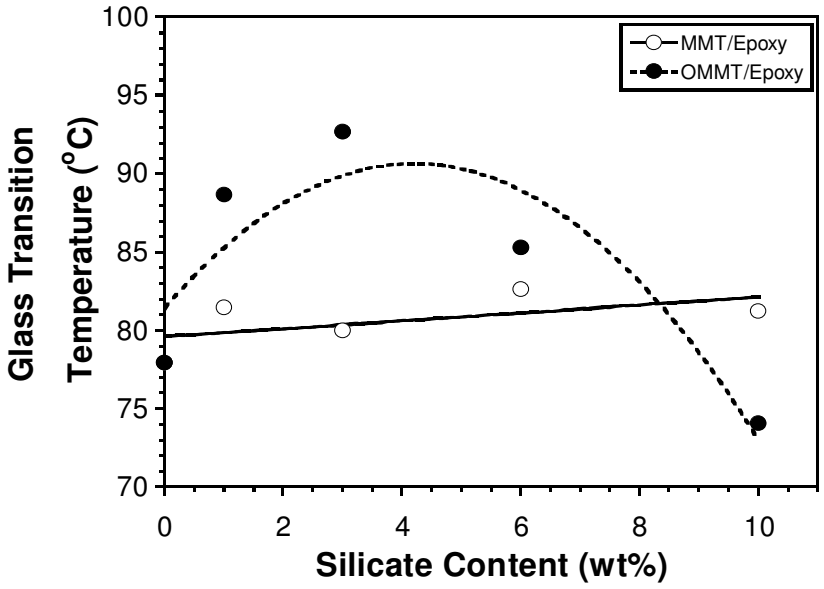

Figure 5.41. Glass transition temperature of the neat epoxy and silicate/epoxy nanocomposites as a function of silicate content.

5.4. Optical Property of the Nanocomposites

Optical transmission values of the neat epoxy and nanocomposites were measured by UV-Visible spectroscopy. Figures 5.42 and 5.43 are the typical examples showing the light transmission spectra in the 200-1100 nm wavelength range of nanocomposites with

1 wt. % MMT and OMMT for four different in thicknesses (1, 2, 4 and 6 mm) of the samples. The transmission values decrease with increasing the specimen thickness, as expected. Surface modified OMMT silicate particle additions to epoxy matrix exhibits better light transmission in comparison with MMT loading.

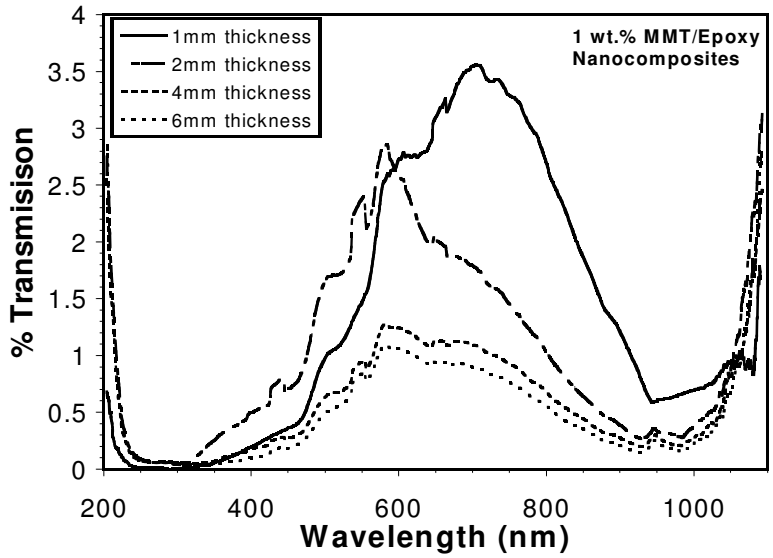

Figure 5.42. Light transmition rate for 1 wt. % MMT/epoxy nanocomposites at various thicknesses.

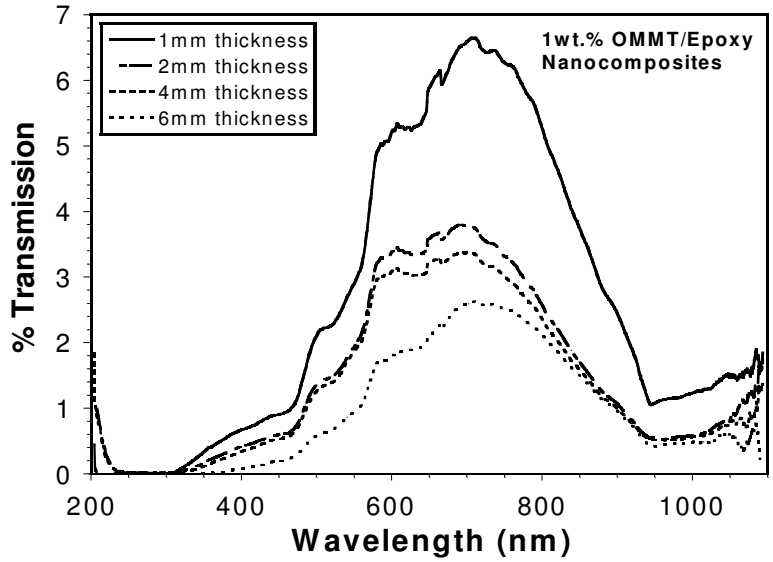

Figure 5.43. Light transmittion rate for 1 wt. % OMMT/epoxy nanocomposites at various thicknesses.

The transmission values at 700 nm wavelength for neat epoxy and nanocomposites made with MMT and OMMT silicates at various loadings are shown in Figure 5.44. Light transmission of neat epoxy at 700 nm was measured to be about approximately 23 %. Optical transmission values are affected by MMT and OMMT silicate incorporation into the epoxy. As the silicate loading increases, transmission value decreases and the materials turned into opaque. Nanocomposites containing OMMT silicate particles have slightly better transmission than those with MMT due to better exfoliation of the organically modified silicate layers in the matrix. Silicate layers with sizes less than the wavelength of visible light do not hinder light's passage. However, the silicate layers have the dimensions in the micrometers the thickness in nanometer range. Therefore, the large surface of the silicate plaques acts to scatter the light transmission and as the content of the plaques increases, the light passage is more hindered.

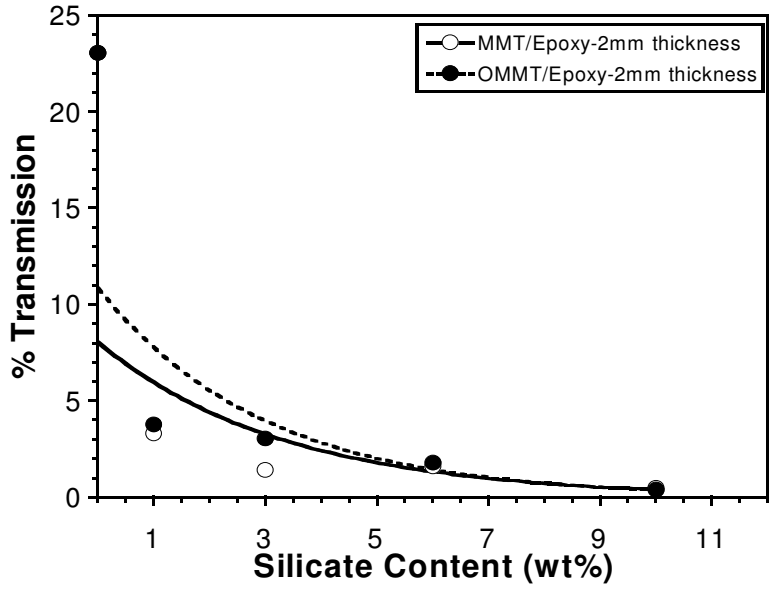

Figure 5.44. Percent transmitance of visible light at 700 nm as a function of silicate content for the neat epoxy and silicate/epoxy nanocomposite samples at 2 mm thickness.

Kagawa et al. (Kagawa et al. 1998) revealed that the light transmittance of the glass particle-epoxy nanocomposites decreased with increase in glass particle volume fraction. Also, Optical properties of montmorillonite/epoxy nanocomposites were studied by Deng et al. (Deng et al. 2004) and it was observed that with increasing OMMT loading, the light transmittances in the whole wavelength range systematically decreases.

This result was concluded such that when the silicate concentration increases, the particle surface per unit volume increases, and the light extinction obtained from the scattering at the interface of epoxy matrix and silicate particles increase.

5.5. Flame Retardancy Behaviour

The UL-94 horizontal flammability test was used to determine the burning time, length and burning rate of MMT and OMMT incorporated epoxy nanocomposites, and the results are listed in Table 5.4. The neat epoxy burns completely at atmospheric conditions, however, partial burning was observed for nanocomposite samples containing MMT and OMMT silicate particles.

Table 5.4. UL-94 flammability tests data for neat epoxy and silicate/epoxy nanocomposites

Flame Retardant Nanocomposite	**Burning Rate (mm/s)**	**Burning Length (mm)**	**Burning Time (s)**
Neat Epoxy	0.34	75	220
3% MMT/Epoxy Nanocomposite	0.28	60	217.5
10% MMT/Epoxy Nanocomposite	0.20	36.5	174
3% OMMT/Epoxy Nanocomposite	0.23	45	192.5
10% OMMT/Epoxy Nanocomposite	0.14	32	221

Figure 5.45 shows the relative burning rate of the neat epoxy and nanocomposites as a function of silicate loading. The burning rate for neat epoxy is 0.34 mm/s. Addition of MMT and OMMT silicate particles into the epoxy matrix increases the flame retardancy of the epoxy. At 10 wt. % silicate loading, the burning rate decreases by 38 and 58 % for MMT and OMMT nanocomposites, respectively. Figure 5.46 schematically illustrates the barrier function of the conventional micron sized particle filled polymer and nanosilicate layers incorporated polymers. The barrier function of the silicate layers reduces the transport of oxygen and waste-gasses and blocks the burning of polymer under the atmospheric conditions so that reduced flammability is observed for nanocomposites. The improvement on the flame resistivity of the composites is greater in the case of OMMT particle additions. Better exfoliation of OMMT silicate particles

within the polymer matrix enhances the flammability resistance of epoxy as compared with MMT. The higher fraction of agglomerates within the MMT/epoxy composites acts more like in conventional filled ones.

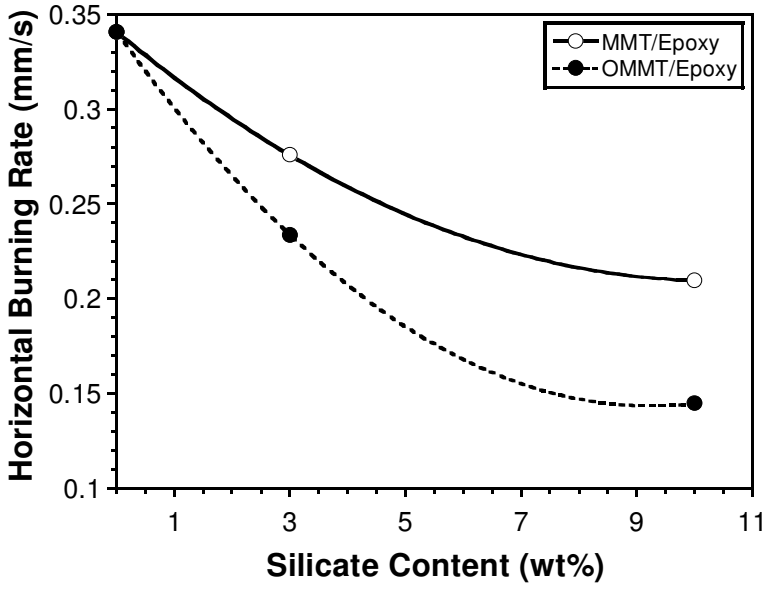

Figure 5.45. Horizontal burning rate of the neat epoxy and silicate/epoxy nanocomposites as function of silicate content.

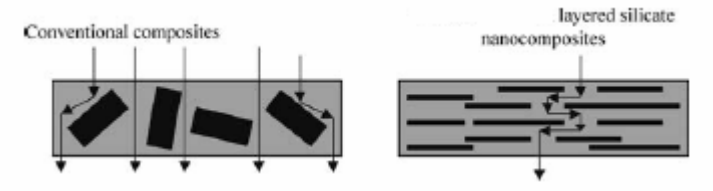

Figure 5.46. Barrier function of the silicate layers (Source: Ray and Okamato 2003)

CHAPTER 6

CONCLUSION

In this study, layered silicate/polymer nanocomposites were developed based on epoxy resins and Na^+ containing montmorillonite as the nano platelet reinforcement. Silicate particles were treated with hexadecyltrimethylammonium chloride (HTCA) through an ion exchange reaction. In this way, Na^+ interlayer cations of the silicate is exchanged with onium cation of the surfactant that turns the hydrophilic silicates to organophilic characteristics. Silicate/epoxy nanocomposites were processed through in-situ polymerization technique by blending of 0-10 wt. % of the silicate particulates within the polymer matrix using ultrasonication. Following blending, composite preparation was completed by polymerization of the cast samples.

Microstructure-property relation within the developed nanosystems was investigated at a fundamental level based on (XRD), scanning electron microscopy (SEM) techniques. Stress-strain behavior of the nanocomposites was measured using mechanical testing. Optical transparency of the materials was analyzed with UV and IR transmittance spectroscopy and thermal behavior was monitored with differential scanning calorimeter (DSC).

From XRD patterns, it was observed that the d-spacing of the silicate particles are expanded from 14.3 Å to 18.1 Å due to surface modification. A greater d-spacing of MMT implies intercalation of the silicate galleries. XRD patterns of the nanocomposites made of MMT and OMMT silicates shows that the characteristic peaks of the silicates are not detectable for the nanocomposites samples. This indicates the further intercalation of the silicates within the polymer matrix. Based on SEM, it was observed that as the clay concentration in the nanocomposites increases, the particle size increases. At high silicate concentrations, larger silicate agglomerations were visible within the epoxy matrix. Organosilicate platelets (OMMT) are better dispersed in the epoxy matrix as compared to those with MMT/epoxy nanocomposites. The tensile modulus of the nanocomposite with 10 wt. % OMMT is improved by 16 %, but with 10 wt. % MMT it is improved by only 12 %. The addition of MMT reduces the tensile strength values of the epoxy while it remains almost constant with OMMT additions. Tensile strain at break values decreases

as the silicate content increases. Flexural modulus of the nanocomposites is increased by 24 % with 6 wt. % OMMT and by 17 % with 10 % MMT with respect to the neat resin. As silicate content increases, the flexural strength values decrease as seen in the case of the tensile strength. Semi empirical models developed to predict the elastic behaviour of the composites that contain non-spherical particles embedded into matrix were used. The predicted and experimentally measured values for MMT-Epoxy and OMMT-Epoxy nanocomposite systems were compared to determine the correlative capability of the models. Predicted values showed some reasonable agreement with experimental data. Among various models, Brodnyan model produced the best prediction of elastic modulus of nanocomposite systems. It was also found that K_{IC} values decrease by 44 and 54% at high concentrations (i.e; with the addition of 10%) of MMT and OMMT silicate particles, respectively. The results indicate that K_{IC} is decreasing significantly at high silicate contents as the void fraction is increasing in the matrix. DSC analysis revealed that incorporation of MMT into epoxy system does not affect the T_g values. On the other hand, it was found that Tg increases with the addition of OMMT silicate particles. Incorporation of silicate leads to an increase in storage and loss modulus and a significant increase of the DMA measured Tg of the nanocomposites. Also, optical transmission values are affected by silicate incorporation. Nanocomposites containing OMMT silicate particles exhibited better transparency than those with MMT. This is associated with a better exfoliation of silicate layers from OMMT within the epoxy matrix. As the silicate layers are dispersed well in the matrix, the nanometer level thickness of the layers does not act to scatter the light passage. Flammability test results showed that the flame retardancy of polymer increases by incorporation of silicate particles. At 10% silicate loading, the burning rate is decreased by 38 and 58 % for MMT and OMMT nanocomposites, respectively.

In general, the mechanical, thermal, optical, and flame retardancy properties of the nanocomposites with OMMT were found to be better than those of nanocomposites with MMT. This is associated with the higher d-spacing of OMMT due to surface modification.

New technologies for modifying the matrix greatly increased the applications of advanced composites. The potential for new or significantly improved properties attainable at such low-volume fractions is the primary motivation for investigating silicate/epoxy nanocomposites for aerospace and automotive applications.

In the future studies, the processing of layered silicate/epoxy nanocomposites may be produced by shear mixing with a three-roll mill and effects of the properties of nanocomposites synthesized by this method can be investigated. Furthermore, the effect of stoichiometric ratio on the material properties of epoxy-amine thermoset system may be studied. The material properties, including the glass transition temperature, modulus of the nanocomposite materials can be measured as a function of stoichiometry.

REFERENCES

Ahmadi S. J., Huang Y. D., Li W. 2004. "Review: Synthetic Routes, Properties and Future Applications of Polymer-layered Silicate Nanocomposites", *Journal of Materials Science*. Vol. 39, pp. 1919-1925.

Ajayan P. M., Schadler L. S., Braun P. V. 2003. *Nanocomposite Science and Technology,* (Wiley-VCH, Newyork, USA).

Avella M., Errico M. E., Martelli S., Martuscelli E. 2001. "Preparation Methodologies of Polymer Matrix Nanocomposites", *Appl. Organometal. Chem.* Vol. 15, pp. 435-439.

Balakrishnan S., Raghavan D. 2004. "Acrylic, Elastomeric, Particle-Dispersed Epoxy-Clay Hybrid Nanocomposites: Mechanical Properties", *Macromol. Rapid Commun*. Vol. 25, pp. 481–485

Braem M., Van Doren V. E., Lambreehts P., Vanherle G. 1987. "Determination of Young's Modulus of Dental Composites: A Phenomenological Model", *Journal of Material Science.* Vol. 22, pp. 2037-2042.

Brodnyan J. G. 1959. "The Elastic Behaviour of a Crystalline Aggregates", *Trans. Soc. Rheol.* Vol. 6, p. 61.

Brown G. M., Ellyin F. 2005. "Assessing the Predictive Capability of Two-Phase Models for the Mechanical Behavior of Alumina/Epoxy Nanocomposites", *Journal of Applied Polymer Science.* Vol. 98, pp. 869–879.

Broutman L. J., Krock R. H.1967. *Modern Composite Materials*, (Addison Wesley, Reading, Massachusetts).

Chang J., Kim S. J., Im S. 2004. "Poly(trimethylene terephthalate) Nanocomposite Fibers by In-situ Intercalation Polymerization: Thermo-mechanical Properties and Morphology (I)", *Polymer*. Vol. 7, pp. 1-11.

Chantler P.M., Hu X., Boyd N.M. 1999. "An Extension of a Phenomenological Model for Dental Composites", *Dental Materials.* Vol. 15, pp. 144–149.

Chen K. H., Yang S. M. 2002. "Synthesis of Epoxy–Montmorillonite Nanocomposite", *Journal of Applied Polymer Science.* Vol. 86, pp. 414–421.

Chen C., Curliss D. 2003. "Preparation, Characterization, and Nanostructural Evolution of Epoxy Nanocomposites", *Journal of Applied Polymer Science.* Vol. 90, pp. 2276–2287.

Counto U. J. 1964. "A variational approach to the theory of the elastic behaviour of multiphase materials", *Mag. Concr. Res.* Vol. 16, p. 129.

Dean D., Walker R., Theodore M., Hampton E., Nyairo E. 2005. "Chemorheology and properties of epoxy/layered silicate nanocomposites", *Polymer.* Vol. 46, pp. 3014–3021.

Deng Y., Gu A., Fang Z. 2004. "The Effect of Morphology on the Optical Properties of Transparent Epoxy/Montmorillonite Composites", *Polym.* Int. Vol. 53, pp. 85–91.

Einstein A. 1956. *Investigation on Theory of Brownian Motion*, (Dover, New York).

Mooney M. 1951. "The viscosity of a concentrated suspension of spherical particles", *J. Colloid. Sci.* Vol. 6, pp. 162-170.

Feng W., Kadi A., Fudel B. 2002. "Polymerization Compounding: Epoxy Montmorillonite Nanocomposites", *Polymer Engineering and Science.* Vol. 42, pp. 1827-1835.

Flandin L., Hiltner A., Baer E. 2001. "Interrelationships Between Electrical and Mechanical Properties of a Carbon Black-filled Ethylene–Octene Elastomer", *Polymer.* Vol. 42, pp. 827-838.

Fischer H. 2003. "Polymer Nanocomposites: from Fundamental Research to Specific Applications", *Materials Science and Engineering C.* Vol. 23, pp. 763–772.

Fornes T.D., Paul D.R. 2003. "Modeling Properties of Nylon 6/Clay Nanocomposites Using Composite Theories", *Polymer.* Vol. 44, pp. 4993–5013.

Gao F. 2004. "Clay / Polymer Composites: The Story", *Materialstoday*. Vol. 23, pp. 50-55.

Gilman J. W. 1999. "Flammability and Thermal Stability Studies of Polymer Layered-silicate_clay/nanocomposites", *Applied Clay Science.* Vol. 15, pp. 31–49.

Giannelis E. P. 1998. "Review: Polymer-Layered Silicate Nanocomposites: Synthesis, Properties and Applications", *Appl. Organometal. Chem.* Vol. 12, pp. 675–680.

Guth E. 1945. "Theory of Filler Reinforcement", *J. Appl. Phys.* Vol. 16, p. 20.

Guth E., Gold O. 1938. "New Foundation of General Relativity", *Phys. Rev.* Vol. 53, p.322.

Kim J., Jackman R. J. 1994, Eisenberg A. "Filler and Percolation Behavior of Ionic Aggregates in Styrene-Sodium Methacrylate Ionomerst", *Macromolecules.* Vol. 27, pp. 2789-2803.

Halpin J. C. 1969. "Conductive rubbers and plastics", *J. Comp. Mater.* Vol. 3, p. 732**.**

Halpin J. C., Kardos J. L. 1976. "The Halpin-Tsai Equations: A Review", *Polm Eng Sci.* Vol. 16, pp. 344-352.

Hasegawa N. 1998. “Preparation and Mechanical Properties of Polypropylene- Clay Hybrids Using a Maleic Anhydride-Modified Polypropylene Oligomer”, *J. Of Appl. Polm. Sci.* Vol. 67, pp. 87-92.

Hashin Z., Shtrikman S. 1963. “A Variational Approach to the Theory of the Elastic Behaviour of Multiphase Materials”, *J. Mech. Phys. Solid.* Vol. 11, pp. 127-140.

Hermans J. J. 1967. “The Elastic Properties of Fiber Reinforced Materials when the Fibers are Aligned”, *Proc Kon Ned Akad v Wetensch B.* Vol. 65, pp.1-9.

Hill R. J. 1964. “Theory of mechanical properties of fibre-strengthened materials: I. Elastic behaviour”, *J. Mech Phys Solids.* Vol. 12, p.199.

Isik I., Yilmazer U., Bayram G. 2003. “Impact Modified Epoxy/Montmorillonite Nanocomposites: Synthesis and Characterization”, *Polymer.* Vol. 44, pp. 6371–6377.

Jordan J., Jacob K. I., Tannenbaum R., Sharaf M. A., Jasiuk I. 2004. “Review: Experimental Trends in Polymer Nanocomposites-a Review”, *Materials Science and Engineering A.* Vol. 12, pp. 35-42.

Kalaprasad G., Joseph K., Thomas S., Pavithran C. 1997. “Theoretical Modelling of Tensile Properties of Short Sisal Fibre-Reinforced Low-Density Polyethylene Composites”, *Journal of Materials Science.* Vol. 32, pp. 4261-4267.

Kagawa Y., Iba H., Tanaka M., Sato H. Chang T. 1998. “Fabrication and Optical/Thermal Properties of Glass Particle-Epoxy Optically Transparent Composites”, *Acta Mater.* Vol. 46, pp. 265-271.

Kornmann X., Thomann R., Mülhaupt R., Finter J., Berglundi L. A. 2002. “High Performance Epoxy-Layered Silicate Nanocomposites”, *Polymer Engineering and Science*. Vol. 42, pp.1815-1826.

Kornmann X., Lindbergb H., Berglunda L.A. 2001.“ Synthesis of epoxy-clay nanocomposites. Influence of the nature of the curing agent on structure”, *Polymer.* Vol. 42, pp. 4493-4499.

Lee A., Lichtenhan J. D. 1999. “Thermal and Viscoelastic Property of Epoxy–Clay and Hybrid Inorganic–Organic Epoxy Nanocomposites”, *Journal of Applied Polymer Science.* Vol. 73. pp. 993–2001.

Lee H., Neville K., 1957. *Epoxy Resins: Their Applications and Technology*, (McGraw-Hill Book Company, Inc., Newyork), pp. 4-12.

Lewis T. B., Nielsen L. E. 1970. “Dynamic Mechanical Properties of Particulate-Filled Composites”, *J Appl Poly Sci.* Vol. 14, pp. 1449-1471.

Lin J., Chang L.C., Nien M.H., Ho H.L. 2005. “Mechanical Behavior of Various Nanoparticle Filled Composites at Low-Velocity Impact”, *Composite Structures.*Vol. 4, pp. 12-21.

Lingois P., Berglund L. 2002. “Modeling Elastic Properties and Volume Change in Dental Composites”, *Journal of Material Science.* Vol. 37, pp. 4573-4579.

Liu W., Hoa S. V., Pugh M. 2005. “Organoclay-modified high performance epoxy nanocomposites”, *Composites Science and Technology.* Vol. 65, pp. 307–316.

Luo J., Daniel I. M. 2003. “Characterization and Modeling of Mechanical Behavior of Polymer/Clay Nanocomposites”, *Composites Science and Technology.* Vol. 63, pp.1607–1616.

Ma J., Xu J., Ren J., Mai Y. 2003. “A New Approach to Polymer/Montmorillonite Nanocomposites”, *Polymer.* Vol. 44, pp. 4619–4624.

McGee S. H., McCullough R.L. 1981. “Models for the permeability of filled polymer systems”. *Polymer Composites.* Vol. 2, pp. 149.

Mooney M. 1951. “The viscosity of a concentrated suspension of spherical particles”, *J. Colloid Science.* Vol. 6, pp. 162-170.

Myskova M. Z., Zelenka J., Spacek V., Socha F. 2003. “Properties of Epoxy Systems with Clay Nanocomposites’, *Mechanics of Composite Materials.* Vol. 39, pp.1-6.

Nielsen L. E. 1970. “Generalized Equation for the Elastic Moduli of Composite Materials”, *J Appl Phys.* Vol. 41, pp. 4626-4627.

Nigam V., Setua D. K., Mathur G. N., Kar K. K. 2004. “Epoxy-Montmorillonite Clay Nanocomposites: Synthesis and Characterization”, *Journal of Applied Polymer Science.* Vol. 93, pp. 2201-2210.

Njuguna J., Pielichowski K. 2003. “Polymer Nanocomposites for Aerospace Applications: Properties”, *Advanced Engineering Materials.* Vol. 5, pp. 769-778.

Qutubuddin S., Fu X. 2001. *Nano-Surface Chemistry*, (New York, NY, USA), pp. 653-672.

Pozsgay A., Frater T., Szazdi L., Muller P., Sajo I., Pukanszky B. 2004. “Gallery Structure and Exfoliation of Organophilized Montmorillonite: Effect on Composite Properties”. *European Polymer Journal.* Vol. 40,pp. 27–36.

Ranta D., Manoj N. R., Varley R., Raman S. and Simon G. P. 2003. “Clay-reinforced epoxy nanocomposites”, *Polym Int.* Vol. 52, pp. 1403–1407.

Ranta D., Becker O., Krishnamurthy R., Simon G.P., Varley R.J. 2003. “Nanocomposites based on a combination of epoxy resin, hyperbranched epoxy and a layered silicate”, *Polymer.* Vol. 44, pp. 7449–7457.

Ray S. S., Okamoto M. 2003. “Polymer/Layered Silicate Nanocomposites: A Review from Preparation to Processing”, *Prog. Polym. Sci.* Vol. 28, pp. 1539–1641.

Salahuddin N. A. 2004."Layered Silicate/Epoxy Nanocomposites: Synthesis, Characterization and Properties". *Polym. Adv. Technol.* Vol. 15, pp. 251–259.

Subramaniyan A. K., Sun C.T. 2006. "Enhancing Compressive Strength of Unidirectional Polymeric Composites Using Nanoclay". *Composites: Part A.* Vol.2, pp. 7-12.

Standard Test Method for Flexural Properties of Unreinforced and Reinforced Plastics and Electrical Insulating Materials, American Society for Testing and Materials (ASTM) D 790M – 86.

Standard Test Method for Tensile Properties of Plastics, American Society for Testing and Materials (ASTM) D 638M - 91a.

Standard Test Method for Plane-Strain Fracture Toughness and Strain Energy Release Rate of Plastic Materials, American Society for Testing and Materials (ASTM) D 5045 – 91a.

Standard Test Method for Rate of Burning and/or Extent and Time of Burning of Self-Supporting Plastics in a Horizontal Position (ASTM) D 635 – 91.

Skoog D. A., Holler F. J., Nieman T. A., 1998. *Principles of Instrumental Analysis*, (Harcourt Brace & Company, United state of America) p.798.

Takayanagi M., Vemura S., Minami S. 1964. "The effect of inclusion shape on the elastic moduli of a two-phase material", *J. Polym . Sci. Part C.* Vol. 5, p. 113.

Tolle T. B., Anderson D. P. 2002. "Morphology Development in Layered Silicate Thermoset Nanocomposites", *Composites Science and Technology.* Vol. 62, pp. 1033–1041.

Thostenson E. T., Li C., Chou T. 2004. "Review: Nanocomposites in Context", *Composites Science and Technology.* Vol. 4, pp. 15-24.

Velmurugan R., Mohan T. P. 2004. "Room Temperature Processing of Epoxy-Clay Nanocomposites", *Journal of Materails Science.* Vol. 39, pp. 7333 – 7339.

Wang J., Pyrz R. 2004. Prediction of the overall moduli of layered silicate-reinforced nanocomposites—part II: analyses. *Composites Science and Technology.* Vol. 64, pp. 935–944.

WEB_1, 2000. Polymer-layered silicate nanocomposites, 12/03/2006. http://www.seas.ucla.edu/mcl/references/Leslie/leslie1.pdf.

WEB_2, 1998. Definitions of Clay Crystals, 23.04.2005 http://www.stadiumturf.com/definitions_of_clay_crystals.htm

WEB_3, 2004. Dynamic Mechanical Analysis, 05.06.06. http://www.impactanalytical.com/dma.html

WEB_4, 2004 UL 94 Test, 08.06.06. www.bolton.ac.uk/fire/UL%2094%20TEST.htm

Wetzel B., Haupert F., Zhang M. Q. 2003. "Epoxy nanocomposites with high mechanical and tribological performance", *Composites Science and Technology.* Vol. 63, pp. 2055–2067.

Whitney J. M., McCullough R. L. 1990. "*Delaware Composites Design Encyclopedia*" Vol 2 Micromechanical Materials Modeling, Technomic Publishing, USA.

Wu Y., Jia Q., Yu D., Zhang L. 2004. "Modeling Young's Modulus of Rubber–Clay Nanocomposites Using Composite Theories", *Polymer Testing.* Vol. 23, pp. 903–909.

Yano K., Usuki A., Okada A., Kurauchi T. and O. Kamigaito. 1993. "Synthesis and Properties of Polyimide–clay Hybrid", *J. Polym Sci, Part A: Polym Chem.* Vol. 31 pp. 2493–2498.

Zanetti M., Lomakina S., Camino G. 2000. "Polymer Layered Silicate Nanocomposites", *Macromol. Mater. Eng.* Vol. 279, pp. 1–9.

Zhang K., Wang L., Wang F., Wang G., Li Z. 2004. "Preparation and Characterization of Modified-Clay-Reinforced and Toughened Epoxy-Resin Nanocomposites", *Journal of Applied Polymer Science.* Vol. 91, pp. 2649–2652.

Zerda A. S., Lesser A. J. 2001. "Intercalated Clay Nanocomposites: Morphology, Mechanics, and Fracture Behavior", *Journal of Polymer Science: Part B: Polymer Physics.* Vol. 39, pp. 1137–1146.

Zhou Y., Shi F. G. 2004. "Epoxy-based Optically Transparent Nanocomposites for Photonic Packaging", *9th Int'l Symposium on Advanced Packaging Materials.* pp.100-103